CHARACTERISTICS OF RUTTING ON HIGH QUALITY BITUMINOUS HIGHWAY PAVEMENTS

By

SAMUEL OTENG-SEIFAH

Bachelor of Science in Building Technology
University of Science and Technology
Kumasi, Ghana
1969

Master of Science in Civil Engineering
Montana State University
Bozeman, Montana
1971

Submitted to the Faculty of the Graduate College
of the Oklahoma State University
in partial fulfillment of the requirements
for the Degree of
DOCTOR OF PHILOSOPHY
December, 1975

CHARACTERISTICS OF RUTTING ON HIGH QUALITY

BITUMINOUS HIGHWAY PAVEMENTS

Thesis Approved:

Phillip L. Marker
Thesis Adviser

James A. Rooker

Robert L. Janes

Robert D. Morrison

N. N. Durham
Dean of the Graduate College

ACKNOWLEDGMENTS

The author wishes to express his gratitude and sincere appreciation to the following individuals:

To his major professor and adviser, Professor Phillip Gordon Manke, for his assistance and encouragement prior to and during this research investigation.

To his committee members, Professors R. L. Janes, T. A. Haliburton, and J. Leroy Folks for their excellent instruction, advice, and interest prior to and during this study.

To the School of Civil Engineering and the Oklahoma Department of Highways for the financial support and assistance which made this study possible.

To the Research and Development division of the Oklahoma Department of Highways for advice and assistance in field sampling.

To P. G. Wilson, A. J. Harris, Gerald Stotts, Maurice Colpitts, and C. K. Sharp for the assistance in preparation of special equipment needed for this study.

To the African-American Institute, and the Department of Structural Technology (Kumasi University) for their interest and financial support which made the author's advanced study in the U.S.A. possible.

To his parents whose early guidance instilled a continuing desire for knowledge.

To his wife, Mary Doris, and their daughter, Sara Bonnie, for the many sacrifices which they have made to enable the author to complete his academic work.

To Mrs. Robin Lee for her assistance in the preparation and typing the manuscript.

TABLE OF CONTENTS

LIST OF TABLES

LIST OF FIGURES

CHAPTER I

INTRODUCTION

Statement of Problem

Rutting, as evidenced by vertical deformations in the wheelpaths on flexible pavement surfaces, is a serious highway performance problem in Oklahoma (55). Rutting is due to traffic action and it affects the quality of ride in two distinct ways. First, rutting tends to define the position of vehicle wheels on the pavement, i.e., wheels slightly displaced tend to be directed back to points of maximum rutting, making steering more difficult at high vehicle speeds. Second, rutting tends to channelize and retain free surface water along the wheelpaths during and after rainfall. This surface water acts at the tire-pavement interface to form an effective lubricant so that the intended frictional resistance at this interface is not mobilized and surface slickness results. In extreme cases, the interfacial phenomenon referred to as "hydroplaning" occurs and this is a definite traffic safety hazard. This channelization also allows drainage of more surface water into intersecting or transverse cracks and thus into the underlying pavement layers to deteriorate the asphalt-bound materials (27), and to soften the subgrade materials.

Method and Scope of Study

Field and laboratory observations indicate three major modes of rutting. Regarding the bituminous bound layers, these modes are: 1) post-construction differential densification of one or more of the pavement layers, 2) shear failure or lateral displacement of material in one or more layers from beneath the wheelpaths, and 3) surface wear or errosion of surface material under traffic. In addition, densification (consolidation) and/or shear failures in the non-bituminous bound base and subgrade materials can influence the total amount of rutting. In a specific case, each of these factors may act singularly or in various combinations.

The primary objective of this research was to investigate rutting on high quality flexible pavements and to detect, where possible, evidence of contribution of the bituminous bound pavement materials to this type of failure. This research did not deal directly with the influence or contributions to rutting of the subgrade soils and the non-asphalt bound base materials.

A transverse profile apparatus was developed to plot the profile of the pavement surface perpendicular to the centerline. Rut depths could be scaled directly and humps outside the wheelpath locations detected from the transverse profile tracings. Heaving or humping adjacent to ruts was considered an indication of outward or lateral creep of material from beneath the wheelpaths.

Four inch diameter (10.16 cm) cores of the asphalt bound pavement materials were recovered at selected points across the pavement. The percent density values of the respective subdivisions of the core samples were determined and compared. Significant differences in the percent density values between materials in the wheelpath locations and

those outside the wheelpaths were considered as evidence of differential densification. Correlation between laboratory densities and field measured nuclear-densities at the selected sites was also attempted.

Stereo photography was employed to obtain quantitative estimates of differential wear in the wheelpath locations. Also, visual rating of the pavement surface conditions was made at each test site so as to provide comparative data for the study of trends at these locations.

Sixteen test sites were selected on two interstate highway systems (I-35 and I-40) in Oklahoma. Performance of four test sites of flexible pavements constructed on each of the following types of base course materials were studied: 1) hot mix sand asphalt (HMSA), 2) soil-cement base (SCB), 3) black base (BB), and 4) stabilized aggregate base course (SABC).

Classical statistical methods, using the Statistical Analysis System (SAS) computer program, was employed in the analysis of test data. Traffic volumes were not counted at the time of testing and the recorded in-service age of the pavement sections at the test sites were estimated from construction completion records obtained from the research section of the Oklahoma Department of Highways (ODH).

CHAPTER II

REVIEW OF PREVIOUS OBSERVATIONS AND RESEARCH

Introduction

An asphalt pavement structure is a layered system composed of an asphalt surface course, an asphalt leveling course, and a base course material supported by the subgrade soil. The following types of base course materials are used by the Oklahoma Department of Highways: 1) portland cement treated soil usually referred to as soil-cement base (SCB), 2) soil-stabilized aggregate material (SABC), 3) an asphalt bound select aggregate material or black base (BB), and 4) a hot mixed sand-asphalt material (HMSA). Sometimes, layers termed "subbase" or "improved subgrade" or both, are also included in the structure.

The load-carrying capacity of an asphalt pavement structure is brought about by the load-distributing characteristics of the layered system. Because the pavement structure consists of a series of layers with the highest quality materials at or near the surface of the pavement (the surface and the binder or leveling courses), the strength of the system is a result of building up thick layers to distribute traffic loads safely over the base course and to the subgrade rather than by the bending action of the slab (98). Wheel loads act on the pavement as compressive load pulses. These loads are then transmitted through the pavement layers to the underlying subgrade soil in the form of stress pulses. During the process of load distribution, the stresses are largest at the

surface (equal to the contact pressure) and decrease non-linearly with increases in depth (16). By proper selection of pavement materials and with appropriate depth and strength of the structure, the pavement layers spread the load stresses until these become small enough to be safely supported by the subgrade.

The Bituminous Mixture

The bituminous mixture consists of graded mineral aggregates (non-mineral aggregates can be used) and an asphalt cement mixed together and compacted in layers to form a solid mass. The compacted mixture utilizes the cohesive strength of the asphalt material, the frictional resistance developed between the aggregate particles and the interlocking resistance that is introduced in the compacted structure of the aggregate combination (76) to distribute the traffic load stresses to the base or subgrade. For a given degree of compaction, the strength components of the bituminous mixture will depend on the individual properties of the mineral aggregate combination and the asphalt binder, and the interaction between these materials.

Mineral Aggregate

Particle Size and Gradation. Much has been written on the effects of aggregate gradation and particle size on the characteristics of the bituminous mixtures, however, opinions and conclusions are not completely consistent.

According to Hargett (76) the term "size of particles" needs qualification in a discussion of the effects of particle size on the properties of the bituminous mixture. Bituminous mixtures are actually affected

by the maximum size of particles, the minimum size of particles, and the gradation of particle sizes within these size limits. Particle size discussed in terms gradation and gradation limits affects the amount of asphalt required for stability, density, workability, and the performance characteristics of the pavement. A large percentage of coarse particles tends to produce harsh mixtures and creates problems in the laydown operations. Poorly graded aggregate combinations have high void ratio, require high asphalt content, and usually produce low stability mixes. On the other hand, fine-grained mixtures are workable but they usually lack the stability developed in a well graded aggregate combination.

With regard to gradation, Regal (80) has noted a tendency for bituminous surfaces to rub and shove when constructed from aggregates having "humps" in their gradation curves. In comparison, Naughton (60) believes that there is a fairly wide band of tolerance within which the gradation curve can shift, without changing, appreciably, the fundamental characteristics of the mixture as regards bitumen requirements, density, and stability.

Benson (12) has pointed out the importance of maximum size of aggregates with regard to bitumen requirements, workability and economy of the mixture. In an experiment utilizing sand with 100 percent passing the No. 4 sieve and 42 to 100 percent passing the No. 20 sieve, it was found that when the percentage passing the No. 20 sieve was increased from 42 to 100 percent, the Marshall stability dropped from 920 to 490 lbs., and the optimum asphalt content increased from 5.5 to 9.2 percent. Also, it was found that as the gradation became denser, degradation decreased. For the materials used, the gradation and aggregate size range did

influence the strength and stiffness characteristics, permeability, asphalt content, workability, economy and skid resistance of the mixture.

Foster's series of tests (29) revealed that the true capacity of dense-graded mixtures to resist traffic induced stresses was controlled by the characteristics of the fine aggregate. In these tests, the mixtures incorporating coarse aggregates exhibited better stress-distributing capabilities than those which utilized only fine aggregates.

Though often associated with low stability, sand mixtures may possess some good desirable properties. From his experience in Virginia, Britton (15) noted the tendency for local sand mixtures to wear or abrade faster than normal mixes. In some cases, the weardown was sufficient for a driver to notice an elevation difference immediately adjacent to the wheelpath. Even so, Britton observed that the sand mixes always provided an excellent skid-resistant surface.

Shape of Particles. The shape of the aggregate particles affects the interlocking resistance that is developed in the compacted mixture. Laboratory tests conducted by Hargett (76) indicated that about 25 percent of the shearing resistance in a dense-graded mixture was developed in the form of interlocking resistance. Also, the shape of the aggregate particles appeared to affect the void content and the workability of the mixture.

In a literature survey, Benson (12) summarized the results of the work of Herrin and Goetz (1954) in the study of the effects of aggregate shape on the stability of bituminous mixtures as follows:

1) When the percentage of uncrushed gravel in the coarse aggregate fraction increased, the strength varied with grading, and decreased as

the grading became denser. This was also true for mixtures incorporating natural sand aggregates.

2) For one-sized grading (zero percent fine aggregate), the strength increased directly and substantially with increasing percentages of crushed gravel. The substantial increases in strength was attributed to changes in internal friction. Cohesion remained essentially the same.

3) In open-graded mixtures (about 39 percent fine aggregates), an increase in the percentage of crushed gravel from zero to 55 percent produced a slight increase in strength; percentages of crushed gravel above 55 gave no further increase in strength. The angle of internal friction did not change for varying percentages of crushed gravel, however, cohesion increased as the percentage of crushed gravel increased from zero to 55 percent.

4) The strengths of dense-graded mixtures were not influenced by the percentage of crushed gravel.

5) In all gradings (one-sized, open, and dense), greater strengths were shown by crushed stone than crushed gravel. The increased strength was attributed to increased cohesion.

6) Regardless of the coarse aggregates used, the strengths of both dense- and open-graded mixtures increased when the fine aggregate was changed from rounded sand to crushed limestone. The increases caused by changes in fine aggregate were much larger than those caused by changes in the angularity of the coarse aggregates. The strength increases were attributed to increases in cohesion.

7) Because substantial strength was derived from internal friction, it was concluded that the aggregate grading was more of a determining factor for strength than the aggregate shape.

In a research study on the properties of mixtures incorporating large-sized aggregates of different particle shapes, Kalcheff (40) found the angularity of aggregates contributed significantly to the strength properties of both the coarse and the fine portions of the mix. Both strength properties were associated with mixtures incorporating crushed stone aggregates.

Surface Texture. Hargett (76) has observed in laboratory tests that frictional resistance accounts for about 50 percent of the shearing resistance that is developed in a dense-graded bituminous mixture. In his concluding remarks, the author stated that the frictional resistance that is developed between aggregate particles depends on the surface texture of the particles, hence the surface texture has significant effect on the stability of the bituminous mixture. This surface property of the aggregate was reflected by large increases in the angle of internal friction.

According to Monismith (62) it is desirable to utilize rough-textured materials with dense gradations and to produce well-compacted mixtures in thick pavement sections because these factors tend to increase mixture stiffness.

Benson's literature survey (12) points out that stability of road aggregates depends primarily on the internal friction and mechanical arrangement or interlocking of individual particles of the mass. The two strength components are affected by the degree of compaction, particle slope or angularity, surface texture, and grading of the aggregate combination.

Other Desirable Properties

To satisfactorily perform as the major medium for stress distribution the mineral aggregate must also be tough enough to withstand the action of rolling during construction and the action of traffic without breaking up or degrading under the imposed loads. The test used for evaluating this property is the Los Angeles abrasion test and is described in detail in AASHO T-96. Also, the aggregates which undergo disintegration under weathering are unsuitable for paving purposes (101).

Bituminous Binder

The asphalt binder performs several tasks in the pavement. 1) It acts as a cementing agent to bind the aggregate particles together and keep them in proper position to transmit the applied loads. 2) It interacts with the aggregate particles to develop the cohesive strength component of the compacted mass. 3) It acts as a waterproffing agent to resist infiltration of moisture, and assists in drainage of surface water. Also it imparts the necessary workability to the system while the mixture is still hot and this assists in compacting the mixture to a dense mass. These functions are very important and any factors which reduce the effectiveness of the binder to perform these tasks will directly affect the overall performance of the pavement structure.

The asphalt material exists in the pavement structure as a thin film. When exposed to weathering, the film loses much of its plasticity and becomes brittle. In this form, the material loses most of its cementing properties and the subsequent cohesive resistance that is developed in the pavement structure. Hargett (76) believes that the inherent development of major increases in shearing resistance in the form of

cohesion, is unreliable and explains further that the strength component developed in the form of cohesion is subject to deterioration or strength loss because of aging and the thermoplastic properties of the asphalt binder.

Several theories are currently used to describe failure modes of asphalt films subject to load stresses. Ford (27) refers to one mode of failure as "film rupture". Film rupture may occur when adhesion of the asphalt cement is not uniform over the entire surface of the aggregate. The asphalt film tends to be thinnest at sharp corners and edges of the aggregate and the effect of traffic may cause the film to fracture. When fractured, moisture will enter the asphalt-aggregate interface to cause further stripping.

Majidzadeh and Herrin (53) have explained the dependence of the tensile strength of materials on the magnitude of the film thickness when tested in thin films by the "strength-thickness" rule. According to this rule, the tensile strength of thin films of a material when tested in tension, increases as the thickness of the film decreases. Experiments with thin films of asphalt cement indicated similar results. The tensile strength decreased as the film thickness increased and the tensile strength approached a constant value which did not change as the film thickness was increased. The film thicknesses used in the experiment ranged from 10 to 1000μ. For the type of asphalt cement studied, the tensile strength-film thickness relationship was linear on a semilogarithmic scale. Three types of failure were observed: brittle fracture occurred in thin films; thick films failed by flow and necking; the failure of intermediate film thicknesses was by tensile rupture and was characterized by the formation of cavities and filaments in the film.

Two theories can be used to accurately predict the tensile strength of asphalts in thin and thick films. These theories are the Hydrodynamic theory (64) and the Theory of Potential Energy and Cavities (51).

Hydrodynamic Theory. According to this theory, the rheological (flow) behavior of thin layers of viscous materials placed between two parallel plates and subject to tension, varies with the thickness of the layer. As the film thickness decreases, the stress required to deform the material increases to a certain value. In a Newtonian liquid subject to tension, the material flows horizontally between the two parallel plates in addition to deforming in the direction of the applied stress, i.e., shear stresses are also present. Because the inward movement of the material in contact with the plates is prevented, the theory assumes that the flow perpendicular to the direction of the applied stress at any other plane is a parabolic function of the distance between the two plates. Hence the inward movement, which is a parabolic function of the film thickness, is considerably smaller in thin films, i.e., a larger stress is required to deform thinner films.

The Theory of Potential Energy and Cavities. According to this theory, the strength of a material that fails in pure tension is partly a function of secondary valence forces between adjacent molecules. With an increase in distance between molecules, the repulsive forces diminish more rapidly than the attractive forces. So the attractive forces govern the strength of the material. The energy associated with the attractive forces is inversely proportional to the sixth power of the distance between the adjacent molecules. Tensile rupture occurs when the applied force equals the maximum force due to the potential of the bonds. Materials with closely packed molecules are characterized by molecules of low

potential energy and have higher theoretical tensile strength than materials with loosely packed molecules.

Because cavities are associated with an increase in volume and are dependent on the tensile strain, it can be concluded that film thickness influences rupture stresses. Mack's experimental and theoretical investigation (51) indicate an optimum film thickness. When tensile strength was plotted against film thickness on a logarithmic scale, it increased linearly with film thickness up to an optimum thickness, then decreased linearly with further increase in film thickness.

Summary

The stress distributing characteristics of a paving mixture result from aggregate-binder interaction. When adequately compacted, the cohesive strength of the asphalt is utilized to bind the aggregates together and prevent dilation of the mixture under loads. The major strength components of the compacted mixture are therefore derived from the internal friction and the interlocking resistance developed in the compacted mixture. To help develop these major strength components, all attempts should be made to exclude moisture in the mixture since moisture tends to weaken the bond between the mineral aggregates and the asphalt cement.

Mix Design

The purpose of the design of asphalt paving mixture is to select and proportion raw materials to obtain a desired product (94). The overall objective, however, is to determine an economical blend and gradation of aggregates and asphalt that yields a mix with: 1) sufficient asphalt to insure adequate coating of the mineral aggregates and a durable pavement,

2) sufficient mix stability to satisfy the demands of traffic without distortion or displacement, 3) sufficient voids in the compacted mixture to allow for a slight amount of additional compaction under traffic loading without flushing or bleeding and loss of stability, yet enough to keep out harmful air and moisture, and 4) sufficient workability to permit efficient placement of the mixture. The Asphalt Institute (61) presents detailed procedures of three major mix design methods. These methods, the Marshall, the Hubbard-Field and the Hveem methods are currently being used with satisfactory results.

The Hveem method uses a stabilometer, a cohesionmeter and swell tests to determine the suitability of a mixture for paving purposes. The stabilometer test utilizes a special triaxial-type testing cell to measure the resistance of the compacted mixture to lateral displacement under vertical loading. The cohesiometer test, on the other hand, measures the cohesive or tensile resistance that is developed in the mix. The swell test measures the resistance of the mixture to the action of water.

The Marshall method uses a stability value and a total deformation value referred to as "flow", to determine the suitability of the mixture. The Hubbard-Field method, utilizes only a stability test to predict the strength characteristics of the mixture.

While stability values of compacted specimens often form the basis for selection of optimum asphalt contents to be incorporated in the paving mixture, stability numbers, as measured by the mix design methods, do not rate mixtures on their capability to withstand stresses induced in the mix. Foster (29) reported that two mixtures described by similar stability numbers which lie on either side of the optimum on a Marshall stability curve will not exhibit the same strength characteristics; i.e., a

lean mix will not exhibit the same strength characteristics as an overly rich mix.

Extensive experiment has also been conducted by Hadley and others (34) to determine correlation between direct tensile test results and those of the Hveem stabilometer and cohesiometer tests. Based on the series of specimens tested, acceptable correlations were found for the following comparisons:

1) modulus of elasticity versus cohesiometer value
2) tensile strength versus cohesiometer value
3) tensile strain versus cohesiometer value
4) Poisson's ratio versus stability, and
5) tensile strain versus stability.

No acceptable correlation was obtained for the following comparisons:

1) modulus of elasticity versus stability
2) tensile strength versus stability

Although, stability values do not directly rate paving mixtures according to their capacities to resist induced stresses they do aid the engineer in determining the optimum asphalt content for the mix. For a given type and gradation of aggregate, the amount of asphalt incorporated in the mixture determines, to a large extent, the thickness of the asphalt film, and directly affects the amount of air voids in the mixture, all other factors remaining constant. The test property curves for hot-mix design data by the Marshall method indicate large decreases in percent air voids as the amount of asphalt (percent by weight) increases. As more void spaces are filled with asphalt, the rate of decrease in air voids gradually decreases with increasing asphalt content. The percent voids in the mineral aggregate (VMA), consists of the volume of voids plus the

volume of asphalt expressed as a percentage of the bulk volume of the compacted mixture. A curve plotting VMA versus the percent asphalt content (by weight) shows a minimum at the optimum asphalt content. Any increase in asphalt content above the optimum results in an increase in VMA and increases the asphalt film thickness between adjacent aggregate particles. Therefore, according to the strength-thickness rule (53), increases in asphalt content above the optimum will directly decrease the tensile strength of the mixture and encourage a flow-type failure. This situation will almost certainly result in premature rutting.

From durability point of view, the amount and distribution of air voids in the compacted mixture is very important (61). Asphalt expands about twenty times more than the aggregate does in the temperature range 50°F to 135°F (22). When expansion takes place, the excess asphalt flows to occupy some of the void spaces in the mixture. Deficiency in voids will therefore encourage flow of the asphalt to the surface of the pavement to create the condition referred to as "bleeding" in the literature (61, 101). Excess voids, on the other hand, will allow free circulation of air and moisture in the mixture to oxidize the asphalt and deteriorate the bond between the asphalt and the aggregate.

Pavement Performance Characterization

Effect of Traffic Loads

Pavement response to loads depends on the nature and magnitude of the applied load. A study of the types of wheel loads actions is, therefore, a prerequisite to the understanding of the nature of stresses that are induced in the pavement structure by traffic. Although many papers have been written about pavement materials response to loading (3, 9, 17,

21, 35, 39, 64, 96, 97, 103, 108, 110), there is a notable absence of experimental data on tire actions on pavement surfaces under normal highway conditions. Because of this lack of information and other unknown variables, the structural design of highway pavements had taken the form of empirical techniques (39, 65). As a result, it is generally recognized that the relationships between traffic loadings and pavement performance developed at road tests apply only to the "conditions at the test site and direct application of the interrelationships in other areas is not valid.

In the absence of experimental data for pavement/tire interactions, however, soil/wheel interactions, usually studied in the field of terramechanics, may be used to characterize the types of actions at the tire/pavement interface. In their study of soil stresses, Wong and Reece (107) rolled a rigid wheel (2000 lb. axle load) over soil materials including loose sand, dry sand, and compacted sand. They observed two stress zones and one main failure surface AD (Fig. 1). Under the action of the wheel, the soil in the region ABC moved upward as the rim moved around the instantaneous center, I. The soil appeared to slide along AC producing positive tangential shear stress. Between points A and D, the soils moved in the opposite direction (backward). The authors (107) remarked that the zone AD was fairly long and approximately parallel to the wheel rim so the squeezing out action was small enough to be neglected.

Onafeko et al. (69), and Kirk (45) have carried out extensive experimental investigation concerning stress fields under slipping rigid wheels on soils. Elsammy and Ghobarah's (23) theoretical approach agrees with the findings of Onafeko and Kirk. At the point of slipping, the soil mass under the rigid wheel tends to flow in the direction of rotation

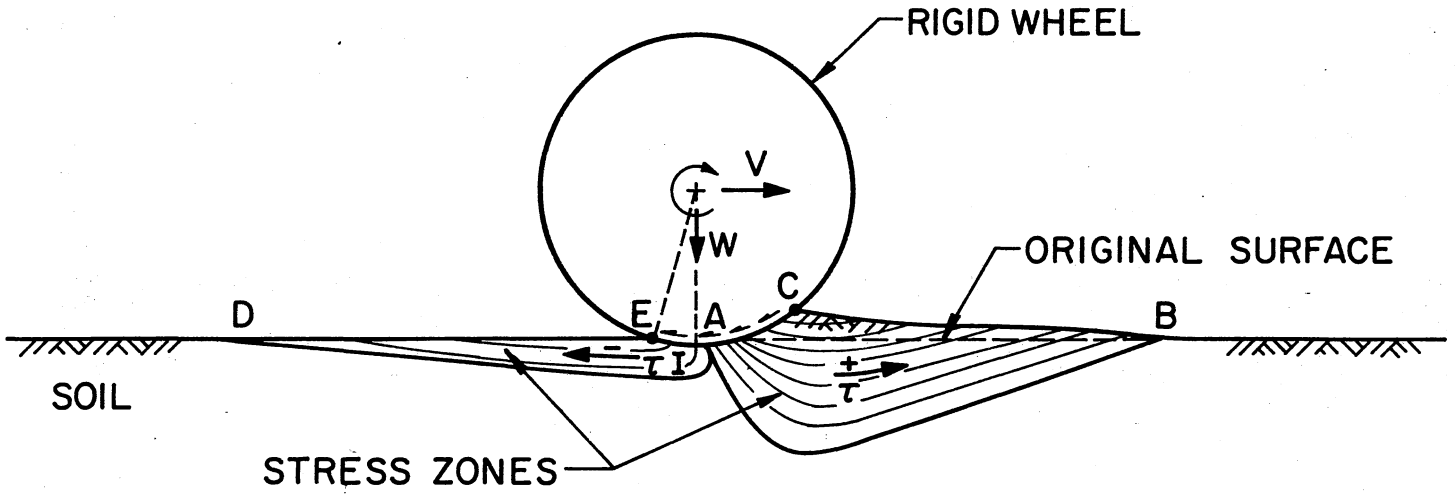

Figure 1. Stresses Under Rigid Wheel (After Wong and Reece (77))

of the wheel. Also the loads on the wheel tend to compress the soil materials immediately under the wheel. The flow zone was characterized by three modes of behavior (Fig. 2):

Mode 1: The soil mass outlined by wedge I was described to be in an active state of equilibrium as the rigid wheel was on the verge of pushing into the soil body. When the soil is in the state of plastic flow, the soil in this zone spreads in a horizontal direction.

Mode 2: The soil mass outlined by wedge II was described as a zone of radial shear failure. The lines that constitute one set in the shear pattern in this zone radiate from the outer edge of the wheel-soil contact surface at point O.

Mode 3: The soil wedge III, on the other hand, was considered to be in a passive state of limiting equilibrium. In the state of plastic flow, the soil in this wedge is compressed laterally and causes the surface to rise.

Grenshaw (31) has conducted detailed experiments to study the effects of wheels on soils. In Grenshaw's experiments, a high-flotation aircraft tire loaded to 5000 lbs was towed through a soil bin containing buckshot clay and Virginia river sand. His major findings may be summarized as follows:

1) prior to the point of planing, the wheel applies a drag load on the soil at the point of tire/soil contact.

2) there is a tendency for incremental increase in rut depth caused by the application of brake torque.

Grenshaw was of the opinion that the drag load response of the wheel on the soils used in his experiments was similar to the drag load response of a wheel hydroplaning on a water-covered hard surface and recognized

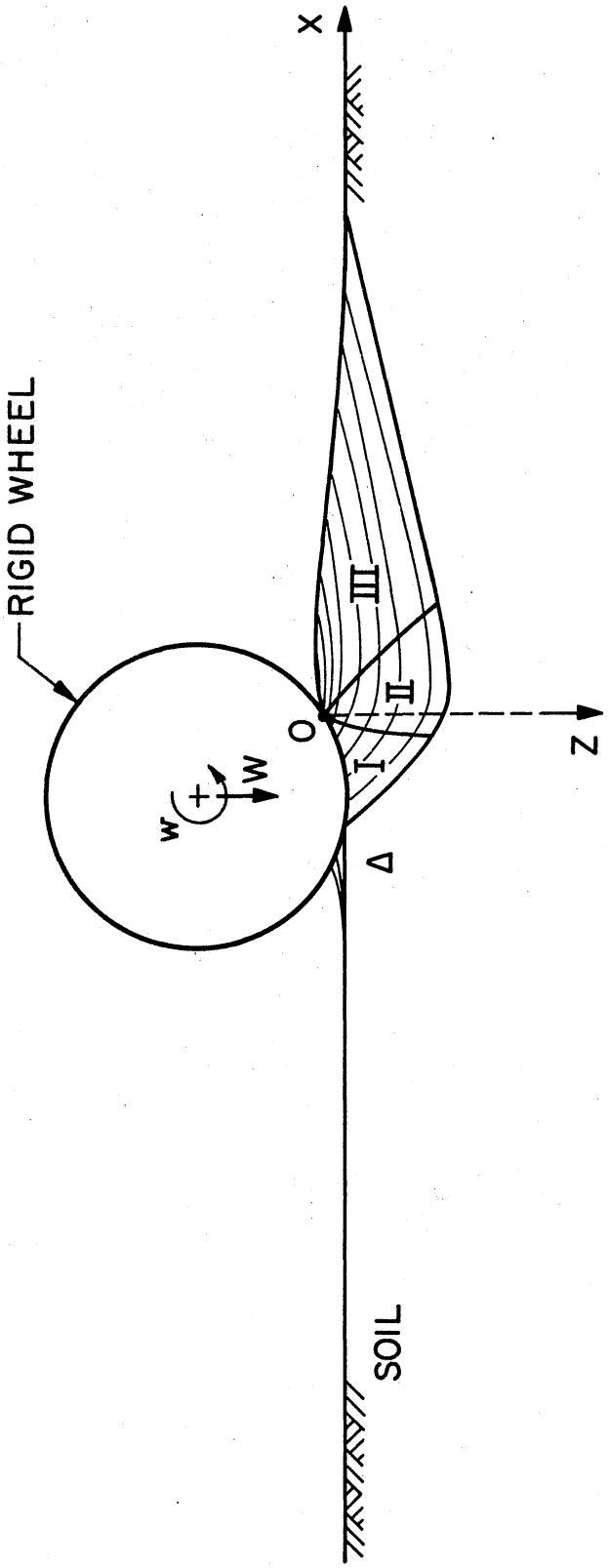

Figure 2. Modes of Behavior of Soil Under Rigid Wheel (After Onafeko (75))

the differences between the two phenomena. The tire on soft soil is near its maximum penetration into the soil whereas the hydroplaning tire is free of the pavement surface at its hydroplaning speed.

Wiendieck (104) has observed three major stress zones (Fig. 3). In his evaluation of stresses under rigid wheels rolling on soft soil, he characterized zone A as a wedge of soil being shoved or bulldozed ahead of the wheel, and zone C as an elastic zone that resists slippage stresses. He referred to the B zones as zones of lateral flow. Wiendieck described the behavior of materials in this zone as tending to undergo downward and sideward movements in a complicated manner. This finding can be used to explain some of the causes of permanent deformations that occur on asphalt pavements in service. These deformations are discussed later.

Summary

Though not exactly the same, the actions of rigid wheels can be used to predict the actions which vehicle tires tend to apply to highway pavements. These types of tire/pavements interaction may be summarized as follows: 1) vehicle wheel loads tend to apply a kneading action on materials in front of the wheel and the direction of stresses is parallel to the direction of the travel (Fig. 3), 2) in the opposite direction, the wheel tends to apply slippage or shear stresses on the pavement, 3) in the direction perpendicular to the direction of travel, the wheel tends to apply shoving action on the materials, 4) the wheel loads also tend to apply compressive stresses on the pavement material directly under the wheel, and 5) all these actions are cumulative; they act on the pavement surface in the form of stress pulses.

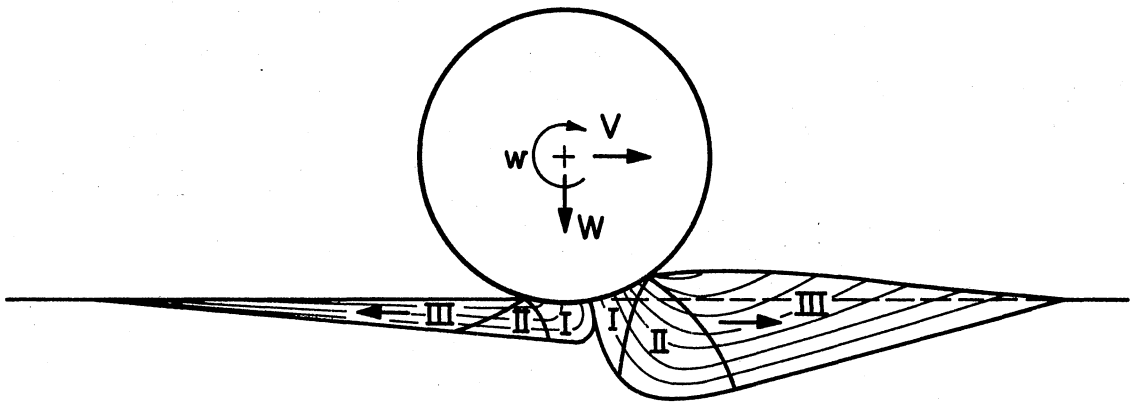

(a) STRESS ZONES UNDER RIGID WHEEL

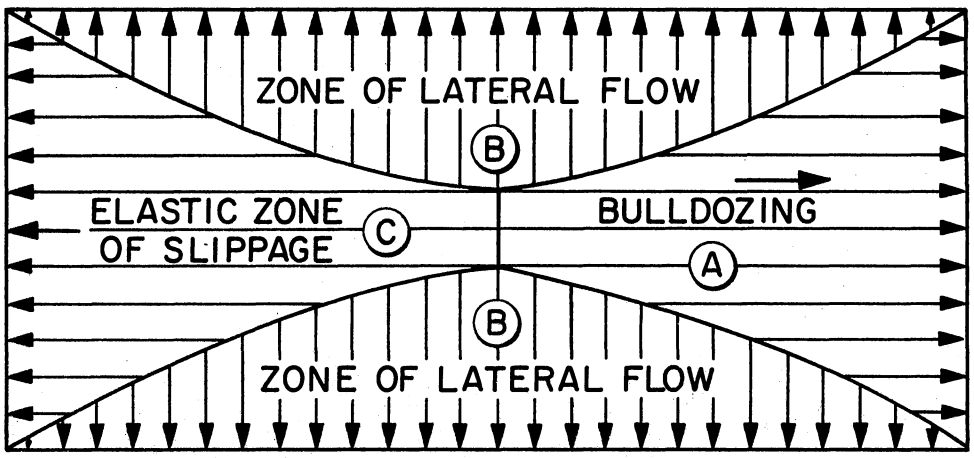

(b) PLAN VIEW OF STRESS ZONES

Figure 3. Stress Zones Under Rigid Wheel

Response to Loading

Elastic Deformations. Under applied wheel loads, bituminous pavements undergo both elastic and plastic deformations (14, 65). These deformations occur in both the longitudinal and the transverse directions to form a deflection basin. The elastic deformations are recoverable upon removal of the load. However, complete recovery is gradual and depends on the magnitude and duration of load, temperature, and stiffness properties of the pavement materials. Sometimes, complete recovery of this portion of deformation is not achieved before subsequent load coverages.

Theories for predicting elastic deformations consider the pavement material as an ideal material of some kind (34, 65, 110) and assume that the primary response of the pavement structure can be defined by its mechanical state (65), as a result of the applied loads. Laws of classical physics are then employed to determine the stress-strain relationships and to formulate constitutive equations (mathematical models) of response. Because of the complexities in the behavior of subgrade materials and the fact that the bituminous pavement constitutes a layered system, deformation values obtained using these methods are approximate. The degree of accuracy resulting from use of any of these theories will depend on how close the assumptions, upon which the theory was developed, relate to the field conditions. Some of the commonly used theories are discussed in the following sections.

Boussinesq's Theory. This theory is based on assumptions of a homogeneous, isotropic, and perfectly elastic mass that extends infinitely in all directions below a level surface. Use of the Boussinesq's deformation equation requires knowledge of the vertical and horizontal stresses. The equations give the elastic deformation (due to flexible circular

plate loaded at the center) at a depth, z, due to elastic strains in the materials between z and infinity, i.e., the equations do not consider any elastic deformations occurring in the pavement thickness itself; the computed deformations are those which occur in the subgrade materials beneath the base course layer (110).

Burmister's Theory. This was the first theory developed to solve the problem of an elastic multi-layered system and was based on the following assumptions: 1) each layer acts as a continuous, isotropic, homogeneous, linearly elastic medium infinite in horizontal extent; 2) the surface loading can be represented by a uniformly distributed vertical stress acting over a circular area; 3) the interface conditions between layers can be represented as being either smooth or perfectly rough; 4) each layer is continuously supported by the layer beneath; 5) inertia forces are negligible; and 6) deformations throughout the system are small (16). Use of this theory requires knowledge of the modulus of elasticity of the individual pavement layers and the subgrade material (9, 110). The determination of these moduli for the subgrade materials and the base course materials are usually done by means of plate-load test (5). Although equally approximate, this theory simulates the field conditions better than the Boussinesq's theory.

Westergaard Theory. Westergaard has also used the elastic theory to investigate stresses and deflections in layered systems (9). His theory considered a thin plate continuously supported by a bed of closely spaced, independent springs referred to as the Winkler foundation (discussed later under discrete models). This thin plate theory neglects the axial stresses perpendicular to the plate and shearing stresses parallel to the plate. Furthermore, the Winkler foundation used by Westergaard

assumes the foundation to act as a discontinuous medium. Nevertheless, Westergaard's charts of influence values are often used to predict subgrade deformations.

Discrete Models. These are response models where a continuum is represented by a system of independent or partially dependent mechanical models. In these models, the Winkler model, the Hetenyi foundation, the Filomenko-Borodick foundation, the Pasternak foundation, the Kerr model and the Tsai-Westmann tensionless foundation are commonly used (65). Although some of these models are sometimes employed to predict flexible pavement deformations, they are used primarily in the design of portland cement concrete pavements. In general, the analytical difficulties associated with these models depend on the closeness with which they approximate the elastic continum.

Plastic Deformations. This portion of the total deformation is unrecovered after removal of the applied load, i.e., the deformation remains permanent. Unlike elastic deformations, plastic deformations are cummulative and depend on the magnitude and duration of loading, temperature and the stress history of the material (9, 37, 65). Basic concepts of material behavior and constitutive laws of plasticity are currently used to predict the onset of plastic behavior. However, because the stress-strain relationships in the plastic range are generally non-linear, plastic deformations are not uniquely determined by stresses. Though seldom used, numerous criteria have been proposed for predicting plastic behavior, and are based on a concept of either stress, strain or energy (65, 100):

1. Maximum Stress Theory: Often referred to as Rankine or Lame-Navier failure criterion, this theory postulates that the maximum

principal stress in the material determines failure, regardless of the magnitude and sense of other principal stresses. Therefore, according to this theory, yielding begins when the absolute value of the maximum stress reaches the yield point of the material as found in simple tension or compression tests. This theory is rarely applied in pavement analysis because it does not consider the influence of two of the three principal stresses and conflicts with experimental information.

2. Maximum Elastic Strain Theory: This theory was proposed by St. Venant (65, 100) and assumes that yielding will occur when the maximum principal strain reaches the value of the yield strain in simple tension or compression. This theory is contradicted by material behavior under hydrostatic tensile or compressive stresses so it is seldom used (65).

3. Maximum Strain Energy Theory: This is often referred to as the Beltrami's energy theory and assumes yielding will occur when the total strain energy per unit volume equals the total strain energy per unit volume at yielding as found in a uniaxial tension or compression tests. Investigators have shown that this theory can be extended from the static to the dynamic case (100).

The Von Mises and the Coulomb-Tresca or Maximum Shear Stress Criteria are recognized as the basic theories currently used to predict the incipience of plastic yielding in soil and bituminous mixtures, and in materials characterized by ductile behavior (65). Both theories neglect the effect of mean stress and require knowledge of the yield stress in a uniaxial state of stress to predict the behavior under any combination of principal stresses. Also, the yield stress is assumed to be identical in tension and compression. Furthermore, the material is assumed to be isotopic. Detailed discussion of these theories are given in the references (65, 100).

Viscoelastic Response. Viscoelasticity attempts to represent the behavior of real materials by combining time-dependent response and time-independent response models (14, 65). Two types of viscoelastic models exist: Linear Viscoelastic and Non-linear Viscoelastic models.

Two basic models are used to develop a linear viscoelastic (one dimensional) model. These models are those of linear elastic spring (elastic model) and the linear viscous model as represented by a dashpot (stress is proportional to the rate of strain). Generally, linear viscoelastic models employ a basic stress-strain rule to combine the two portions of the model. The basic rule states:

> When two models are placed in series, the stress is the same in each model, but the total strain is the sum of the strain in each model. When two models are placed in parallel, the strain is the same in each model, but the total stress is the sum of the stresses in each model.

The linear viscoelastic models in current use are the Kelvin and the Maxwell models. These models have been discussed in detail by Nair and Chang (65).

Linear viscoelastic models are the most widely used in bituminous pavement analysis because of their relative simplicity and the closeness with which they predict field behavior. Barksdale and others (9) have compared measured and computed responses using a linear viscoelastic model. They computed both elastic and permanent deflections for a 3-layer pavement system on the AASHO test road (96). The computed response was in close agreement with the measured response. In their concluding remarks, it was stated that the viscoelastic theory appeared to give a realistic approximation of the actual behavior of a bituminous pavement system.

Non-linear viscoelastic models only exist as theoretical tools. They have not been applied to the analysis of pavement structures because of the complexity of the theory, the difficulty in experimentally determining the material functions, and the problems associated with developing solutions to the non-linear boundary value problems (65).

Summary

The elastic theories used to analyze pavement material response are based on assumptions of ideal materials which do not exist in the field. Also, these theories require experimental determination of material functions. Because of the fact that experimental determinations are also subject to error, the elastic models do not give any realistic approximation of actual field behavior. Nevertheless, some of them do provide reasonably good tools for predicting the onset of plastic behavior. Even so, the closeness of prediction depends to a larger extent, on how well the theoretical assumptions simulate the field conditions. Because the materials of a flexible pavement system have time dependent stress-strain properties, due to consolidation, creep, and temperature effects, the viscoelastic approach appears to be an important improvement over the elastic methods for predicting performance parameters now recognized as relevant in the design and analysis of bituminous pavements.

Phenomenon of Rutting

Field and laboratory observations indicate different modes of rutting. Foster (29) has observed a situation in which high asphalt content mixes shoved out from under the path of traffic wheels and bulged up on the sides (lateral creep). Similarly, studies by Regal (80) indicated

a tendency for bituminous surfaces to rub and shove when constructed from aggregates having "humps" in their gradation. At a symposium on Pavement Evaluation, Hartronft (73) cited an example of decreases in density of stone base course materials between wheelpaths and referred to this as an apparent permanent loss of density. This situation may be due to lateral creep of material from beneath the wheelpaths to this location thus resulting in dilation of the material.

Wissa (30), and others (59) are of the opinion that pavement mixtures undergo densification under traffic. In a general discussion on the effects of load repetition of bituminous mixtures, Wissa remarked that, with repetitions of loads, strains to reach a maximum strength tend to decrease as densification occurs, i.e., densification tends to increase the stiffness of the bituminous mixture. In a detailed study of the performance of full-depth asphalt bases, Shook and others (88) found surface rutting to be related to the vertical compressive strain and the vertical compressive stress on the subgrade surface. Studies by Nabil (41) has confirmed this relationship. In his concluding remarks, Nabil noted that present technology is able to recommend criteria for precluding excessive rutting but is not developed enough to confidently predict the actual amount of rutting that might occur for any given design situation. Marks and Ford (57) have also studied the effect of density on surface performance of bituminous mixtures. In their field investigation, study cores obtained adjacent to initial reference cores indicated increased densities in the surface course materials ranging from 0.5 percent to 7.5 percent of Marshall Laboratory density. It was also found that the average rut depth increased with increases in the percent density change of the natural gravel mixtures used in the study.

Shoving or lateral displacement (lateral creep) and post-construction densification do not appear to be the only factors that contribute to rutting. Wear of surface materials can also contribute significantly to rutting as was reported by Britton (15). Evidence of pavement wear has also been observed in performance studies using studded tires (24).

Rut depths on high class pavements are usually very small (maximum values around 0.5 in. (1.27 cm), however, data from large scale road tests show that rutting on highway pavements can be substantial. Ramsey (79) has reported rut depths up to 1.8 in. (4.572 cm) on granular base course materials in Nebraska. The British full-scale design experiment (48) also shows rut depths exceeding 3.0 ins. (7.62 cm). Similarly, data from the AASHO road test (96) suggests excessive rut depths in the order of 4.0 ins. (10.16 cm).

Summary

Three major factors (relative to the bituminous bound layers) appear to contribute to rutting of flexible highway pavements. These factors include: 1) post-construction densification; 2) lateral creep of material from beneath the wheelpaths, and 3) attrition or errosion of surface materials under traffic. In addition densification (consolidation and/or shear failures in the non-bituminous bound base and subgrade materials can also influence the total amount of rutting. In a specific case, each of these factors may act singularly or in various combinations.

Mechanisms of Rutting

Densification

The mechanism of densification is best understood by considering the stress conditions occurring under the action of a moving load. When a wheel load moves past an element of material located beneath the surface of the pavement system, the element is subject to stress states similar to that shown in Fig. 4 (14). Consider a particular situation in which the moving load is at position A. If the surface frictional resistance were neglected, the orientation of the major and minor stresses acting on an element located under position B will be as shown by broken lines. As the load moves past position A towards position B, the orientation of the principal stresses gradually changes and finally assume the orientation indicated by the bold lines when the load reaches position B. That is, each element of material under the pavement surface is subject to a simultaneous build up of principal stresses (σ_1 and σ_3). As these stresses build up, a rotation of the principal stress axis occurs. The tendency of this rotation and stress build up is to, encourage reorientation of aggregate particles in the paving mixture, followed by degradation (if the stresses are large enough) and, finally, a decrease in void content or an increase in density. If the paving mixture is already at its maximum density, then dilation (increase in void ratio) will tend to take place.

The mechanism of densification may also be explained by any of the viscoelastic response models or systems consisting of a combination of elastic springs and dash pots. Representing the materials beneath the thin wearing surface by a viscoelastic medium and assuming no lateral

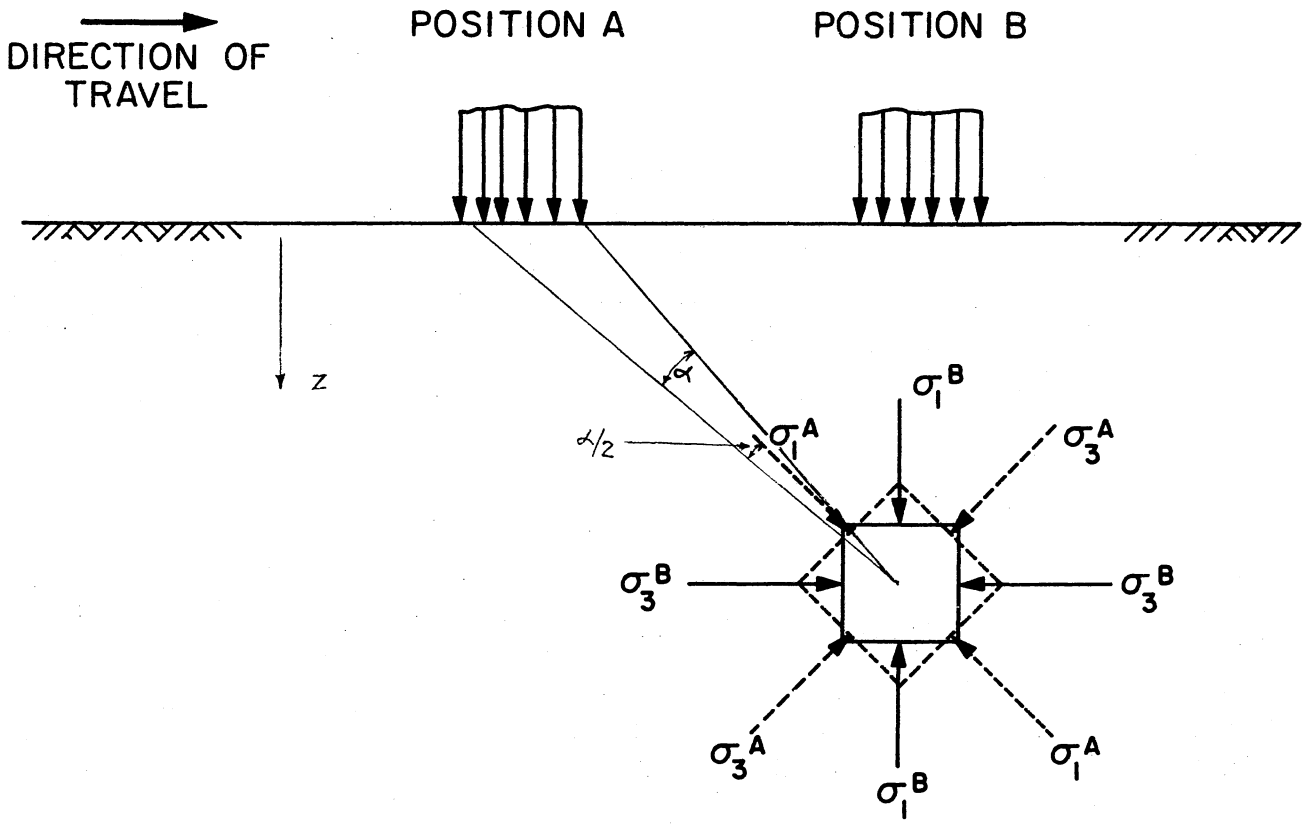

Figure 4. Rotation of Principal Stress Axes of an Element Under a Moving Load

escape of material occurs, it can be inferred that the unrecovered portion of deformations upon removal of the load, directly decreases the volume of the material, and is a measure of densification due to the applied load.

Densification can also occur as a result of temperature cycling. Ellis and others (22) have noticed significant increases in density of Marshall briquettes subject to temperature cycling. They attributed this type of densification to the behavior of the asphalt binder during heating and cooling. Asphalt cement increases in volume by approximately 3.0 percent over a 100^{o}F (37.7^{o}C) rise in temperature. Over the temperature range of the experiment, the asphalt binder was considered to have expanded in volume about twenty times more than the aggregate in the mixture. This expansion caused the binder material to flow into the air voids in the briquette. Upon cooling the asphalt cement contracted and pulled the aggregate particles closer together by the action of surface tension. This caused the air voids to decrease and the briquette to shrink. Their experimental data associated increasing densification with: 1) high absorptive aggregates, 2) low viscosity asphalt cement, and 3) high asphalt content. It is believed that this type of densification is not a contributing factor to pavement rutting. Nevertheless, thermal densification will develop large contraction stresses in the paving mixture.

Review of compressive stress distribution in materials under load reveals large stresses approaching or approximately equal to the contact pressure, in the surface (wearing) course. These stresses become smaller at greater depths Fig. 5a. This indicates greater densification in the surface layers. When the surface layers attain maximum densities no more

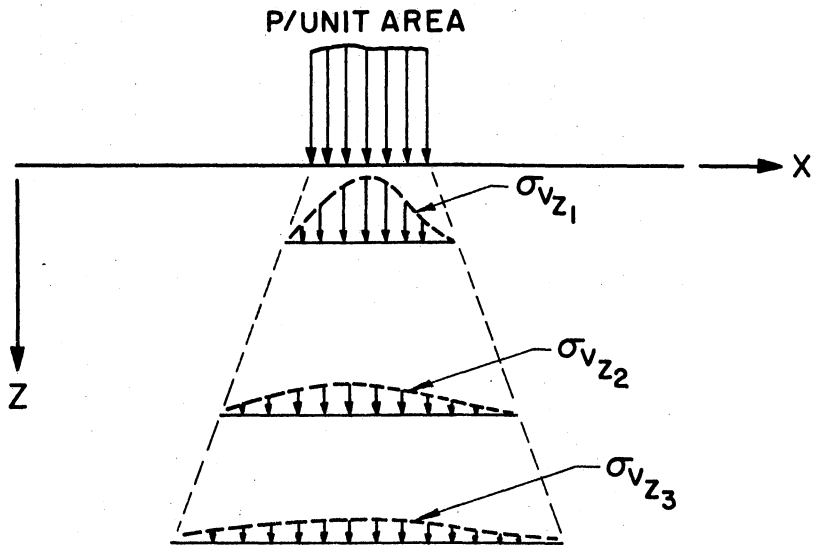

(a) DISTRIBUTION OF VERTICAL STRESSES

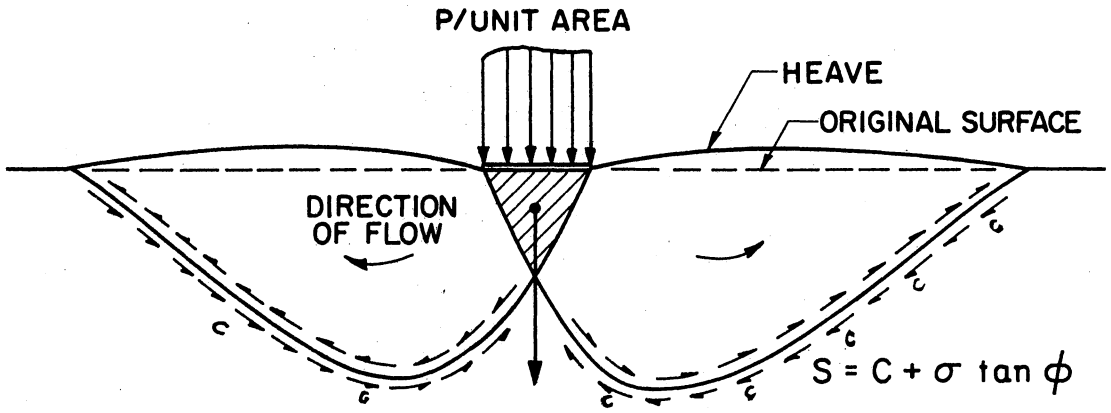

(b) SHEAR FAILURE

Figure 5. Behavior of Material Under Loaded Areas

densification can occur in these layers and any further densification will occur in the underlying layers. That is, densification in the pavement materials layers is cummulative.

The contribution of densification to rutting can be illustrated by considering a column of material defined by rigid boundaries at the sides and at the base (Fig. 6). Assume this column of material changes in volume from V_0 to V_1 as a result of the applied load P. The height H_0 of the column is reduced to H_1 and the density of the column of material is increased. The increase in density reduces the void content in the material. The percent change in void content can thus be shown to be directly proportional to loss in height of the column of material. That is, differential densification contributes directly to rutting on bituminous pavements.

Lateral Displacement

In addition to tensile and compressive stresses, the vertical compressive stress pulses acting on the pavement tend to induce shearing stresses in the pavement layers. The induced shearing stresses are resisted by the cohesive strength developed by the asphalt-aggregate interaction and the inter-particle frictional resistance developed in the compacted mixture. When the induced shearing stresses exceed the shearing strength of the mixture, plastic flow of the materials beneath the loaded area occurs (110). Lateral flow of materials from beneath the loaded area is evidenced by upheaval of surfaces adjacent to the loaded area (Fig. 5b).

In bituminous pavement structures, lateral creep may occur in the surface layer, base course, or in the subgrade soil. These modes of

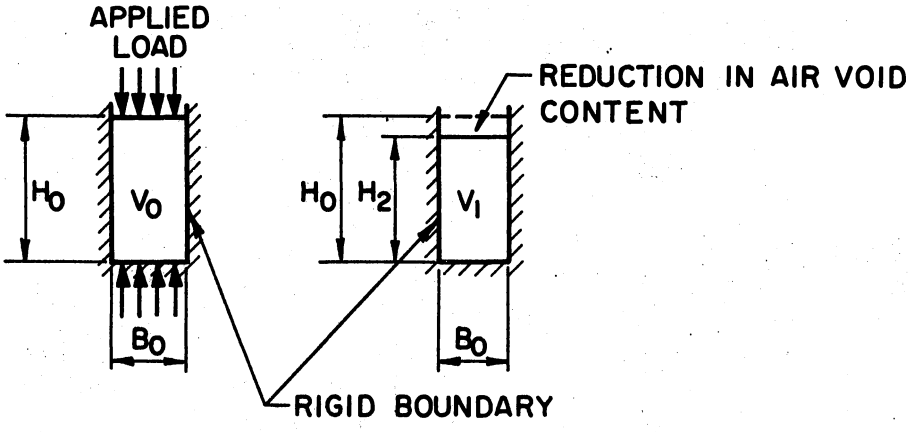

INCREASE IN PERCENT DENSITY $\propto$ DECREASE IN VOID CONTENT,

AND

$\propto$ PERCENT DECREASE IN SPECIMEN HEIGHT

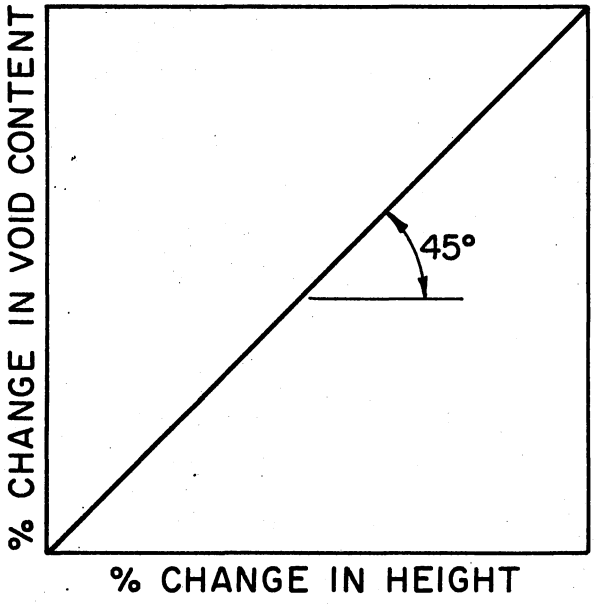

Figure 6. Effects of Densification on Layer Thickness

failure are illustrated in Figures 7, 8, and 9. Lateral creep will contribute to rutting, however, the amount of this contribution is difficult to determine. If an initial transverse profile graph of a new pavement surface was made prior to traffic use, then any subsequent upheaval of the surface adjacent to the wheelpaths could be measured. The amount of upheaval of the adjacent surfaces will provide an estimate of the rut depth resulting from lateral flow of material from beneath the wheelpath. Estimates obtained this way are highly approximate because of volumetric changes the pavement materials undergo in service, and the complex behavior of the subgrade soil. Nevertheless, lateral creep can occur in bituminous pavement structures (96) and upheaval of surfaces adjacent to the wheelpaths is a good indication of this phenomenon.

Surface Wear

Wear of pavement surfaces is due to frictional stresses developed at the tire-pavement interface as a result of resistance to rotation of the tire offered by the surface materials. It is a complicated phenomenon and depends on several factors including: The nature of vehicle tire, type of tread or stud, strength characteristics of the surface mixture, nature of traffic and environmental conditions. On bituminous pavements, the slippage stresses which the tire applies to the pavement surface tend to polish, fracture loosen and pulverize the matrix.

According to Keyser (43, 44) bituminous surfaces are worn by a combination of three processes: 1) pulverization, cutting and attrition of the surface matrix; 2) fragmentation and loosening of the mineral aggregate; and 3) loosening and dislodging of the aggregate particles. Keyser

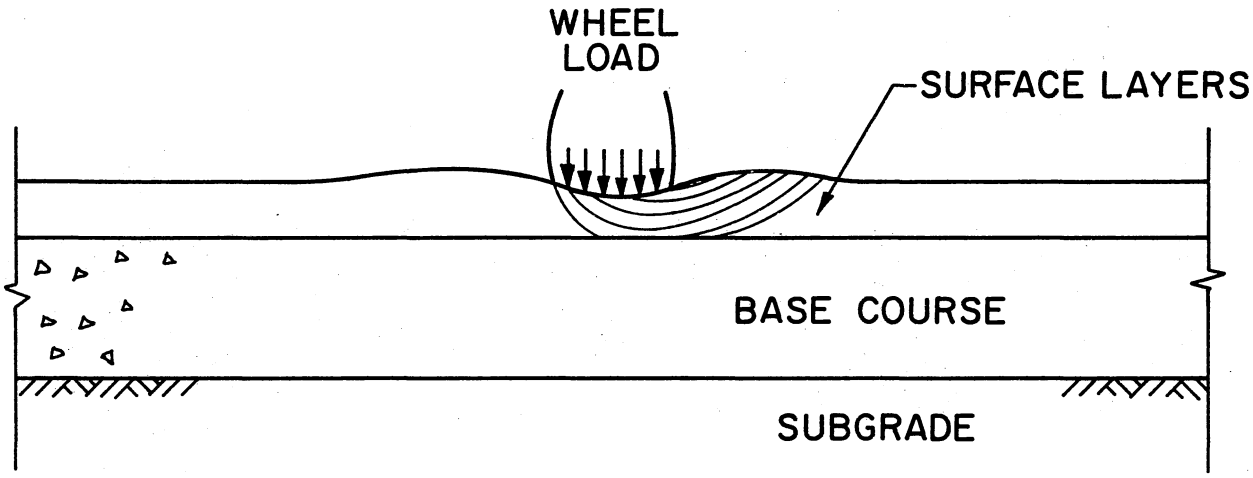

Figure 7. Lateral Creep (Shear Failure) in Surface Layers

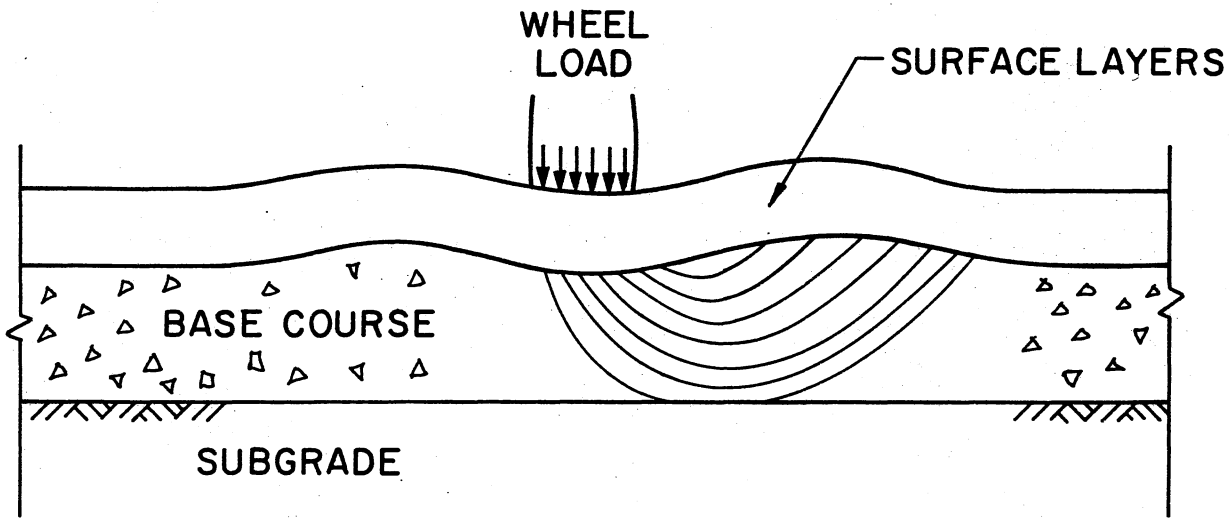

Figure 8. Lateral Creep (Shear Failure) in Base Course

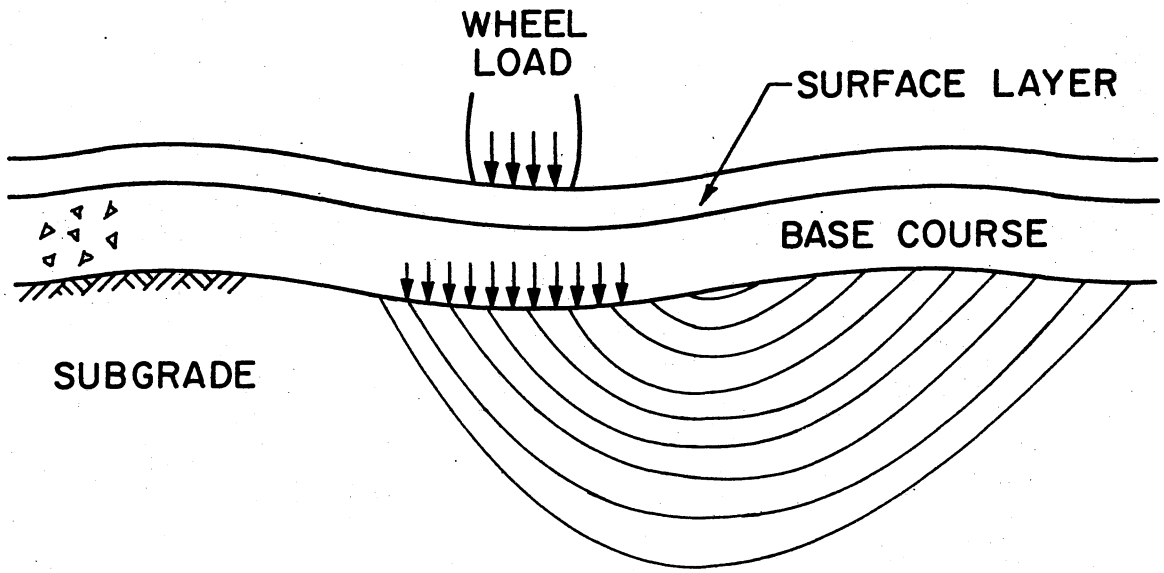

Figure 9. Lateral Creep (Shear Failure) in Subgrade Soil

performed detailed laboratory and field studies using studded tires and explained the mechanism of wear as follows:

a) The surface matrix wore rapidly at the beginning of the test. The rate of wear of the aggregates which was lower than that of the mortar was also higher at the beginning. On surfaces incorporating hard (lamprophyre) aggregates, the mortar and the sharp edges of aggregates wore rapidly until the asperity or the projection of the coarse aggregate was approximately equal to the stud protrusion. At this stage, the tire and the studs were chiefly supported by the rounded surface aggregate particles and the rate of wear of the mortar remained constant and followed the rate of wear of the coarse aggregates. On limestone surfaces, the nature of wear depended on the relative wear resistance of the constituent coarse aggregate and the mortar. Where the aggregate was more resistant, the rate of wear stabilized when the coarse aggregate had worn to a constant average protrusion value less than the stud protrusion. At that stage, the tire and studs were supported partly by the aggregate and partly by the mortar. The surface of the stone particles was much rougher than that obtained on the lamprophyre aggregates and was not rounded.

b) When the exposed aggregates reached a depth of embedment of about .05 in. (1.20 cm), the aggregates wore out rapidly by fragmentation, loosening, and dislodgement.

c) The powder produced by the wear of the lamprophyre mixture had a fairly uniform size, with particles ranging between 0.03 mm and 0.09 mm. For the limestone mixtures the size of the powder particles was between 0.02 mm and 0.15 mm. The difference in sizes was attributed to the difference in hardness and structure of the two aggregates. Limestone,

being a soft crystalline aggregate was pulverized and fragmented more easily than the hard armorphous lamprophyre aggregates.

Effects of Environment. Wear was lowest at near freezing temperatures and increased with an increasing or decreasing temperatures. This behavior of the wear versus temperature curve was attributed to changes in both rigidity of the rubber tires supporting the studs and the stiffness of the bituminous mixture with temperature. The hardness of the tires increased at low temperatures and decreased at high temperatures, so the force required to push the stud into the tire to become flush with the pavement surface changed with changes in temperature. At low temperatures the unit pressure was higher thus causing more wear. The asphalt cement, on the other hand, behaves as a viscoelastic, semi-solid material with less cohesion at 70°F (21.1°C) than at lower temperatures. When the stud comes in contact with the mixture, it penetrates deeper into it, displacing the aggregate particles thus producing more wear by shear and dislodgement. At low temperatures, the asphalt becomes brittle. So during the indentation process the matrix was partly crushed and chipped by fracture thus producing a higher rate of wear.

When the test track was kept wet, the rate of wear on the lamprophyre mixture doubled, whereas, the wear ratio between the wet and dry conditions for mixtures incorporating limestone aggregates ranged from 1.3 to 1.7. The increased rate of wear was attributed to loss in adhesion and loss in hardness and strength of the aggregates and the matrix due to absorption of water by the surface particles.

For pavements receiving all year round traffic with standard automobile tires, surface wear takes place at very slow rates, and magnitudes of wear are usually very small. In the case of traffic using studded

tires during the winter months, however, wear takes place rapidly and magnitudes become relatively large in short periods of time depending on the wear-resistance of the surface materials. Preus (78) has observed depths of wear on both bituminous and portland cement concrete pavements for traffic using studded tires and for traffic using standard, non-studded tires. On one portland cement pavement the depth of wear was 0.32 after estimated 1.7 million studded tire passes. The depth of wear after 2.3 million studded tire passes on the same pavement was 0.4 in. (1.01 cm). The depths were measured under a 10.0 ft. straight edge, and the midpoint wear depth was 0.1 in. (2.54 cm). On a bituminous surface incorporating gravel aggregates the wear depth was 0.41 in. (1.02 cm) after estimated 1.0 million studded tire passes (after 6 winters). The surface wear effect on texture was much the same as that of the portland cement concrete. In all cases, the wear pattern gradually widened as a result of lateral shift of traffic to avoid driving in the roughened wheelpaths.

Preus's laboratory study of wear using non-studded tires showed 0.008 in. (0.02 cm) wear depth on a bituminous surface compared with 0.006 in. (0.015 cm) on a portland cement pavement, after 4.0 million tire passes. Under field conditions, however, greater depths of wear can be expected on bituminous surfaces. This increased wear is due to loss in adhesion and strength of the surface mixture resulting from the presence of water and changes in temperature.

CHAPTER III

EXPERIMENTAL DESIGN

By definition, the terminology "design of experiment" refers to: the specification of treatments whose effects are to be investigated, the selection and the arrangement of the experimental units to which specific treatments are to be applied, and the specification of measurements to be made on each experimental unit (26).

Initially, it was planned to use a purely statistical approach in this investigation. However, as in the case of many other field research programs, existing limitations required some departure from the classical statistical approach. Some of these limitations pertained to: 1) safety of the research personnel on high-speed highways, 2) time restrictions related to completing certain phases of the study within an established time frame, 3) existence of a particular base course material at an appropriate experimental design location on the Oklahoma interstate highway system, and 4) precise transverse location of the wheelpaths in the respective traffic lanes.

For this investigation, types of base course materials were referred to as "treatments". Test sites were selected on flexible pavement sections of interstate highways constructed on four types of base course materials. These base course materials are the four major types commonly specified by the Oklahoma Department of Highways: Hot Mix Sand Asphalt

(HMSA), Soil-Cement Base (SCB), Black Base (BB), and Stabilized Aggregate Base Course (SABC) (92).

The individual test sites were considered as "experimental units" and were picked from locations on the two interstate highways in Oklahoma. These highways, Interstate 35 (north-south) and Interstate 40 (east-west), roughly divide the state into four quadrants. To be able to detect possible regional differences resulting from climatic variations and the subsequent differences in subgrade moisture contents, variations in subgrade soil types and differences in traffic characteristics, it was thought that the "completely randomized block design" (26) would be most effective. However, the field limitations mentioned above did not permit use of the randomized block design. Tentative selection of the test sites (experimental units) was based on performance data obtained from the research section of the Oklahoma Department of Highways. This information indicated the design average daily traffic volumes (design ADT) of the two interstate highways and the construction completion dates and existing paving materials of respective pavement sections on these highways. The data also included Benkelman beam deflections and "A-frame" rut depth measurements at approximately 176.0 yd. (160 meter) intervals. From this performance data, possible test sites were selected, making sure that they were evenly distributed over the entire state.

Preliminary site visits were made to these test sites to: 1) evaluate the extent of sight distance available to on-coming motor vehicles, 2) check the vertical and the horizontal alinement, 3) check for the existence of the indicated type of base course materials, 4) visually examine and rate the surface characteristics including estimates of the extent of rutting, 5) study the general geometric design characteristics in the

vicinity and, 6) mark out suitable test sites as possible candidates for final selection. Whenever a site was found to lie on curved section (horizontal or vertical) or near interchanges, a substitute test site in the same vicinity was picked. Each tentative test site was permanently identified by attaching a 4.0" x 6.0" orange painted sheet metal marker to the right-of-way fence. For the test sites on Interstate 35, the markers were located at measured odometer distances north of the appropriate south boundary line of the county in which the test site was located. If the location of the site happened to be in the southbound traffic lanes, the distance was measured in the northbound traffic lanes. The location was temporarily identified in the northbound lane and then projected transversely to the west right-of-way fence adjacent to the southbound lanes, where it was permanently marked as described above. The sites on Interstate 40 were similarly identified. The only exception was that all distances were measured east of the west county line in the eastbound traffic lane.

In order to assure the safety of the study personnel on these high speed highways, the governing criteria for site selection was that the test sites had to lie on straight tangent sections. This was needed so that drivers of on-coming vehicles could be given sufficient distance to effectively perceive and react safely to the changed road conditions caused by the study operations. A minimum of one-half mile (804 meters) of unabstructed sight distance was considered necessary to meet this safety requirement.

To keep the volume of experimental data within the limits practical to the planned time schedule, a total of sixteen test sites meeting the aforementioned requirements were finally selected for investigation.

These included four test sites, comprising two minimum and two maximum rut depth sections of pavements constructed on each of the four types of base course materials (HMSA, SCB, SABC, and BB). The resulting allocation of base course materials (treatments) to the test sites (experimental units), though not completely randomized, was considered as a completely randomized experiment (26, 89) instead of the intended randomized block design. In other words, eventhough the effects of regional differences on performance were somehow allowed for, the final site selection procedure did not permit direct classical statistical investigation of the influence of regional differences on the performance of the individual types of base course materials.

The data collected from both the field and the laboratory portions of this investigation are referred to as "measurements" in the above statistical definition of "design of experiment". Specification of types of measurements to be made on the test sites were dictated by the prevailing field conditions and lack of desirable information on individual test sites. Absence of initial in-place densities of the asphalt-bound paving materials at the selected test sites required the determination of percent densities instead of the existing bulk densities alone. To obtain the percent density values, two other laboratory values were required: the in-place bulk specific gravities and the maximum theoretical specific gravities of the existing pavement materials (56). Standard procedures for measurement of the theoretical specific gravity were reviewed in terms of their relative advantages and Rice's Method (91) was found to be the most appropriate. This procedure, in turn, required that "undisturbed" samples (47) be taken from the layered system at appropriate points across

the pavement surface. Four inch diameter core specimens were considered convenient.

It was also decided that a nuclear technique (19) be employed to measure the in-place bulk densities in addition to the laboratory methods of measurement of bulk specific gravities of the core samples. The major reason for this additional field measurement was to determine, if possible, a correlation between the nuclear measurements and the conventional laboratory measurements. If good correlation were found, the destructive laboratory procedure could be replaced by the faster non-destructive nuclear method for all future research or field testing involving measurement of in-place bulk densities.

In order that the pavement surface configuration could be clearly observed, and to accurately measure the rut depths in the wheelpaths and possible heaves immediately outside the wheelpaths, it was decided that continuous plots of the transverse profiles at the individual test sections be made. Most of the existing profilometers or road meters (71) were found to be incapable of producing the required continuous tracings. Furthermore, the sizes of those which could possibly be modified to do the job made them unfeasible, so a portable transverse profile gage was developed for this research investigation. In addition to plotting the transverse profiles, the cross-slopes of the pavement surface could also be determined with this equipment.

Some means of measuring or estimating the amount of attrition in the wheelpaths was desirable. It was found that a qualitative estimate of attrition could be made by means of stereo-photography (84, 85). Stereo-pairs of 35 mm photographs taken at appropriate transverse points on the pavement surface were required. Comparison of projections of the surface

aggregates in the wheelpaths with those outside the wheelpaths would provide estimates of relative attrition or frictional wear of surfaces in the wheelpaths.

For comparative purposes, two other sets of data were needed. These were: 1) estimates of the in-service pavement age, and 2) pavement surface condition rating (qualitative) (105). The final field layout of test points at a given test site is illustrated in Fig. 10. The geographical locations of the test sites selected for this study are described in Appendix A.

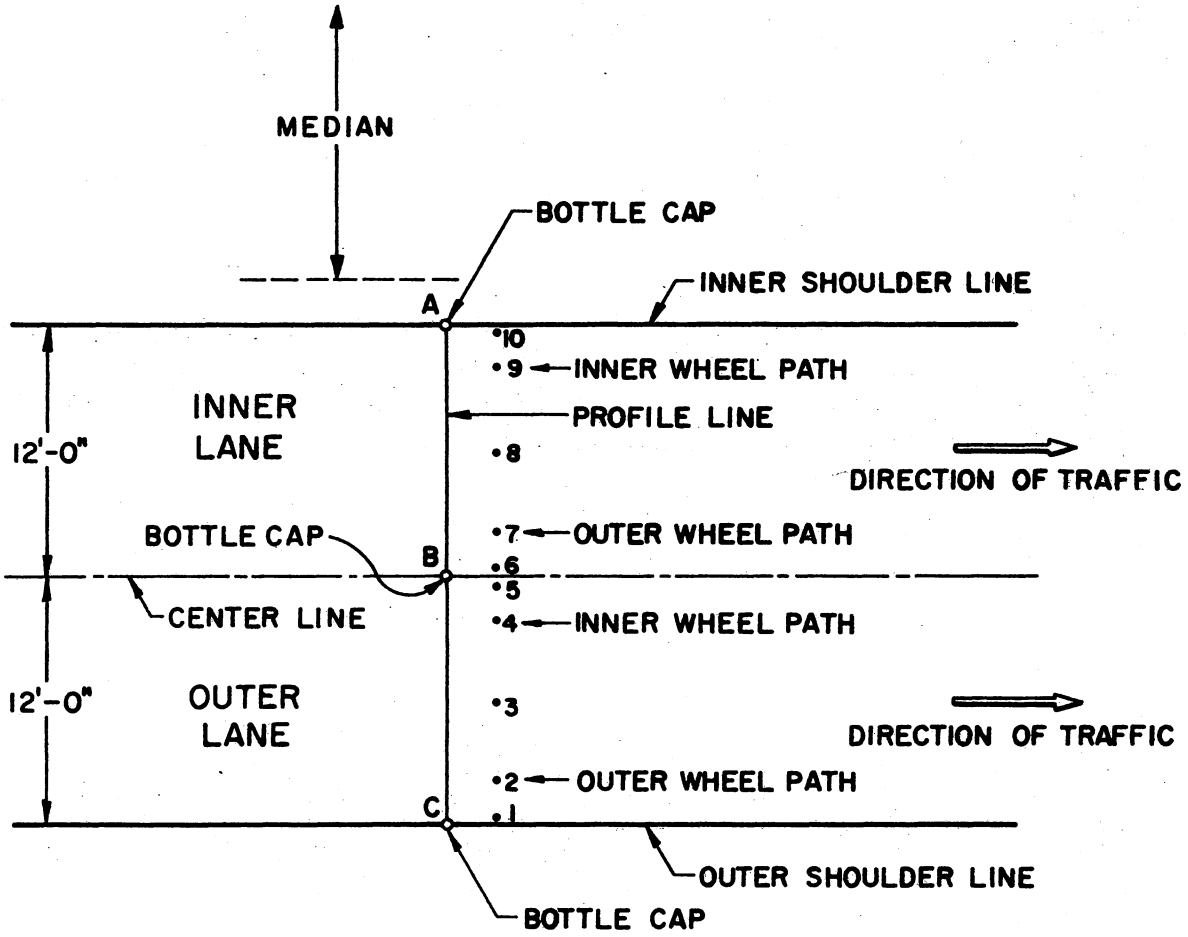

Figure 10. Layout of Transverse Test Points

CHAPTER IV

DEVELOPMENT OF TRANSVERSE PROFILE GAGE AND EQUIPMENT

A continuous transverse profile tracing apparatus, the "transverse profile gage", was developed for this and future research because the existing profilometers were designed primarily for longitudinal profile studies. The few that were designed for transverse profiles, on the other hand, were too large to handle and cost more than small to medium sized research programs could afford. Furthermore, successful operation of these equipments required trained personnel and special instrument vehicles.

The portable types including the "A-frame" and the electronic rut depth gage (96), for example, are only capable of producing point estimates of rut depths. Also, their operational procedures require knowledge of the transverse location of the wheelpath whose rut depth is to be estimated, and their accuracy depends, to a large extent, on the curvature or configuration of the rut. Because these variables are usually unknown, measurements made with this equipment are only approximate and can be highly erroneous, making them unsuitable for research studies which require reasonably accurate measurements of rut depths or upheaval of pavement surfaces.

The transverse profile gage was developed to provide a portable and accurate means of obtaining continuous transverse profile graphs. In

addition to the measurement of rut depths and heaves outside of the wheelpaths, the plotted transverse profile graphs provide permanent records of these conditions at a specific time in the service life of a pavement and can be used in future studies. The equipment could also be employed to check the transverse profile tolerances usually specified in the construction of highway pavements.

Transverse Profile Gage

Essentially, the transverse profile gage consists of: 1) a straight edge, 2) a cross-slope device, 3) a trolley system, 4) an "X-Y" recorder, and 5) electrical installation equipment.

Straight Edge

The straight edge was designed to serve as a guide rail and a datum plane for the trolley system. The major design requirements were: 1) that the unit be subject to a minimum amount of temperature distortion, 2) that its weight be kept to a minimum to facilitate transportation to and handling at the site, 3) that its length be sufficient to span, at least, one traffic lane of an interstate highway without picking up vibrations from high speed vehicles in the adjacent traffic lane, and 4) that its supports be adjustable in height to provide means of increasing or decreasing the relative elevations of the datum plane at the support points.

Temperature distortion was a major problem in the selection of a suitable member. In addition to the unavoidable expansion and contraction, a metallic section undergoes twisting and warping when subjected to sudden temperature change. These distortions could add to the factory

or mill imperfections which alone might be greater than was desirable. For example, a standard American wide flange steel section could come from a mill with an "out-of-square" of 0.25 in. at any cross-section. Factory tolerances and temperature suseptibility of similar aluminum-alloy structural sections are equally high, if not worse.

The weight of the member was also a problem. The unit had to be transported to and from the site and it also has to be handled several times at the site. Under the expected conditions, it was considered that any member that was heavier than one person could conveniently handle would create both handling and safety problems. Also, the weight of the member would encourage flexural deflections. For this study, flexural deflections exceeding 0.05 in. (0.127 cm) were considered excessive.

To provide a member that was less subject to temperature distortion and yet light in weight, the straight edge was made from magnesium-alloy carpenter's framing levels. Two standard 6.50 ft. long carpenters levels (1.0 in. wide x 2.25 in. deep I-section) were spliced together on the web with two 1.5 in. wide x 8.0 in. long aluminum-alloy plates, 0.3125 in. (0.794 cm) thick to provide continuity. The spliced connection was bolted along the mid-depth of the web with four 0.25 in. (0.635 cm) diameter bolts so the built-up member could be taken apart by removing two bolts for transportation to and from the site. The built-up member had a finished length of 13.0 ft. (3.96 cm). The member was also bracketed at its mid-length with a dismountable heavy gage steel bracket (38 in. long) to provide the desired rigidity and to provide a means of support at the mid-span (Fig. 11).

The straight edge was supported at the ends and at the center. The end supports utilized 12.0 in. lengths of standard 10.0 in. x 2.5 in.

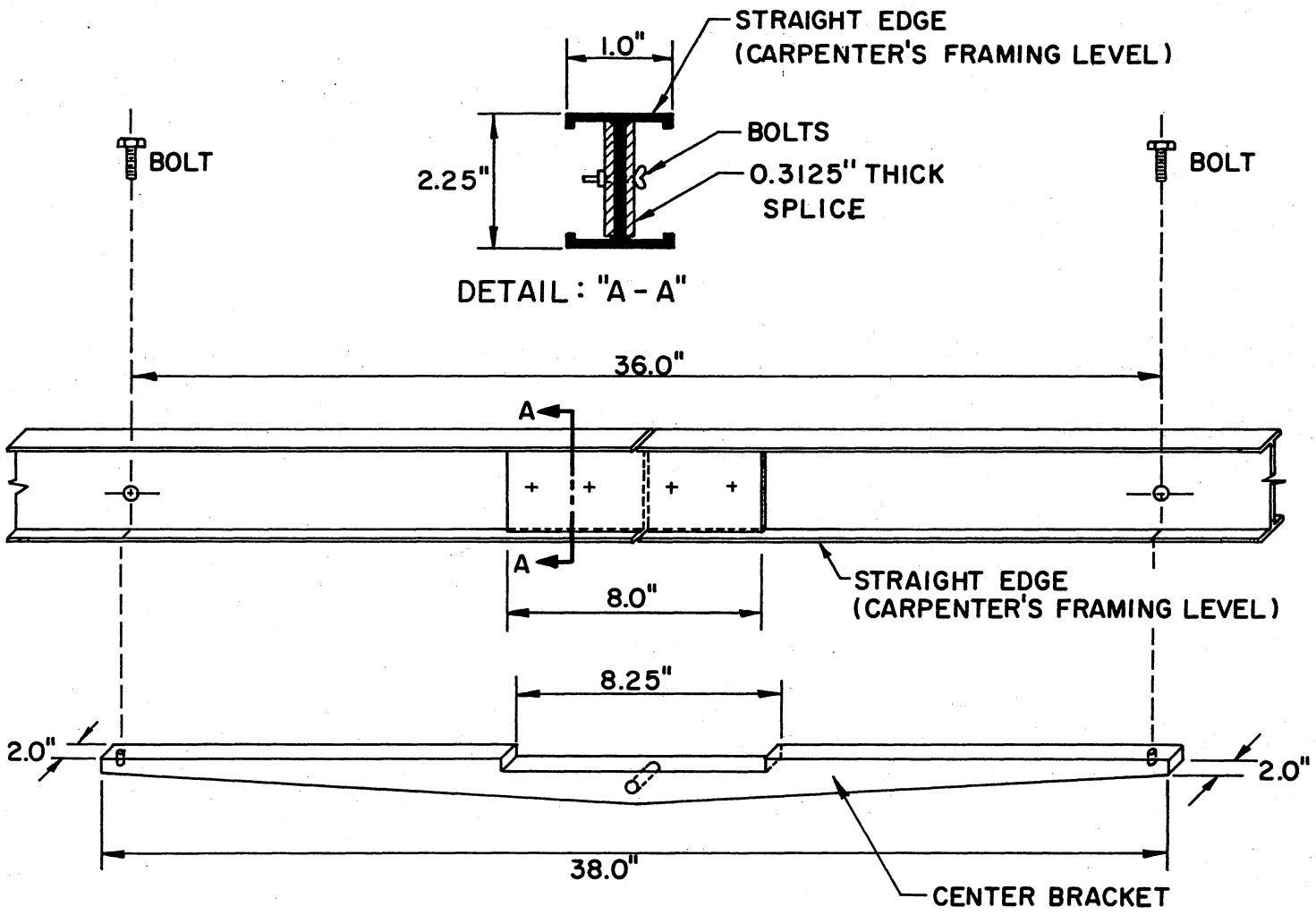

Figure 11. Fabrication of Straight Edge

(25.4 cm x 6.35 cm) structural steel channel sections as base plate which were supported on three leveling screws. These screws were 0.75 in. (1.905 cm) diameter bolts, 3.0 in (7.62 cm) long, with spherically shaped ends so the height of the base plate from the pavement surface could be varied and the entire base leveled by adjusting the screws. The stem of the end support system utilized a standard 2.0 in. x 2.0 in. (5.08 cm x 5.08 cm) structural steel angle 12.0 in (30.48 cm) long which was centered and welded at its lower end to the side of the base plate such that the stem stood vertically when the base plate was level. A 0.5 in. dia. x 3.0 in. long (1.27 cm x 7.62 cm) steel bolt was screwed to the stem to provide a horizontal abutment for the straight edge (Fig. 12). The straight edge was fastened to the face of the stem by a 0.5 in. (1.27 cm) diameter bolt.

The base plate for the center support system was built from three pieces of 0.5 in (1.27 cm) thick steel plates and one piece of a standard 8.0 in. x 6.0 in. (20.32 cm x 15.24 cm) structural steel T-section as shown in Fig. 12. The threaded steel rod was bolted at its lower end to the horizontal leg of the T-section to form a vertical shaft which supported the center bracket of the straight edge. A brass nut, bevel-pointed at the contact end, provided a bearing surface for the bracket. The brass nut also provided a means of adjusting the elevation of the straight edge at this point. A second brass nut firmly held the bracket at a desired elevation when tightened.

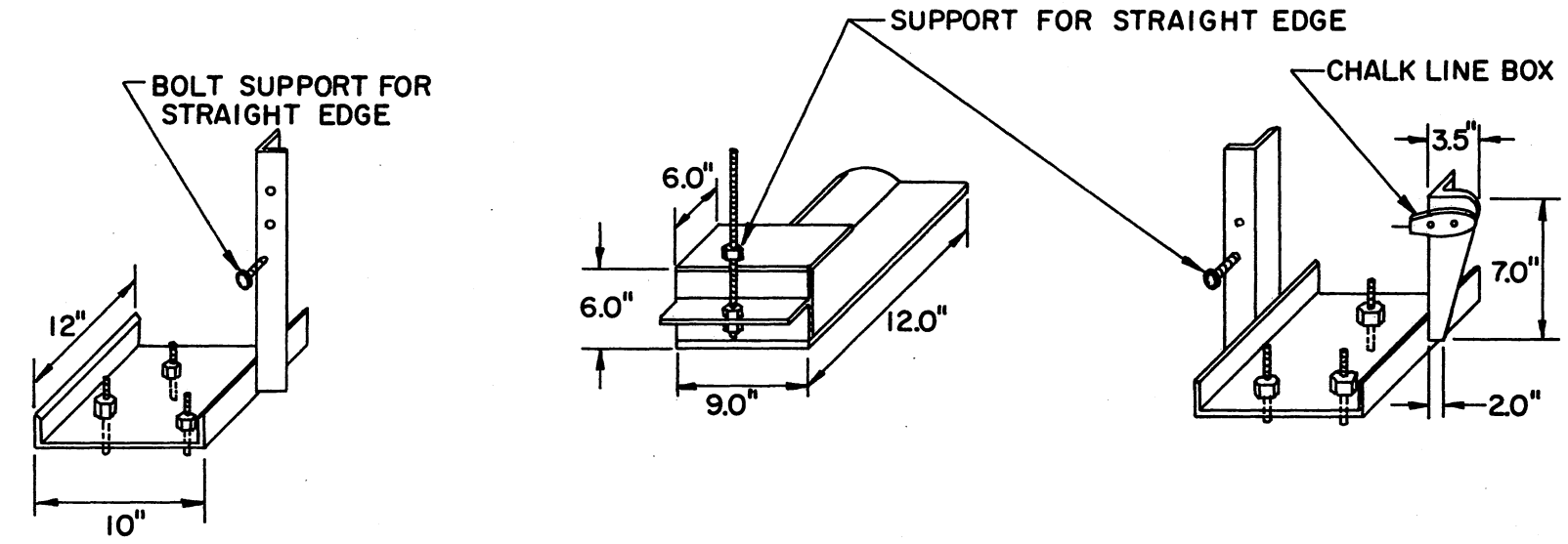

Figure 12. Straight Edge Support System

Cross-Slope Device

This is a simple accessory that was attached to the straight edge to estimate the average cross-slope of the pavement surface for each traffic lane of the highway.

A selected 15.0 in. (38.1 cm) length was cut from a standard 1.0 in. x 1.0 in. (2.54 cm x 2.54 cm) extruded aluminum-alloy angle. One leg (vertical) of the member was notched at a distance of 1.0 in. (2.54 cm) from one end. The other leg (horizontal) was also notched at a distance of 12.0 in. (30.48 cm) from the same end. The vertical leg was pivotted to the face of the stem of one support of the straight edge by bolting through the notch such that the angle would lie flat on the top surface of the straight edge when freed to do so. A dial gage with thousandths of inch graduations was attached to the web of the straight edge (by a bolt) at a distance of 12.0 in. (30.48 cm) from the end of the straight edge so that the neck of the dial gage shaft would freely slide into the notch cut through the horizontal leg of the angle section. A torpedo type spirit level was placed on the top surface of the horizontal leg to complete the fabrication of the device.

To measure the average cross-slope of a highway pavement, the straight edge was first set up transversely across the pavement so that the height of the top flange (straight edge) above the pavement surface was equal at the two end support points. Any mid-span deflection of the straight edge was removed by adjusting the height of the center support (a detailed procedure for setting up the profile gage is discussed later). The aluminum angle was adjusted to lie flat on the top of the straight edge. This position established the datum line parallel to a line joining the pavement surface at the end support points. The dial gage was

set to zero and the free end of the aluminum angle was raised vertically until the bubble in the spirit level moved to a level position. The observed dial gage reading gives the average cross-slope of the pavement surface in inches per foot.

The Trolley System

This portion of the transverse profile gage consists of: 1) a 15-turn, 2-ohm Helipot helical potentiometer, 2) a 0.5 in. dia. x 4.75 in. long (1.27 cm x 12.06 cm) 2-ohm linear potentiometer with 1.5 in. (3.81 cm) travel, 3) 5.0 in. (12.70 cm) diameter teflon actuating wheel, 4) four 1.5 in. dia. x 2.5 in. long (3.81 cm x 6.35 cm) nylon rail track wheels, and 5) a 9.0 in. x 12.0 in. (22.86 cm x 30.48 cm) aluminum suspension plate 0.5 in. (1.27 cm) thick. Functionally, the helical potentometer scales the transverse displacements while the vertical potentometer gages the vertical displacements of the actuating wheel (Fig. 13).

The rail track wheels were cut from a 1.75 in. diameter nylon rod and machined so that the cylindrical web would freely track along the flanges of the straight edge (Fig. 14). The four track wheels were bolted along their cylindrical axes to the upper portion of the steel suspension plate. The two rows (upper and lower) of track wheels were centered to freely fit the straight edge, as explained above, and to provide a smooth ride along the entire span of the straight edge.

The actuating wheel was cut from 0.75 in. (1.91 cm) thick teflon sheet. The outer circumference was slightly crowned and grooved. A 0.1875 in. diameter circular rubber ring was placed in the groove on the outer circumference of the wheel to provide for a smoother ride and to minimize permanent circumferential deformations on the relatively plastic

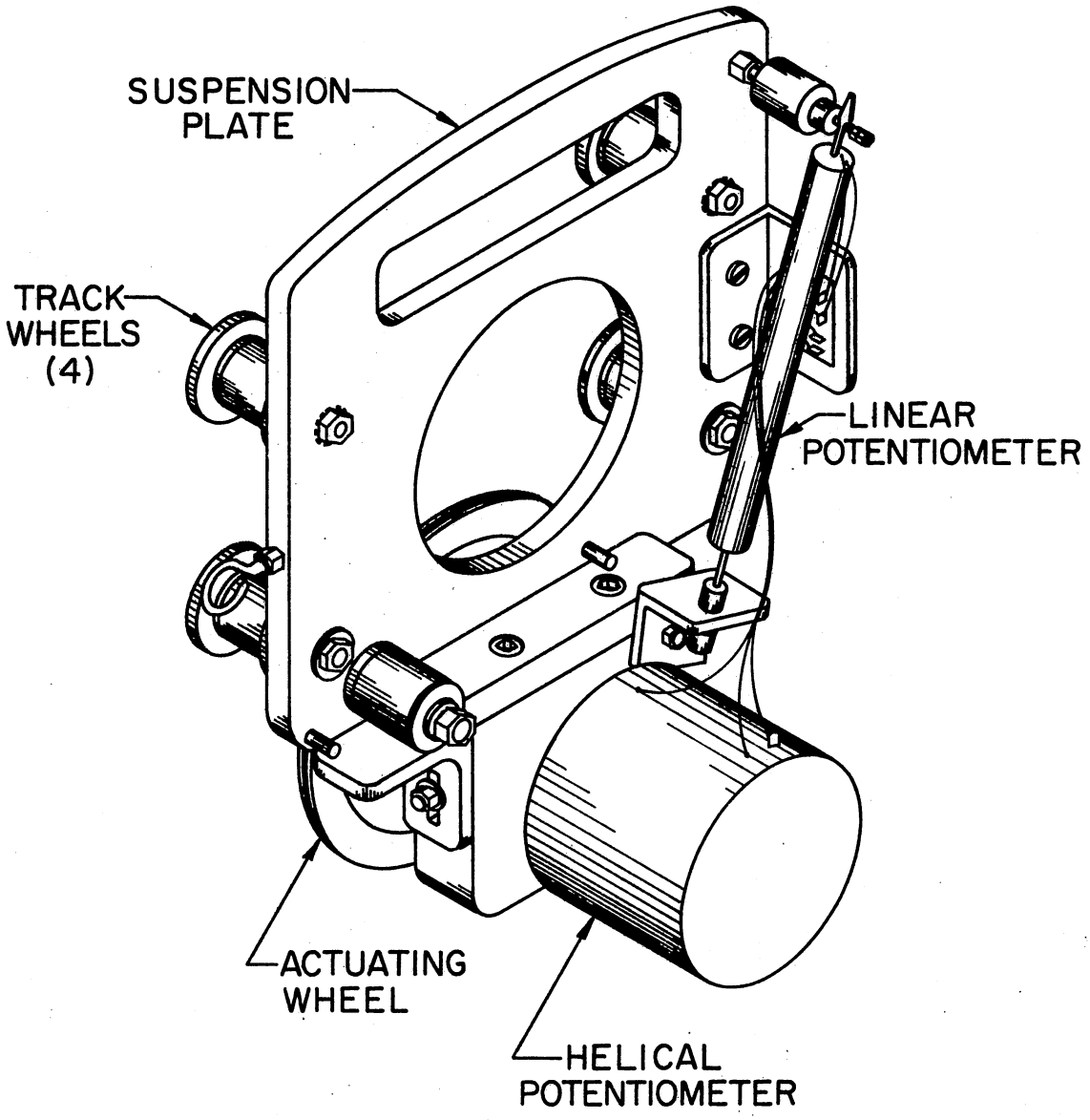

BACK VIEW

Figure 13. Transverse Profile Gage: Trolley Unit

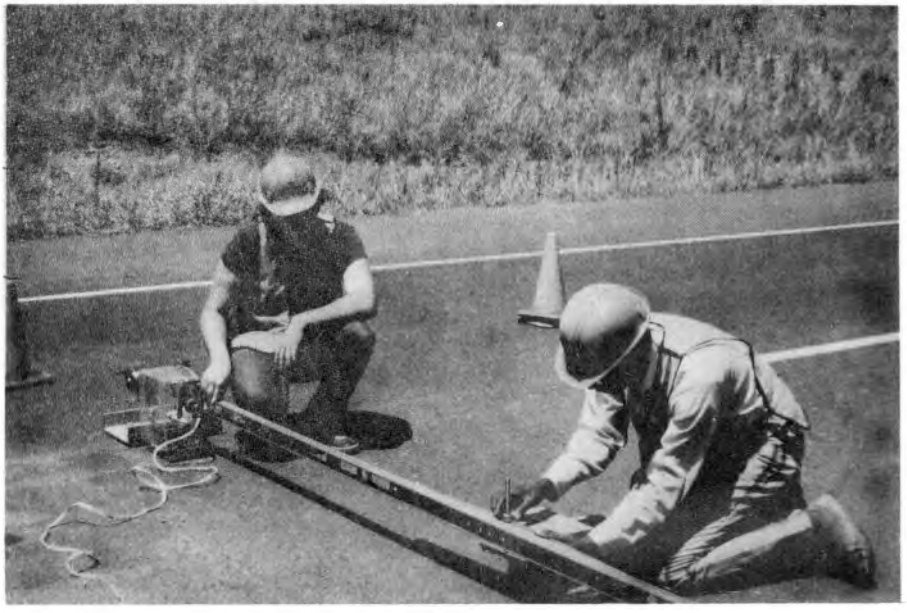

Figure 14. Straight Edge and Trolley Unit--(Photo.)

teflon wheel. Also, the rubber ring could easily be replaced without having to machine a new actuating wheel should excessive wear occur or the rubber material become fatigued.

The mounting ring on the shaft of the helical potentiometer was fitted to an opening cut at the centroid of the actuating wheel. The protruding end of the potentiometer shaft was bolted to one end of a pivot arm the other end of which was hinged to the aluminum suspension plate. There was sufficient tolerance at the hinged connection for free rotation of the wheel system about this point. The wheel system was sufficiently mass-weighted (5 lbs. approximately) to keep the actuating wheel in continuous contact with the traveled surface.

The vertical potentiometer was similarly mounted by attaching one end to the suspension plate and the other to the axle of the actuating wheel such that the stem of the potentiometer remained approximately vertical when the shaft of the potentiometer was at its midpoint of travel. This was designated as the datum for the vertical potentiometer so that both positive (subsidence) and negative (upheaval) deformations could be measured. The sensitive portions (the potentiometers) of the trolley system were shielded with a plexiglass cover attached to the suspension plate.

A small reel of fine copper cable was bolted onto one end support for the straight edge and the end of the cable was hooked to the aluminum suspension plate as shown in Fig. 13. The trolley could be manually cranked in one direction at a fairly uniform speed from one end of the straight edge to the other. In this way, induced structural vibrations in the straight edge could be minimized and undue deflections that might result from "push loads" on the trolley system eliminated.

Electrical Installation System

Fig. 15, shows a diagramatic sketch of the electrical installation system which was employed to provide a source of electrical power to the trolley system and to the "X-Y" recording equipment. Using a standard automobile battery cable, electrical current from a 12 volt pickup battery was passed through a safety switch and through a low resistance relay switch system to the 200 watt/115 volt D.C. to A.C. inverter. The inverter supplied the appropriate alternating current (AC) to the Hewlett Packard "X-Y" recorder. The potentiometers used direct current from the storage battery. Both the input to and the output from the potentiometers were passed through an input-output socket unit which was attached to the trolley system. In this fashion, the number and lengths of the electrical leads could be minimized and the displacement output leads from the potentiometers to the "X-Y" recorder pulled together into a single 6-wire conductor cable.

The negative to ground (vehicle chasis) system of electrical installation was adopted. The equipment power switch which was attached to the dash of the pickup was installed on the electrically negative conductor. This was done because the size of the electrically positive conductor (battery cable) would not permit the installation of the standard power switch on the positive conductor. The low resistance electrical power relay switch system was installed on the positive conductor to serve as a circuit breaker, i.e., electrical current from the storage battery would flow through the installation system only when the equipment power switch were turned to the "ON" position. If the positive conductor had been directly connected to the storage battery, the electrical circuit would be complete whenever the bare end of the positive conductor

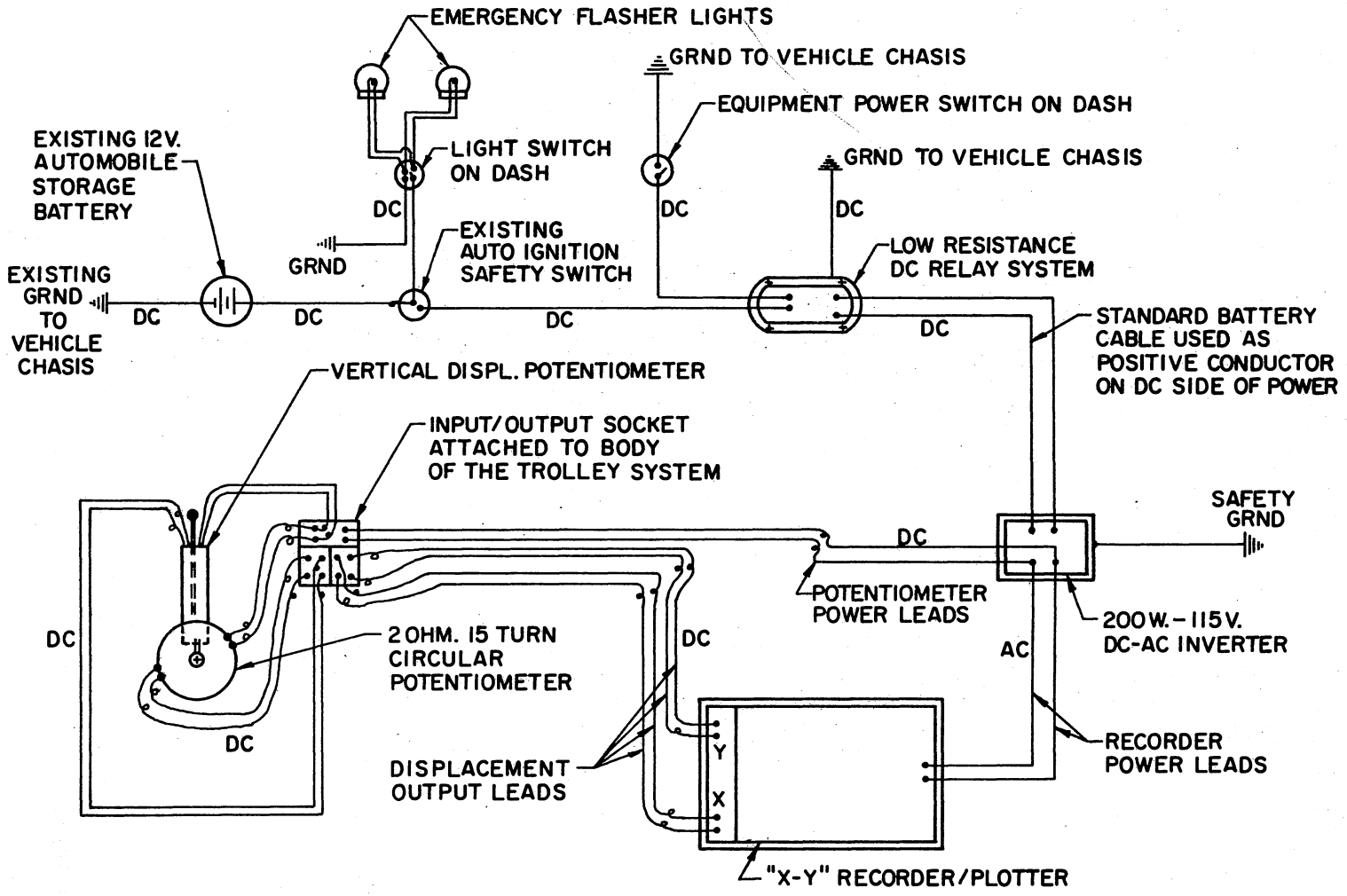

Figure 15. Electrical Installation Diagram

contacted any metallic part (body) of the vehicle, a condition that would create a serious fire hazard. A second safety provision was built into the system by passing the positive conductor cable through the vehicle's ignition safety switch system. A third safety provision consisted of grounding the inverter to take care of probable stagnant electrical power on this unit.

Fig. 15 also shows the electrical circuit diagram employed to power the emergency flasher lights which were utilized to provide additional warning to on-coming vehicular traffic of the restrictions created by the study operations. The detachable type dome flasher lights with magnetic base were placed on the cab of the pickup when in use. The complete set up of the transverse profile gage including the electrical installation system is shown in Fig. 14.

Calibration of the Transverse Profile Gage

Trolley Unit

The first set of tests made on the performance of the profile gage were those involving linearity and reproducibility of results. A parking lot on the campus of Oklahoma State University (OSU) which had some rutted areas, was selected for the preliminary testing. Having obtained permission from the OSU, Department of Safety and Security, a section of this parking lot was blocked to traffic and the profile gage was set up in this location.

Helical Potentiometer. Initially, a plot of the pavement surface was made so that the surface characteristics could be studied and the suitability of the location for calibration purposes evaluated. A fine chalk line was then drawn along the path of the gage actuating wheel.

Using a steel tape, distances of 1, 3, 6, 9, and 11 feet were measured from the starting point and marked off along the chalk line of the pavement. A trial scale was selected on the "X-Y" recording equipment. The trolley unit was then reeled along the measured path. The recorded distances were compared with the measured distances traversed. This process was repeated numerous times using different "X-Y" recorder scales. A high degree of accuracy and reproducibility of the profile tracings was observed in these trials. Subsequently, a horizontal scale of 0.5 volts/in. was selected as the most convenient and practical for field work and a calibration factor was determined for this scale setting.

Vertical Potentiometer. From the initial plot of the surface profile of the parking lot area, a relatively level section along the path of the profile gage was selected on the plot and the corresponding location on the pavement surface was identified by moving the actuating wheel back and forth until the position of the plotter pen coincided with the midpoint of the selected section. A 0.125 in. (0.62 cm) thick plexiglass plate 2.5 in. wide and 6.0 in. long (6.35 cm x 15.24 cm) was taped to the pavement surface at this point with masking tape. A vertical scale of 0.5 volt/in. on the recording equipment was selected, the actuating wheel was reeled slowly over the plexiglass plate and the profile of this surface obstruction plotted. This process was repeated several times using the same vertical scale on the recorder. Comparison of the plotted heights of the same 0.125 in. (0.62 cm) thick plate on the various profile traces showed excellent reproducibility. This procedure was repeated using other plotter scales of 1.0, 2.0, 5.0, and 10.0 volt/in. and for plate thicknesses of 0.25, 0.375, 0.5, 0.75, and 1.0 in. Convenient

recorder scales of 0.5 and 1.0 volt/in. were selected for field usage and calibration factors for these settings were determined.

Cross-Slope Device

The specified procedure for measurement of cross-slope was followed by three operators, each recording the observed average gradient of the same parking lot area without moving the supports of the straight edge. The reported results were as shown in Table I.

TABLE I

TEST RESULTS

Operator No.	Observed Gradient in./ft.	Average of Obsns. in./ft.
1	0.0028	0.0027
2	0.0026	
3	0.0029	

Eventhough the observed cross-slope values did vary slightly from one operation to the other, the data shows that results would be reasonably reproducible. Subsequent calibration checks showed similar reproducibilities.

Laboratory Calibration

To check for any adverse effects of wind and temperature on the accuracy and reproducibility of the profile gage the calibration processes described above were repeated in the Asphalt Laboratory of the School of Civil Engineering, at OSU where the air was relatively still and where the room temperature was held approximately constant at 77°F.

A selected 14.0 ft. long two by four plank with a smooth surface was placed on the concrete floor and the profile gage was set up such that the path of the (gage) actuating wheel followed the longitudinal center line of the plank. Measured distances were marked on the top surface of the two by four and the various (height) calibration plates were taped to the plank (one at each trial). A new set of calibration data was obtained and compared with the previous field calibration data.

Good agreement between the two sets of calibration data was observed. This substantiated the validity of the field calibration data and showed very little variance in the performance of the profile gage for the conditions under which the two sets of the calibration data were obtained. The profile gage was subsequently considered acceptable for the purposes for which it was designed. That is, 1) to measure the average cross-slopes of highway pavements in inces per foot to 2 decimal places, and 2) accurately plot the transverse profile of pavement surfaces so rut depths and/or heaves outside the wheelpaths could be detected and measured to the nearest hundredth of an inch.

CHAPTER V

TEST PROCEDURES

This research investigation can be divided into two parts or phases relative to the procedures employed in collecting data and core samples at the field test sites and those used in the laboratory to analyze the pavement materials and stereo-photographs.

Field Testing

Safety

Safety of research personnel on the highway was a deciding factor in the design of the field operations. Selection of test sites was based primarily on the availability of adequate sight distance to oncoming motor vehicles. All field work was terminated or cancelled whenever there was any form of precipitation at the test site. Similarly no work was carried out whenever visibility was poor or whenever traffic volumes became larger than a single traffic lane could handle. While these actions were expensive in terms of both time and money, they were considered necessary to minimize the danger of traffic accidents.

Workmen, research equipment and highspeed traffic do not operate too well together on an interstate highway without some means of separation. To avoid any unfortunate accident, one lane of the highway was kept open to traffic while the other was blocked for field tests. Each field test site was preceded by appropriate advance signing to warn the

motorist at 880 yds. (800 meters) from the work area. This was followed by directional signals, a flagman and finally a physical barrier to block the lane undergoing field tests to vehicular traffic. The directional markers and barriers were then switched to allow work in the other lane. All signing, signalling, blocking and flagging were done by personnel from Research and Development, and other respective Divisions of the Oklahoma Department of Highways.

Setting Up the Profile Equipment

Having blocked the test lane to all vehicular traffic, a chalk line was used to mark the pavement surface perpendicular to the center line. Two bottle caps were nailed to the pavement surface to mark the ends of this transverse line at the shoulder and the center line of the pavement.

The straight edge (gage rail) was then set up, as described previously, directly over the chalk line by shifting the end supports laterally. The trolley unit was moved to one end of the gage rail (the bottle cap point) and the height of the support at this end was adjusted so that the vertical potentiometer shaft was positioned at the midpoint of its effective travel distance. The trolley unit was then moved to the other end and the height adjusting process was repeated. This assured that the two ends of the gage rail were the same height above the pavement surface.

A string line was stretched along the top surface of the gage rail between the end support points. The height of the rail at the middle support point was then adjusted until the top surface of the rail just touched the string line. Adjustment of the middle support was also made for the lateral alinement or straightness of the straight edge. In this

way, the top surface of the straight edge was set parallel to an imaginary line joining the bottle cap points at the edges of the pavement lane. This imaginary line was considered as the datum for subsequent profile measurements.

Profile Tracings

After making the appropriate output and input power connections, the helical potentiometer was set to zero by moving the trolley unit to its starting position at one end of the straight edge. The trolley unit was reeled from this point to the other end of the straight edge and the resulting linear and vertical displacements were recorded on a standard 8.5 in. x 11.0 in. graph paper by the "X-Y" recorder. This was in the form of a continuous plot on the graph paper and this tracing indicated the transverse profile of the pavement surface (at a selected recorder scale) along the path of the actuating wheel.

Measurement of Cross-Slope

The cross-slope device was attached to the straight edge and connected to the indicator dial gage. With the device lying flat on the top surface of the straight edge, the dial gage was set to zero. The free end of the cross-slope device was then raised vertically until the bubble in the torpedo level moved into a level position. The observed gage reading was recorded as the average cross-slope (in inches per foot) of the pavement surface.

Location of Wheelpaths

If the theory of rutting on bituminous highway pavements is valid, then the most frequently traveled pavement surfaces, i.e., those areas receiving the greatest number of wheel coverages; will show a concave profile. The relatively less traveled surfaces, on the other hand, will remain practically unchanged from the original profile or will possibly show some convexity. On medium to heavily rutted pavements, therefore, the points where the surface profile changes direction (a maximum or minimum point on the plot) would very closely define the location of the center of the wheelpaths and the approximate midpoint of the distance between the wheelpaths, respectively.

The following procedure was used to locate the vehicle wheelpaths and the approximate midpoint of the wheelpaths on the pavement surface. After obtaining an accurate plot of the transverse profile of the pavement surface, points of maximum depression and points of maximum upheaval as indicated where the surface profile significantly changed direction were marked on the plotted transverse profile. The actuating wheel of the trolley unit was wheeled back and forth on the pavement surface until the position of the plotter pen coincided with one of the identified points on the profile tracing. The corresponding point on the pavement surface was then marked. This process was repeated until all the required points (center of wheelpaths and midpoint of the distance between wheelpaths) were identified on the pavement surface. Five points per traffic lane were selected along the profile line for further tests. These points are shown in Fig. 10.

Measurement of Rut Depths. Lack of an original profile of the pavement surface at a test site made it rather difficult to determine the

total subsidence or upheaval the surfaces had undergone since the roadway was opened to vehicular traffic. For this reason, the observed profile measurements were referred to as minimum values of the variables whose magnitude were being measured, and were based on measurements from defined datum plane. That is, rut depth was measured as the maximum vertical displacement of the surface in the wheelpath from a straight line whose ends formed tangents to the transverse profile curve at the adjacent points of maximum elevation. All rut depth measurements were scaled directly from the profile tracings and recorded in inches.

Lateral Creep. Upheaval of the pavement surfaces immediately outside the wheelpaths is some indication of increases in thicknesses of pavement layers beneath those surfaces and is an indication of lateral creep of material from beneath the wheelpaths. It was known from design records that the surface of the pavements studied had uniform cross-slope for lanes in the same traffic direction. Since an original transverse profile of the pavement surface was not available, a straight line joining the end support points of the straight edge was assumed to be the original surface. Based on this assumption, upward displacements of the pavement surfaces above this base line were scaled directly from the profile tracings at points between the wheelpaths. The maximum upward displacement so measured was considered as the probable heave resulting from lateral creep of materials from beneath the wheelpaths. Even very small displacements could be measured. Measurements of heave were recorded in inches.

Stereo-Photos

An offset line, parallel to and 12.0 in. from the profile line in the direction of traffic, was marked on the pavement. The selected test points on the profile line were laterally transferred to this offset line. Stereo-photographs of the pavement surface were then taken at these points. The stereo-photo box described by Schonfeld (86), a 35 mm Kodak Retina IV single reflex camera, and an automatic 80 shot electronic flash accessory were used to make these photographs. Interpretation of these photographs is described later under Laboratory Tests.

Nuclear Density Measurements

A Troxler Series 2400 Compac Surface Density/Moisture Gage was used to obtain the nuclear density measurements. Following both the manufacturer's Instruction Manual (99) and the ASTM Method of Test (95), a standard count for the nuclear gage was taken in the morning and at noon of each day of operation. Prior to each standard count, a series of tests were made to check for drift (99) and malfunction (95, 99). Tests for reproducibility of results were also conducted at each test point to make sure the recorded density counts were representative for the pavement materials beneath the respective test points. Using the backscatter method of test (99), density counts were obtained for each of the previously selected test points. These counts were later converted to density units (pounds per cubic foot) using the manufacturer's calibration data.

Surface Condition Rating

A surface condition evaluation was included in this investigation to establish, in terms of suitable qualitative index, the overall condition

of the pavement surface at the test locations. The surface condition rating format suggested by Winnitoy (105) was modified to include the following conditions:

1. General structural condition,
2. Degree of weathering,
3. Uniformity,
4. Crack condition, and
5. Surface wear/excess asphalt

Each of these conditions was rated in terms of serviceability indices ranging from 1.0 to 5.0. A typical rating form is shown in Fig. 16.

Core Drill Operations

The core drill equipment and personnel were provided by the Research and Development Division of the Oklahoma Department of Highways. Using a 4.0 in. diameter (10.16 cm) core drill, the angular speed and the rate of penetration were regulated to obtain core specimens with minimum possible disturbance of the material layers. Ten cores of full thickness ranging from 6.0 in. (15.24 cm) to 14.0 in. (35.56 cm) of the asphalt bound pavement materials were cut at the selected test points along the previously described offset line and at the same points where the nuclear density measurements were obtained. Each core specimen was immediately identified, wrapped in plastic bags, and stored in a heat insulated container. Individual core specimens in the container were isolated from each other by placing layers of sponge rubber between any two specimens before transporting them from the site to the OSU Civil Engineering Laboratories for further tests.

SURFACE CONDITION RATING

Rated by _____ Date _____ Base Course type _____

Site Description _____ Age of pavement (months) _____

Rated for (Job) _____ Pavement on: cut / fill / Nat. grade

Rating Code	Gem. Str. Condition	Surf. Wear Excess Asphalt	Weathering	Uniformity	Crack Condition			Remarks
					Opening	Abrasion	Multiple	
5	--Good	--None	--None	--Good	--Hairline 1/16	--None	--None	
4	--Long crk	--Slight	--Slight	--Streaked	-- 1/8	--Slight	--Slight	
3	--Map crk	--Moderate	--Moderate	--Crk-filling	-- 1/4	--Moderate	--Moderate	
2	--Allig crk	--Severe	--Severe	--Blotchy	-- 1/2	--Severe	--Severe	
1	--Erosion	--Abrasion/ bleeding	--Erosion	--None uniform	--Greater than 1/2	--Abrasion	--Erosion	

Figure 16. Surface Condition Rating Form

Laboratory Testing

Cutting Core Specimen

Following the ASTM methods of test: D-2726 and D-2041 and the OSU Asphalt Laboratory Manual (56), each pavement core was cut into five subdivisions with a diamond edged concrete saw. The subdivision included the surface course, leveling course, and top third, middle third, and bottom third of the base course materials. Only the asphalt bound pavement materials were included in these subdivisions. The average thicknesses of the individual subdivisions were measured, recorded, and then marked on the cores before sawing. Separation of the core into layers was done so that the specific gravities of individual layers could be compared and differences in densities detected (see analysis of data).

Bulk Specific Gravity

The extent of water absorption of the core samples was evaluated by comparing the results of two series of tests. In one series, the bulk specific gravities of five samples comprising the subdivisions from one core specimen cut from a pavement constructed on Black Base (BB) material were determined by weighing the sample in air, then weighing it is water and computing its bulk specific gravity from the relationship (56):

$$\text{Bulk Sp. Gr.} = \frac{\text{weight of sample in air}}{\text{weight of sample in air} - \text{weight of sample in water}}$$

The five samples were then allowed to dry at room temperatures ($77^{o}F$ or $25^{o}C$ approx.) and their specific gravities were remeasured with the samples coated with paraffin. Comparison of the results from the two series of tests on the same samples showed very large differences. The

observed specific gravities of the uncoated samples were much larger than the specific gravities of the same samples coated with paraffin. Apparently, the uncoated samples absorbed sufficient water during the process of weighing the samples in water to result in an appreciable reduction of value in the denominator of the Bulk Specific Gravity equation. Subsequently, it was concluded that the extent of water absorption of the field core samples were high enough to appreciably affect their observed bulk specific gravity values. Based on this finding, it was decided that all the core samples be coated accordingly.

Following the test procedure described in reference 31, each sample was coated with paraffin which had a specific gravity of 0.866 at 77°F (25°C), and a melting point of 122°F (50°C) and was allowed to cool at room temperature before its weight in water was determined. The paraffin coating was peeled off immediately after the "weight-in-water" process by first dipping the coated specimen in a bath whose temperature was set at 122°F (50°C) approximately (melting point of paraffin).

Rice's Specific Gravity

The ASTM test procedure (91) for the determination of the maximum theoretical specific gravity (Rice's vacuum saturation method) was slightly modified so existing equipment in the OSU Civil Engineering Asphalt Materials Laboratory could be used. The following modifications were made:

1) Container: 0.5 gallon (1.8925 liters) Mason fruit jar with rubber gasket, conical cap with #40 US Standard mesh strainer, and a hose connection was used instead of the suggested 1000 ml volumetric flask. Each jar was calibrated prior to use.

2) Vacuum Pump: A Nelson vacuum pump capable of holding 14.7 psi (30 in. Hg) vacuum pressure was used to evacuate the entrapped air. The specimen was subjected to full vacuum for 15 minutes.

3) Preparation of Test Samples: The core sample used in the bulk specific gravity test was heated in a temperature controlled oven until the asphalt in the sample attained a fluid consistency. Using a spatula, the particles of the sample were separated by stripping the coarse aggregates clean of lumps of fine material and by breaking down lumps of the fine materials portion as fine as possible, while the mixture was still hot, without fracturing the mineral particles. The separated mixture was allowed to cool to room temperature by thoroughly stirring the mixture to prevent the particles from caking together. Where the volume of a core sample was significantly larger than was specified, the standard "quartering" method of sampling was employed to reduce the volume of the separated sample to a convenient size.

4) To facilitate release of entrapped air a wetting agent (liquid calgon) was added to the deaired-distilled water used in the test.

Percent Density

The percent density values for the individual test samples were calculated using the relationship:

$$\text{Percent Density} = \frac{\text{Bulk Specific Gravity}}{\text{Rice's Specific Gravity}} \times 100$$

The percent density values, expressed as a percentage of the maximum theoretical specific gravity (voidless mix), may be used to determine the volume of voids in the sample as follows:

Percent Air Voids = (100 - Percent Density Value)

Also, comparison of the percent density values for the core samples at the individual test points on a test site can be made and differences detected. Significant differences in percent density values could then be assumed as resulting from densification under traffic (see analysis of data).

Stereo-Photo Interpretation

Wear is a contributing factor to rutting of bituminous highway pavements. In surface mixtures incorporating non-polishing aggregates, only the fine materials and the asphaltic binder tend to wear or abrade under traffic. This leaves the larger non-polishing aggregate particles projecting above the partially worn background fines, in the form of angular to sub-angular pyramid depending on the polish-resistant characteristics of the material. In the case of mixtures made with polishing aggregates, both the surface aggregates and the background fines tend to wear under traffic though at different rates depending on the relative wear-resistance of the surface materials. In either case the amount of wear due to traffic action is greater on heavily traveled surfaces (wheelpaths) than on less frequented surfaces (surfaces other than wheelpaths).

Based on this duscussion, the projection of the coarser aggregate particles at the pavement surface would be relatively higher in the wheelpaths than outside the wheelpaths. This assumes that the background fines do not wear to an extent that would permit the dislodging of the surface aggregates, that raveling due to stripping of the asphaltic binder from the aggregates does not occur, and that bleeding of excess asphalt onto the surface does not take place. If these assumptions are

reasonable, then comparison of the projections of surface aggregates in the wheelpaths with those outside the wheelpaths will give a reasonably good estimate of the differential wear that occurs.

To obtain estimates of these projections, the stereo-slide pairs were viewed under a telescopic lens with six power magnification on a flourescent light desk. By comparing the heights of projections with that of a calibrated wedge scale which was placed on the pavement at the time the photographs were taken, estimates of maximum projections were recorded in terms of the calibrated scale. These scale values were later converted to inches by means of a calibration curve.

Other surface characteristics were observed during the microscopic study. These included the degree of polishing of the surface, geometry of projections, raveling, bleeding, fracture of surface aggregates, cracking and erosion. This supplementary information aided the evaluation of the general condition of the pavement surfaces of the individual test points at a test site.

CHAPTER VI

TEST RESULTS AND DISCUSSION

Density Measurements

The percent density values for the individual core subdivisions were computed from the bulk specific gravity and the Rice's specific gravity values. The percent air void content values were calculated directly from the percent density values as follows:

Percent Air Void Content = (100 - percent density value)

If the initial percent density values were known, then comparison with the test values would directly indicate the changes in density caused by traffic compaction. The contribution to rutting of these changes could then be estimated, using the procedure discussed earlier. Because the initial values were unknown, classical statistical methods were employed to test for differences in the observed percent density values. Significant point differences were considered as changes resulting from traffic action.

Tests for evidence of differences were conducted for each test site using the Statistical Analysis System (SAS) standard computer program (Appendix C), (10). The computer program gave the Observed Significance Level (OSL), (26) and acceptance or rejection of the null-hypothesis (no differences) depended on the choice of a significance level. Choice of this significance level depends on several factors including: 1) expected

variability in the initial values, 2) degree of certainty or accuracy required, 3) accuracy of test results, and 4) consistency with which the tests were conducted. For this study, a value of 0.1 was considered as the significance criterion for the rejection or acceptance of the hypothesis of no differences. The results of the computer analysis for the individual test sites are discussed in the following paragraphs under the four types of base course materials.

HMSA Materials

All the four test sites showed strong evidence of layer differences in the percent density values. The observed significance level was 0.0001 in each case. The percent density of the surface materials (surface and leveling courses) appeared to be essentially the same and ranged from a high value of 99 percent to a low value of 90 percent. The percent density values of the HMSA base course materials did contribute a greater portion of the observed variability and ranged from a high value of 93 percent to a low value of 77 percent.

The computer analysis did not show strong evidence of point differences in the percent density values for test site #10. The observed significance level was 0.2465. However, a plot of percent density values versus transverse location of test points indicated peak values occurring at the wheelpath locations (Fig. 34) for both the surface and the base course materials and is an indication of some differential densification (wheelpath versus outside wheelpaths) at these locations. For the surface materials the maximum values occurred at test points #2 and #7, which are the respective transverse locations of the outer wheelpaths in the outer and the inner traffic lanes. For the base course materials,

the maximum values occurred at test points #2 and #9 and were the outer and the inner wheelpath locations in the outer and the inner traffic lanes, respectively.

The Analysis of Variance (AOV) for test site #60 indicated strong evidence of point differences in the percent density values. The observed Significance Level (OSL) was 0.0001. Although the data showed some scatter, a plot of percent density versus transverse test point (Fig. 35) associated the peak values with wheelpath locations. For the surface materials, the maximum values occurred at test points #2, #4, and #9. For the base course materials, however, the curves indicated one major peak value (86 percent density), and this occurred at the transverse location of the inner wheelpath in the outer traffic lane.

Similar behavior of the percent density curves was recorded for test site #70 (Fig. 36). The AOV indicated strong evidence of both layer and point differences. Unlike those of test sites #10 and #60, the curves show consistent differential densification in the surface course materials in the wheelpaths. In the inner traffic lane, a differential value of 2 percent density units was recorded at both wheelpath locations. For the outer traffic lane, the maximum differential densification was 5.6 percent density units and occurred at the outer wheelpath location. The percent density values for the leveling course materials were consistently high and uniform across the pavement. Even so, a differential densification of 1.6 units was observed at the same outer wheelpath location. At the inner wheelpath location (outer lane), however, both the surface course and the base course materials showed similar differential densification and these were 2.8 and 3.4 percent density units respectively.

The percent density curves for test site #120 (Fig. 37) exhibited behavior similar to that of test site #70. Major differential densification occurred in the surface course materials and relatively uniform percent density values in the leveling course material are indicated. Owing to the uniform distribution of density values in the base course materials it can be assumed that the major densification at this site occurred in the surface materials.

Black Base Materials

Unlike the pavement sections on the HMSA base course materials, the percent density values of both the surface and the base course materials of pavement sections utilizing the black base as the base course materials were found to be relatively high and ranged from about 90 to 98. Nevertheless, the analysis of variance on the percent density values did indicate strong evidence of point differences for all four of the test sites and strong evidence of layer differences for three test sites.

For test site #30, the analysis did not indicate any strong evidence of layer differences. Accordingly, the percent density values of the layers were averaged for each test point and a percent density versus test point curve was plotted for this test site (Fig. 38). The density curve showed two peak values corresponding to the outer and the inner wheelpath locations in outer traffic lane. The differential densification at these wheelpath locations was estimated as 1.6 percent density units for each layer. The AOV indicated a strong evidence of point differences and is an indication of this differential densification.

In the inner traffic lane, the plotted density values exhibited considerable scatter. In fact, the only peak value shown by the curve occurred at a non-wheelpath location. The recorded density values for the materials in this lane were considered inconsistent and this can be attributed to experimental error in the density determinations. However, the average density values were lower than in the outer lane, indicating the compactive influence of traffic in the more frequently traveled right hand lane.

The AOV on the values for test site #50 indicated significant layer and point differences in the percent density values. This indicated that averaging of layer values corresponding to a given transverse test point was not legitimate so separate curves were plotted for each layer (Fig. 39). Although the percent density values did not vary too much from one layer to another, peak values were associated with wheelpath locations. The maximum differential densification occurred at test point #4 which is the transverse location of the inner wheelpath in the outer lane, and this was estimated as 4.8 percent density units. The density curve for the base course material showed very little change across the roadway and density values ranged from 87 to 90 percent of the maximum theoretical density obtained by Rice's method. The curve for the leveling course materials showed similar behavior except that peaks were more distinct in the inner traffic lane and density values were slightly higher (90 to 92 percent density). For the surface course materials major peak values occurred at test points #4 and #8. The occurrence of peak value at test point #8 is similar to that observed at test site #30. In this case, however, major densification in the inner traffic lane appeared to occur in the leveling and base course materials so that the peak value

observed at test point #8 in the surface material did not have any significant influence on the total densification recorded at the adjacent wheelpath locations.

The density curves for test site #20 (Fig. 40) indicated higher percent density values in the base course materials than in the leveling course materials. The base course materials averaged 92 percent compared with an average of 90 percent in the leveling course materials. This type of situation should be avoided in pavement construction. That is, a low density layer between two layers of higher density materials will almost certainly result in pavement rutting due to either differential densification and/or lateral creep of material in the sandwiched layer. The curves for the base and leveling courses did not show major peak values, however, the surface course materials which had relatively high percent density values (98 percent average) did indicate differential densification as large as 3.6 percent density units. Densification was observed at all four wheelpath locations in the surface layer.

On test site #40, the density curves indicated the lowest percent density values in the surface course materials (Fig. 41). It was, therefore, not suprising that differential values as high as 4.2 percent density units were observed at the inner wheelpath location in the outer traffic lane. When surface materials have relatively low density, their load-distributing capability is reduced and this will tend to encourage concentration of stresses in the underlying layer. This may explain the substantial difference in density values occuring between the leveling course materials in the outer traffic lane and those in the inner traffic lane. In the outer lane the leveling course materials had percent density values approaching 98 percent as compared to 95 percent in the inner

traffic lane. On the other hand, when material layers have sufficient density to withstand the applied loads, they tend to be stable under traffic and this is shown by the uniformity of the percent density values of the base course materials.

SABC Materials

The percent density curves for all the pavement sections utilizing this type of base course materials showed peak values in both the surface and the leveling course materials at the wheelpath locations and this is an indication that densification extends into the base course. In three of the pavement sections tested, the measured percent density values for the leveling course materials were found to be higher than those of the surface course materials. The AOV on the percent density values indicated strong evidence of point differences for all four test sites and strong evidence of layer differences for three of the test sites.

That the AOV did not indicate strong evidence of layer differences for test site #100 is not surprising because the surface course materials which showed larger values in the outer traffic lane had percent density values lower than those of the leveling course materials in the inner traffic lane (Fig. 42). If the initial density values were approximately equal in both lanes, then it can be inferred that the change in trend is due to mass densification of the surface course materials which must have had relatively low initial densities. This is evidenced by the surface density values approaching those of the leveling course materials at the wheelpath locations in the inner traffic lane. According to the density curve, peak values occurred at the four wheelpath locations and a maximum differential densification of 2 percent density units was

observed at the outer lane compared with 5 percent in the inner traffic lane.

Except for the transverse test point #7, the percent density values recorded for the leveling course materials indicated higher values than those of the surface course materials for the pavement section at test site #80. Accordingly, large differential densification was observed at the wheelpath locations in the surface materials (Fig. 43). Maximum differential values of 5 units were observed at test points #2, #7, and #9 in the surface course materials. A value of 3.5 percent density units of differential densification was observed at test point #7 in this layer. The density curve for the leveling course materials was relatively uniform for the materials in the outer traffic lane but showed significant peaks in the inner traffic lane. The maximum differential densification of 3.0 percent density units in this layer was observed at test point #9. No substantial differential densification was observed in the outer traffic lane because of the probable high initial densities. The observed percent density values ranged from 97.1 to 98.7.

The density curves for test site #90 (Fig. 44) indicated similar trends. The surface course materials exhibited relatively lower percent density values than the leveling course. The curves showed peak values at the wheelpath locations in both layers and suggest that differential densification extends into the base course. Maximum differential densification of 3.5 percent density units were observed at the wheelpath locations in the outer traffic lane. The densities of all the materials in the outer traffic lane were consistently higher than those in the inner lane and this is an indication again of the compactive influence of more frequently applied traffic loads.

The density curves for site #110 (Fig. 45) exhibited different behavior in that the surface layer indicated higher density materials at all the transverse test points except at points #5 and #6. Nevertheless, peak values were observed in both the surface and leveling course materials at the wheelpath locations, and this was particularly true in the surface layer. Densification of about 3.0 units was noticed at the wheelpath locations in both pavement lanes.

Soil-Cement Materials

The percent density curves plotted for the four test sites utilizing soil-cement base course materials showed the densities of the surface course materials approaching those of the leveling course materials in the outer traffic lane and much lower values in the inner traffic lane. There can be no direct explanation for this behavior since the initail densities of the materials are not known. Considering the rigidity of the soil-cement materials and heavier traffic volumes in the outer traffic lanes, however, it can be inferred that this behavior is due to a greater rate of densification occurring in the outer traffic lanes. The rigidity of the base course materials may also have facilitated compaction of the leveling course materials during construction resulting in denser leveling course materials. Because the surface course materials had relatively lower initial densities, densification of materials in this layer was much easier especially during the early stages of pavement life and may have resulted in the observed high density materials in the outer traffic lanes.

For test site #130, the densities of the surface course materials were essentially the same as those of the leveling course materials in

the outer lane and ranged from 96 to 98 percent density (Fig. 46). The maximum differential densification was 1.5 percent density units for each layer and this occurred at the outer wheelpath location in this lane. For the materials in the inner lane, the percent density values of the surface course materials ranged from 95.5 at the outer wheelpath location to 92.6 at the shoulder compared with the average value of 98 recorded for the leveling course materials in this lane. Differential densification of 2.0 percent density units was observed at the outer wheelpath location. Generally, the curves showed peak values at all the wheelpath locations and is an indication of densification at these transverse locations.

The materials at test site #140 indicated behavior similar to those at test site #130 (Fig. 47). Density values were much higher in the outer traffic lane and ranged from 96 to 99 percent density. Those in the inner traffic lane ranged from 91.5 to 96.8. The density curves peaked at the wheelpath locations and differential densification was similar to that observed at test site #130.

For site #170, the AOV did not indicate any strong evidence of layer differences. Accordingly, averaging of the percent density values was performed for the two layers and a density curve was drawn (Fig. 48). The curve indicated peak values at the wheelpath locations. The differential densification occurring at the two wheelpath locations in the outer traffic lane may be estimated at 2.0 percent density units and is approximately equal to that observed at the inner wheelpath location in the inner traffic lane. The significant differential densification was identified by the AOV when it recorded a very strong evidence of point differences in the percent density values of materials at this test site.

The percent densities recorded for the materials on test site #180 (Fig. 49) showed maximum values at test point #3 which is located between the two wheelpaths in the outer lane. No explanation for this can be given except that the profile tracing indicated a lateral shift of traffic toward this point. Nevertheless, some peak values occurred at the wheelpath locations especially in the surface course materials. In the outer traffic lane, a maximum differential densification of 5.5 percent density units was observed at the outer wheelpath location in the surface course materials. In the leveling course materials, the differential densification was 2.5 units at this location. In the inner traffic lane, observed densification was equal at both wheelpath locations in the surface course material and may be estimated as 1.6 units. In the leveling course materials, maximum densification occurred at the inner wheelpath location in this lane and this was 1.5 units. The behavior of materials at this test site was different from those observed earlier in that the density curves for the two layers stayed approximately parallel to each other. Like the other test sites utilizing soil-cement base course materials, the percent density values for the surface course materials were lower than those of the leveling course materials.

Profile Measurements

As was noted earlier, one profile tracing was made for each pavement lane and the two tracings for a test site were put together to obtain the continuous transverse profile tracings shown in Appendix B. On these tracings, the transverse location of the test points have been marked and numbered sequentially. The test points identified as #1 and #10 refer to the locations of the outer and the inner shoulder lines

respectively (Fig. 10). Points #2 and #4 refer to wheelpath locations in the outer pavement lane and points #7 and #9 are the locations of the outer and the inner wheelpaths in the inner lane. The measured values of relative subsidence or rut depths are identified as "positive" values, whereas "negative" values refer to heaves. These measurements were scaled directly from the original tracings and are presented immediately below the profile tracings (Appendix B) as "profile measurements".

The characteristics of the transverse profiles of the pavement sections studied are discussed in the following paragraphs under the four types of base course materials. It must be pointed out that the measured subsidence and/or heave cannot be considered as the true displacement that occurred since "initial" profile traces, i.e., traces made at the time the pavement was first opened for traffic, were not available and an assumed profile line was used as a basis for comparison.

Also, subgrade behavior may have a significant influence on the determined values. If major subsidence occurred in the subgrade soil, lateral displacement of the bituminous materials (as evidenced by upheaval of the pavement surfaces) will not be apparent and erroneous conclusions may be drawn. Similarly, if substantial heave or swelling occurred in the subgrade materials at the pavement shoulders due to changes in moisture content, the observed subsidence or rut depths will be magnified by the amount of heave and lateral displacement of materials may be inferred. The determination of heave was, however, based on the assumption that any moisture-associated heave at the pavement shoulders would not be sufficient to significantly affect the measurements in the traffic lanes. That is, moisture-associated heaves at the shoulders would result in relatively uniform or large radii surface curvatures and these are different from

the small radii humps associated with shear failure or lateral creep which occurs immediately adjacent to the wheelpaths.

HMSA Sections

At test site #10 (Fig. 17) heaves of 0.2, 0.5, and 0.4 inches were determined at the test points #1, #3, and #8, respectively, indicating lateral creep of materials from beneath the wheelpaths to these locations. Also, lateral shift of traffic towards the inner pavement lane can be observed on the profile tracing. This is indicated by the widening of the outer wheelpath in the outer pavement lane towards the inner lane. This widening may have subdued the magnitude of heave at test point #3. Visual examination of the pavement surface at this test site also indicated hairline longitudinal cracking at test point #3 and wider longitudinal cracking at the outer shoulder and at the pavement center line (between points #5 and #6). This is an indication of overstressing (tensile) of the pavement materials at these locations. No cracking was observed in the inner lane.

The density data at this test site showed large differential densification in all the pavement layers at test point #2 and minimum densification at test point #4. Comparing the magnitudes of differential densification and the rut depths at test points #2 and #4, it may be concluded that a major portion of the observed heave at test point #3 was contributed by lateral creep of base course material from beneath the outer wheelpath. However, if the peaking of the density curve for the base course materials at test point #2 is considered, it can be argued that substantial consolidation of the subgrade soil may have occurred at

this location and this may have contributed to the rut depth in this wheelpath.

The performance of test site #60 was different from that of test site #10 in that subsidence at the midsections of both pavement lanes was observed (Fig. 18). In the outer pavement lane, the subsidence was 0.078 in. (0.2 cm) compared with 0.214 in. (0.54 cm) recorded in the inner lane. Nevertheless, heaving was noticed at the pavement center line (between points #5 and #6). The magnitude of heave was estimated at 0.125 in. (0.32 cm) and was attributed to lateral creep of materials. A study of the surface profile at this location and evidence of large differential densification occurring in the pavement materials at test point #4 relative to point #5, suggests that the observed heave was due to lateral dispalcement of the bituminous materials from beneath the adjacent wheelpath in the outer lane.

Although no surface cracking was apparent at this test site, indicating good structural integrity, it must be pointed out that the surface subsidence is detrimental to traffic safety because this will impair effective drainage of surface water. Major rutting occurred in the outer pavement lane. Rut depths of 0.43 in. (1.09 cm) and 0.30 in. (0.76 cm) were noticed at test points #2 and #4 respectively.

The performance of the pavement section at test site #70 was similar to that at test site #60. Subsidence was apparent in both traffic lanes (Fig. 19). In the outer lane, a subsidence of 0.125 in. (.32 cm) was determined at the center compared with 0.036 in. (0.091 cm) in the inner pavement lane. Rutting, however, was more pronounced at this site. Rut depths of 0.574, 0.464, 0.125, and 0.143 in. (1.458, 1.186, 0.32, and 0.36 cm) were noticed at test points #2, #4, #7, and #9 respectively.

The values indicate maximum rutting at the wheelpath locations adjacent to the shoulders. Since shear failure is likely at the unsupported pavement edges, i.e., lower lateral confining pressures at these locations, some of this rutting could be attributed to lateral creep. However, the density curves at this location indicated strong evidence of differential densification. No upheaval was indicated at this site, however, a slight hump at the pavement center line could be some indication of lateral displacement of materials from beneath the adjacent wheelpaths.

Based on rutting alone, site #120 (Fig. 20) may be considered as the one that showed the best performance in this group of pavement sections. Only two rut depths were large enough to be measured and these were 0.38 in. (0.965 cm) and 0.16 in. (0.41 cm) and occurred at the inner wheelpath locations in the outer and the inner pavement lanes respectively. However, visual examination of the pavement structure indicated considerable surface cracking (longitudinal, transverse/map cracking, etc.), and raveling especially in the outer pavement lane. The surface cracks and the wide depression basin in the outer lane indicate a base failure. This concept was further substantiated by the fact that in several of the cores at this location, the hot sand base material completely washed out during the coring operation. Evidently, considerable stripping had occurred in this layer.

Black Base Sections

Careful study of the profile tracing for test site #50 (Fig. 21) revealed sharp humps at the pavement center line and at test point #3 (between the wheelpaths in the outer lane). This was considered an indication of shoving or lateral creep of materials from beneath the

adjacent wheelpaths. However, more positive evidence of lateral creep could not be determined because the initial transverse profile at this site was unknown. Rut depths of 0.786, 0.464, 0.232, and 0.09 in. (2.0, 1.18, 0.59, and 0.23 cm respectively) were measured at test points #2, #4, #7, and #9 respectively. These indicate deeper rut depths at the outer wheelpath locations in both pavement lanes, and may be related to the effects of cross-slope on weight distribution to the vehicle wheels. The cross-slope of the pavement section was measured at 0.275 in. per foot (2.29 cm/meter). A subsidence of 0.411 in. (1.04 cm) was noticed at the midsection of the outer lane as compared with 0.054 in. (0.137 cm) in the inner lane. Densification of the bituminous materials cannot account for this total vertical deformation, however, this test site is in a fill section and there is a possibility of subgrade consolidation beneath the outer lane.

At test site #20 (Fig. 22), subsidence was noticed at the midsection of the outer lane whereas evidence of heave was established at a similar location in the inner traffic lane. Magnitudes, however, were very low: the subsidence was 0.078 in. (0.2 cm) and the heave was 0.054 in. (0.137 cm). Rut depths of 0.25 in. and 0.571 in. (0.635 and 1.45 cm) were noticed at test points #2 and #4 respectively in the outer lane, compared with 0.161 and 0.170 in. (0.409 and 0.43 cm) at test points #7 and #9 respectively in the inner pavement lane. No direct explanation could be given for the occurrence of deeper rutting at the inner wheelpath locations in both pavement lanes.

Evidence of lateral creep was noticed at all locations adjacent to wheelpaths in the outer pavement lane at test site #30 (Fig. 23). The largest heave was observed at the midsection of this lane and this was

0.233 in. (0.59 cm). Large longitudinal cracking in the wheelpath was observed at test point #2 and this is an indication of excessive flexural stresses in the pavement structure. The apparent tilting of the surface profile between test points #2 and #1 towards the pavement center also supports this idea. Deep rutting 0.607 in. (1.54 cm) at this location will channelize surface water along the longitudinal crack and, subsequently, to the underlying materials. The deep rutting and cracking in the outer lane and the substantial elevation difference (between the inner and the outer lanes) observed at this site can be attributed to deterioration of the base course materials and possibly to softening and volume change of the subgrade.

At test site #40 (Fig. 24), the outer pavement lane appeared to be at a lower elevation than the inner lane. While this could be due to failure to achieve proper grade at the time of construction another explanation might be general subsidence of materials in this lane. Also the leveling course materials in this lane had higher percent density values relative to those observed in the inner pavement lane. This suggests that the densification of the leveling course materials contributed to the apparent subsidence in this pavement lane. Rutting was heavy in the outer lane and lateral shift of traffic towards the inner pavement lane was evident on the profile tracing. Rut depths of 0.643 in. and 0.607 in. (1.63 and 1.54 cm) were measured at points #2 and #4 respectively, compared with 0.094 in. and 0.233 in. (0.24 and 0.59 cm) observed at test points #7 and #9 in the inner pavement lane. Upheaval of approximately 0.078 in. (0.198 cm) was noticed at test points #3 and #5.

SABC Sections

Evidence of lateral creep was observed at all the four test sites utilizing this type of base course material. Substantial rutting occurred on both pavement lanes at all four of the test sites, and this suggests relative flexibility or instability in the base course materials.

At test site #80 (Fig. 25), a heave of 0.2 in. (0.51 cm) was observed at test point #3. The rut depths measured at the adjacent wheelpath locations (test points #2 and #4) were 0.482 in. and 0.571 in. (1.22 and 1.45 cm). A study of the percent density curves for the bituminous materials in this lane indicated relatively uniform density values at the three test points for each layer and this suggests that differential densification in these materials did not contribute appreciably to rutting. The substantial rutting observed in this pavement lane, therefore, can be related to lateral creep and differential densification in the stabilized-aggregate base course materials. Base failure was evidenced by wide longitudinal cracking in and between the wheelpaths. These cracks were developing into map cracking patterns and it was not surprising that base stabilization operations (lime injection) were being carried out at this test site at the time of testing.

The profile tracings made at test site #90, #100, and #110 (Figs. 26, 27, and 28), indicated trends similar to that observed at test site #80, i.e., deep rutting and upheaval of surfaces adjacent to the wheelpaths were in evidence. It should be noted that these pavement sections were relatively old (ages ranged from 158 to 165 months) and the fatigue life of the unbound base materials is a factor relating to the apparent deterioration in this layer. Thus, age of the pavement structure should

be considered in an overall performance evaluation of the bituminous bound layers.

Soil-Cement Sections

Rutting was minimal at test site #130 (Fig. 29). The maximum rut depth was 0.2 in. (0.51 cm) and occurred at test points #2, #4, and #9. Evidence of lateral creep was observed at test points #1 and #3 where heaves of 0.184 and 0.062 in. (0.47 and 0.16 cm) were measured. Although differential densification occurred in the pavement at the wheelpath locations, these values were not large and since the total thickness of the materials that could undergo densification was also small, a major portion of the observed rut depths can be attributed to lateral creep of the bituminous materials. It may be recalled that a differential densification of 2 percent density units occurring in a 6 in. thick layer will result in a differential change in thickness equal to (.02 in. x 6 in.) 0.12 in. (0.3048 cm). The thicknesses of the core specimens from the pavement sections constructed on soil-cement base course materials ranged from 6 to 8 in. (15.24 to 20.32 cm) so any section that showed rut depths greater than 0.2 in. (0.508 cm) and differential densification less than 3 percent density units (assuming these were computed based on the initial values), could not be considered as deriving its rut depths from differential densification alone.

Some evidence of lateral creep was also observed at test site #140 (Fig. 30). However, the magnitude of heave was very small 0.03 in. (0.076 cm) and this occurred at test point #3. Rut depths measured at the outer pavement lane were 0.289 and 0.257 in. (0.73 and 0.65 cm) at

the outer and the inner wheelpath locations, respectively. The inner pavement lane did not show any appreciable rutting.

The pavement at site #170 (Fig. 31) showed deep rutting at all the four wheelpath locations and substantial heave of surfaces at the shoulder and the pavement midsection in the outer lane. The observed rut depths were 0.5, 0.5, 0.3, and 0.2 in. (1.27, 1.27, 0.76, and 0.51 cm) at test points #2, #4, #7, and #9, respectively. The magnitudes of heave were 0.125, 0.25, and 0.03 in. (0.32, 0.635, and 0.076 cm) and these occurred at test points #1, #3, and #5, respectively, in the outer pavement lane. The magnitudes of rutting and heaving indicate substantial lateral displacement of the bituminous materials must have occurred. Considerable differential densification at these locations was inferred from the density curves but this cannot account for the total amount of rut depth observed.

Subsidence of 0.217 in. (0.55 cm) was recorded at the midsection of the outer pavement lane at test site #180 (Fig. 32). A review of the density curves for this test site, however, indicated large differential densification in the pavement materials at this location (5.5 and 2.0 percent density units in the surface and leveling course materials, respectively) so that the observed subsidence can be attributed to densification of the bituminous materials. Lateral shifting of traffic, as evidenced on the profile tracing, toward the inner pavement lane resulted in densification of the materials at that location. Rut depths of 0.478, 0.289, 0.043, and 0.055 in. (1.21, 0.75, 0.11, and 0.14 cm) were observed at test points #2, #4, #7, and #9, respectively.

Cracking appeared to be the major problem associated with the pavement sections which utilized soil-cement as base course materials. All

four pavement sections on this type of base showed transverse cracking at regular intervals of 50 to 60 ft. (15.24 to 18.29 cm). Between the wheelpaths in the outer pavement lanes dendritic type cracking had developed at irregular intervals along the longitudinal cracks. The transverse cracks showed no symptoms of surface distortion or break-out of material adjacent to the crack joint. These cracks were, of course, considered as reflection of shrinkage cracks in the soil-cement materials. Nevertheless, traffic action will subsequently cause erosion of materials at the cracked joints (interface). Also, surface water will drain through these cracks to deteriorate the bituminous materials and soften the subgrade soil. Considering the action of water and the effects of freeze-thaw circles during the winter months at the cracked joints, it may be concluded that these cracks are detrimental to the structural integrity of pavement system and require appropriate remedial action.

Surface Wear

The method of test for wear of pavement surfaces at the wheelpath locations was described under "Test Procedures" and was based on the assumption that wear of the matrix would not be sufficient to cause complete dislodgement of the surface aggregates. It was originally planned to use a classical statistical method (AOV) to test for differences in the test data which will be an indication of differential wear resulting from traffic action. Use of this statistical method implied data sets of full size, i.e., if any of the classification variables had blank or missing values in an observation, that observation will be excluded from the analysis.

Surprisingly, the state of wear observed at most of the sites (at the time of testing) had passed the fracturing stage and substantial dislodgement was noticed. Surface raveling was observed at a number of the pavement test sections. Furthermore, some of the stereo-pairs of photographs made of the pavement surface at some of the sites were very poor due to a malfunction of the camera shutter system. These situations weakened the effectiveness of the statistical test method proposed and resulted in a departure from the intended method of analysis.

A new method of analysis (non-statistical) was devised and this consisted of comparing the maximum projections of the surface aggregates observed at the wheelpath locations in a given pavement lane with those observed at the adjacent non-wheelpath locations. Because the aim of this analysis was to detect evidence of differential wear (not magnitudes of wear), the surfaces at the pavement shoulders (test points #1 and #10) were excluded from the analysis. Absolute arithmetic mean differences were used so differential wear on pavement surfaces incorporating either polishing or non-polishing aggregates or both could be detected. Averaging of differential values indicated conservative results, i.e., the differential values obtained this way are minimal. Table II shows a classified summary of the results of this analysis. The results indicated differential wear values at all the test sites where comparisons were possible. As would be expected, the larger values occurred in the wheelpaths of the outer traffic lane. While the determined magnitudes of wear were smaller than anticipated, the results indicate that wear is definitely a contributing factor to rutting on flexible pavements.

TABLE II

DIFFERENTIAL WEAR

BASE COURSE MATL.	SITE #	AGE MO.	DIFFERENTIAL WEAR (INS.)[1] AT WHEELPATH LOCATIONS	
			INNER LANE	OUTER LANE
HMSA	10	36	0.012	0.020
	60	169	0.016	0.023
	70	169	0.018	0.027
	120	105	0.016	0.029
BB	20	82	0.008	0.071
	30	56	***	***
	40	56	***	0.016
	50	86	0.015	0.016
SABC	80	165	0.016	0.031
	90	165	0.023	0.078
	100	158	***	***
	110	158	***	***
SCB	130	148	0.010	0.017
	140	148	0.005	0.014
	170	169	0.028	0.039
	180	169	0.031	0.031

*** MISSING VALUES

1. CONVERSION: 1.0 in. = 2.54 cm

CHAPTER VII

CONCLUSIONS AND RECOMMENDATIONS

Conclusions

Based on the test procedures employed and the pavement sections studied, the following conclusions are made:

1. The transverse profile gage provides a portable and accurate means of obtaining continuous profile tracings of a pavement surface.

2. In addition to measurement of surface deformations, the plotted profile graphs provide permanent records of these conditions at a specific time in the service life of a pavement and can be used for future studies.

3. The profile gage can be used to follow the development of surface deformations at sites on stage construction pavement sections. The transverse profile information and other test data, e.g., Benkelman beam deflections, can provide guidance in determining the optimum time for placing subsequent overlays. The gage is currently being used for this purpose.

4. With slight modifications to increase its portability, the profile gage can be employed to check surface tolerances on concrete bridge floors. This capability has been demonstrated.

5. On flexible pavements, densification under traffic loadings occurs in all asphalt bound material layers with the greatest amount of densification in evidence at the wheelpath locations in the outer

pavement lane. Densification contributes a significant amount to the total surface rut depth, particularly where a thick layer of low density (below 92 percent density) asphalt base is used.

6. Lateral creep or instability in the bituminous pavement materials, as evidenced by surface heaves immediately adjacent to the wheelpaths, was found on 12 of the 16 test sites. This occurred in high as well as low density materials and contributed greatly to the total rutting at these locations. Evidence of lateral creep was observed on all types of base course materials. More prominent surface heaves were noticed at sites where the bituminous material layers had low densities.

7. Lateral shift of traffic towards the inner pavement lane was noticed on pavement sections where rut depths exceeded 0.5 in. (1.27 cm). This was indicated by the widening of the wheelpaths in the heavily traveled right hand lane towards the inner traffic lane. Apparently, drivers tend to avoid driving in rutted wheelpaths and steer to the left rather than towards the pavement shoulder. On two lane facilities, this reduces the lateral vehicle clearance and can result in hazardous driving conditions.

8. Surface wear or attrition in the wheelpaths on heavily traveled traffic lanes is an important contributing factor to rutting on flexible pavements.

9. No satisfactory correlation between laboratory density values and the values obtained using the surface nuclear density gage was found. The accuracy of measurements obtained using the surface or back scatter method (nuclear method) appeared to depend on the pavement surfaces material characteristics, particularly, surface roughness as well as experience with the operation of the equipment. See Appendix E.

10. The analysis of data using the multiple regression (multivariate) methods (28) indicated negative correlation coefficient between rut depth and age of pavement, i.e., greater rut depth values were associated with more recent pavement sections. The older pavement sections might have been overlaid or they were built to resist rutting better than the more recent ones. This indicates that, if rutting should be a major problem, it will occur during the early stages of pavement life.

11. A negative correlation coefficient was found between rut depth and surface (differential) wear in the wheelpaths and this confirms the afforementioned finding that motorists tend to avoid driving in deep ruts by shifting to less rutted pavement surfaces.

12. The importance of drainage in flexible pavement construction was indicated by the negative correlation coefficient observed between rut depth and the cross-slope of the pavement surface. Apparently, surfaces with greater cross-slope tend to drain surface water faster during and after rainfall thus reducing infiltration of water into the pavement structure to deteriorate the bituminous materials and soften the underlying subgrade soil.

Recommendations

In view of the results of this research investigation, the following recommendations are made:

1. Investigate modifications to increase the portability of the transverse profile gage so it can provide faster means of monitoring pavement surface deformations and for checking surface tolerances on concrete bridge floors.

2. In order to follow surface deformations due to traffic action, profile tracings at a site should be made prior to opening the highway to traffic. This will provide an initial tracing at time "zero" for subsequent comparisons.

3. Following the above recommendation, additional (or further) studies could ascertain exact amounts of surface heave, and determine the bituminous pavement layer(s) responsible for this type of displacement. With careful monitoring of specially constructed test sections, it should be possible to distinguish between surface heave resulting from lateral creep (shear failure) in these layers and that due to changes in the environment, e.g., swelling of subgrade soils. Higher stability values for the respective layers may be required.

4. Increased surveillance of operations at hot-mix plant sites and more stability checks on the mixture being produced could be instituted to insure conformance with the stability requirements for a given type of mix. Special studies of this nature on selected projects would indicate the adequacy of present inspection and check test procedures.

5. To minimize the contributions of densification and lateral creep to rutting, construction methods and specifications should be reviewed to determine if changes are necessary to insure adequate compaction and density of all asphalt bound pavement materials.

6. The accuracy of current laboratory procedures for determining percent density values of both laboratory and field compacted specimens should be investigated. Error in the determination of the maximum specific gravity of a mixture can easily result in very low in-place density values. Due to this error, the measured percent density values of field

specimens can be above the specified minimum value but the actual density of these specimens may be a great deal below the desired value.

7. A comprehensive study of the effectiveness of the various types of base course material used in flexible pavement construction in Oklahoma should be made. A feasible appraoch to such a study would be to use stage construction test sections at various geographical locations in Oklahoma. That is, for a given type of base, design and construct test sections with varying thicknesses of the surface course material and follow subsequent behavior in terms of appropriate performance variables including 1) rutting, 2) surface roughness, 3) longitudinal cracking, 4) transverse cracking, and 5) slope variance. Other material variables, e.g., initial density of material layers, layer thickness, type of section, etc., may be included to provide a set of data for classical statistical analysis using mutivariate methods.

BIBLIOGRAPHY

(1) "A Method for Rating the Condition of Flexible Pavements". Highway Research Board Circular 476, August, 1962.

(2) Adlen, J. H., and R. T. Marshall, "Resilient Response of Granular Materials Subjected to Time-Dependent Lateral Stresses". Highway Research Record 12, December, 1973.

(3) Ali, G. A., R. J. Krizek, and J. O. Osterberg, "Influence of Poisson's Ratio on the Surface Deflection of Layered Systems". Highway Research Record 337, 1970.

(4) "Asphalt Overlays and Pavement Rehabilitation." Asphalt Institute Manual Series No. 17 (MS-17), November, 1969.

(5) "Asphalt Paving Manual." Asphalt Institute Manual Series No. 8 (MS-8), August, 1965.

(6) "Asphalt Surface Treatments and Asphalt Penetration Macadam." Asphalt Institute Manual Series No. 13 (MS-13), November, 1969.

(7) Barksdale, R. D., "Laboratory Evaluation of Rutting in Base Course Materials". Proceedings 3rd International Conference on the Structural Design of Asphalt Pavements, Vol. 1, London, England, 1972.

(8) Barksdale, R. D., and R. G. Hicks, "Material Characterization and Layered Theory for Use in Fatigue Analysis". Highway Research Board Special Report 140, 1973, pp 20-48.

(9) Barksdale, R. D., and G. A. Leonards, "Predicting Performance of Bituminous Surface Pavements". Proceedings 2nd International Conference on Structural Design of Asphalt Pavements, Ann Arbor, Michigan, 1967.

(10) Barr, A. J., et al., A User's Guide to the Statistical Analysis System. North Carolina State University Press, Raleigh, August, 1972.

(11) Beagle, C. W., "A Study of Non-Destructive Methods to Determine the Density of Deep-Lift Asphalt Concrete Base Construction". Association of Asphalt Paving Technologists, Proc. Vol. 39, 1970, pp 671-682.

(12) Benson, F. J., "Effects of Aggregate Shape, Size, and Surface Texture on the Properties of Bituminous Mixtures - A Literature Survey". Highway Research Board Special Report 109, 1970, pp 12-22.

(13) Blight, G. E., "Permanent Deformation in Asphalt Materials". ASCE Journal of Transportation Engineering, Volume 100, No. TE 1, February, 1974.

(14) Bonitzer, J., and P. H. Leger, "Studies on Pavement Design". Proceedings International Conference on Structural Design of Asphalt Pavements, August, 1967.

(15) Britton, W. S. G., "Effects of Aggregate Size, Shape and Surface Texture on the Durability of Bituminous Mixtures". Highway Research Board Special Report 109, 1970, pp 23-24.

(16) Burmister, D. M., "The General Theory of Stresses and Displacements in Layered Systems". Journal of Applied Physics, Vol. 16, 1945, pp 89-302.

(17) Burmister, D. M., "The Theory of Stresses and Displacements in Layered Systems and Application to the Design of Airport Runways". Highway Research Board Proceedings Volume 23, 1943.

(18) Chou, Yu T., and R. L. Hutchinson, "Response of Flexible Pavements to Multiple Loads". ASCE Journal of Transportation Engineering, Proceedings Volume 101 No. TE 2, May, 1975, p 247.

(19) Defoe, J. H., and A. P. Chritz, "Evaluation of Nuclear Method for Asphalt Testing". Highway Research Record Report No. R-745, July, 1970.

(20) Dormon, G. M., "The Extension to Practice of Fundamental Procedure for Design of Asphalt Pavements". University of Michigan Press, 1962.

(21) Drake, W. B., and J. H. Havens, "Re-Evaluation of Kentucky Flexible Pavement Design Criterion". Highway Research Board Bulletin 233, 1959, pp 33-56.

(22) Ellis, D. S., et al., "Thermally Induced Densification of Asphalt Concrete". Proceedings Association of Asphalt Paving Technologists, Vol. 38, February, 1969, p 660.

(23) Elsamny, M. K., and A. A. Ghobarrah, "Stress Field Under Slipping Rigid Wheel". ASCE Journal of Soil Mechanics and Foundations Division, Volume 98 No. SM 1, January, 1972, pp 13-25.

(24) "Evaluation of Studded Tires - Performance Data and Pavement Wear Measurement". Highway Research Board Special Report 61, p 66.

(25) "Factors Influencing Flexible Pavement Performance". Highway Research Board Special Report 22.

(26) Finney, D. J., An Introduction to the Theory of Experimental Design. University of Chicago Press, Chicago, 1960.

(27) Ford, M. C., Jr., "Stripping in Bituminous Mixtures". (Unpublished Ph.D. dissertation, Oklahoma State University, Stillwater, 1973).

(28) Ford, M. C., Jr., and J. R. Bisset, "Flexible Pavement Performance Studies in Arkansas". Highway Research Board Bulletin 321, 1962, pp 1-15.

(29) Foster, C., "Dominant Effect of Fine Aggregate on Strength of Dense-Graded Asphalt Mixes". Highway Research Board Special Report 109, 1968, pp 1-3.

(30) "General Discussion of Effects of Aggregate Size, Shape, and Surface Texture on Properties of Bituminous Mixtures." Highway Research Board Special Report 109, January, 1968, pp 33-41.

(31) Grenshaw, B. M., "Soil-Wheel Interaction at High Speed". Journal of Terra Mechanics, Vol. 8 No. 3, 1972, pp 71-78.

(32) Grey, R. L., "Evaluation of Bituminous Compaction Procedures Using Nuclear Gages". Highway Research Record 361, 1971.

(33) Haas, R. C. G., and W. R. Hudson, "The Importance of Rational and Compatible Pavement Performance Evaluation". Highway Research Record 116, 1971.

(34) Hadley, W. O., et al., "Correlation of Direct Tensile Test Results with Stability and Cohesiometer Values for Asphalt Treated Materials". Proceedings Association of Asphalt Technologists Volume 39, 1970, pp 745-765.

(35) Hofstra, A., and J. G. Klomp, "Permanent Deformation of Flexible Pavements Under Simulated Road Traffic Conditions". Proceedings, 3rd International Conference on Structural Design of Asphalt Pavements, London, England, Volume 1, 1972.

(36) Hout, G. L., et al., "Nuclear Measurement of Bituminous Pavement Densities". Canadian Technological Association, Proceedings Volume II, November, 1966, pp 115-134.

(37) Hveem, F. N., "Pavement Deflections and Fatigue Failures". Highway Research Board Bulletin 114, 1955, pp 43-87.

(38) Hveem, F. N., "Devices for Recording and Evaluating Pavement Roughness". Highway Research Board Bulletin 264, 1960, pp 1-26.

(39) Hudson, W. R., and B. F. McCullough, "Flexible Pavement Design and Management: Systems Formulation". NCHRP Report No. 139, 1973.

(40) Kalcheff, I. V., "Research on Bituminous Concrete Properties With Large-Sized Aggregates of Different Particle Shape". Highway Research Board Special Report 109, 1970, pp 27-32.

(41) Kamel, Nabil, "Developing Structural Design Models for Ontario Pavements". Transportation Research Record 521, 1974, p 60.

(42) Kennedy, T. W., "Tensile and Stochastic Characteristics of Black Base Materials". Highway Research Board Volume 43, No. 12, December, 1973.

(43) Keyser, J. H., "Design Criteria for Wear Resistant Bituminous Pavement Surfaces". (Paper prepared for presentation at the 51st Annual Meeting of the Highway Research Board, 1972.

(44) Keyser, J. H., "The Effect of Studded Tires on the Durability of Road Surfacings". Highway Research Record 331, 1970.

(45) Kirk, G., "Radial and Shear Stress Distribution Under Rigid Wheel and Pneumatic Tires Operating on Yielding Soils with Consideration of Tire Deformation". Journal of Terra Mechanics Volume 6, No. 3, 1969, pp 73-98.

(46) Klomp, A. G. J., and G. M. Dormon, "Stress Distribution and Dynamic Testing in Relation to Road Designing". Proceedings Australian Road Research Board, 1964.

(47) Lambe, T. W., and R. V. Whitman, Soil Mechanics. John Wiley & Sons Book Company, New York, 1969, p 75.

(48) Lee, A. R., and D. Croney, "British Full-Scale Pavement Design Experiments". Proceedings, International Conference on Asphalt Pavements, University of Michigan, August, 1962, pp 114-136.

(49) Leslie, L. K., "Radial and Shear Stresses Under Rigid Wheels". Journal of Terra Mechanics, Volume 7, No. 3 and 4, 1970, pp 117-122.

(50) "Load Carrying Capacity of Roads as Affected by Frost Action". Highway Research Bulletin 40, 1951.

(51) Mack, C., "Physical Properties of Asphalts in Thin Films". Industrial Engineering Chemistry, Volume 49, No. 422, 1957.

(52) Mahone, D. C., and S. N. Runkle, "Pavement Friction Needs". Highway Research Record 396, 1972.

(53) Majidzadeh, K., and M. Herrin, "Modes of Failure and Strength of Asphalt Films Subject to Tensile Stresses". Highway Research Record 67, 1965, pp 98-121.

(54) Majidzadeh, K., and R. R. Stander, Jr., "Effect of Water on Behavior of Sand-Asphalt Mixtures Under Repeated Loadings". Highway Research Record 273, 1969, pp 99-109.

(55) Manke, P. G., and M. C. Ford, Jr., "Evaluation of Bituminous Mixes in Pavement Structures". An Interim Report Presented to the Oklahoma Highway Department, June, 1973.

(56) Manke, P. G., "Asphalt Mix Design Procedures". Laboartory Manual for CIVEN 5653, Department of Civil Engineering, Oklahoma State University, 1970.

(57) Marks, D., and H. O. Ford, "Density of Bituminous Surface Courses". Proceedings, 55th Annual Tennessee Highway Conference, Bulletin No. 40, January, 1974, pp 1-13.

(58) McClean, D. B., et al., "Estimation of Permanent Deformation in Asphaltic Concrete Layers due to Repeated Traffic Loading". Highway Research Abstracts, Volume 43, No. 12, December, 1973.

(59) McLeod, N. W., "Influence of Viscosity of Asphalt Cements on Compaction of Paving Mixtures in the Field". Highway Research Record 158, 1967, pp 76-115.

(60) McNaughton, M. F., "Discussion of Paper by W. H. Campen". Proceedings, American Association of Paving Technologists, Volume 12, 1952, pp 237-254.

(61) "Mix Design Methods for Asphalt Concrete." The Asphalt Institute Manual Series No. 2 (MS-2), 1969.

(62) Monismith, C. L., "Influence of Shape, Size and Surface Texture on the Stiffness and Fatigue Response of Asphalt Mixtures". Highway Research Board, Special Report 109, 1970, pp 4-11.

(63) Morris, J., and R. C. G. Haas, "Designing for Rutting in Asphalt Concrete Pavements". Paper presented at the Annual Conference, Canadian Technical Asphalt Association, Vancouver, November, 1972.

(64) Mylonas, C., and N. A. Bruyne, "Theoretical Investigation of Stresses in Joints". Adhesion and Adhesives, ed. Elsenier Press, Houston, 1951, p 51.

(65) Nair, K., and C. Y. Chang, "Flexible Pavement Design and Management: Materials Characterization". NCHRP Report 140, 1973.

(66) Nicholas, F. P., Jr., "Deflections as an Indicator of Performance of Flexible Pavements". Highway Research Record 13, 1963, pp 44-65.

(67) Norman, O. K., and R. C. Hopkins, "Weighing of Vehicles in Motion". Highway Research Board Bulletin 50, 1952, p 27.

(68) "Oklahoma Drivers Manual". Oklahoma Department of Public Safety, Oklahoma City.

(69) Onafeko, O., and A. R. Reece, "Soil Stresses and Deformations Beneath Rigid Wheels". Journal of Terra Mechanics, Vol. 4, No. 1, 1967, pp 59-80.

(70) "Optimization of Density and Moisture Content Measurements by Nuclear Methods". Highway Research Special Report 125, 1971.

(71) "Pavement Evaluation Using Road Meters". Highway Research Special Report 133, Washington D.C., 1973.

(72) "Pavement Rehabilitation: Materials and Techniques". Highway Research Special Report 9, 1972.

(73) "Pavement Evaluation." Proceedings, American Association of Asphalt Technologists, Volume 38, 1969, p 660.

(74) Please, A., and F. E. Mayer, "Resistance to Plastic Flow of Bituminous Base Courses Made With Gravel Aggregates". Chemistry and Industry, No. 37, 1968, pp 1238-1245.

(75) Porter, H. C., "Permanency of Clay Soil Densification". Texas A & M University Experiment Station, Series 67, 1942.

(76) "Prepared Discussions on Effects of Aggregate Size, Shape and Surface Texture on Properties of Bituminous Mixtures." Highway Research Board Special Report 109, 1970, pp 25-26.

(77) "Present Practices and Techniques Used in Pavement Rehabilitation." NCHRP, Synthesis No. 9, 1972.

(78) Preus, C. K., "Studded Tire Effects on Pavements and Traffic Safety". Highway Research Record 418, 1972, pp 44-54.

(79) Ramsey, W. J., and O. L. Lund, "Experimental Lime Stabilization in Nebraska". Highway Research Record 263, December, 1969, p 9.

(80) Regal, F. V., "Factors Governing Selection of Aggregates: Practice in Missouri". Proceeding, 13th National Asphalt Conference, 1940, pp 181-186.

(81) "Revised Method of Thickness Design for Flexible Highway Pavements at Military Installations". U.S. Army Waterways Experiment Station, TR No. 3-582, August, 1961.

(82) "Rice's Method Measurement of Specific Gravity". ASTM Designation: D2041.

(83) "Roadway Surface Properties". Highway Research Record 28, 1963, p 97.

(84) Rosenthal, P., et al., "Performance Data and Surface Wear Measurements". NCHRP Reports, No. 61 and 66, 1969.

(85) Schonfeld, R., "Photo Interpretation of Skid Resistance". Highway Research Record 311, 1970.

(86) Schonfeld, R., "Skid Numbers from Stereo-Photographs". Ontario Department of Highways, Report No. RR 155, January, 1970.

(87) Shook, J. F., et al., "Use of Loadmeter Data in Designing Pavements for Mixed Traffic". Highway Research Record 42, 1963, pp 41-56.

(88) Shook, J. F., and J. R. Lambrechts, "Performance of Full-Depth Asphalt Bases on San Diego County Experimental Base Project". Transportation Research Record 521, 1974, pp 47-59.

(89) Snedecor, W. J., and W. G. Cochran, Statistical Methods. (6th ed.) Iowa State University Press, 1972.

(90) Spangler, E. B., and W. J. Kelly, "GMR Road Profilometer - A Method for Measuring Road Profile". Highway Research Record 121, 1965, pp 27-54.

(91) "Specific Gravity of Compacted Bituminous Mixtures". ASTM Designation: D2726, 1971.

(92) "Standard Specifications for Highway Construction". Oklahoma State Highway Commission, 1967.

(93) "State of the Art: Compaction of Asphaltic Pavements". Highway Research Special Report 131, Washington, D.C., 1972.

(94) "State of the Art: Compaction of Asphaltic Pavements". Highway Research Board, Special Report No. 131, 1972.

(95) "Tentative Method of Test for Density of Bituminous Concrete in Place by Nuclear Method". ASTM Designation: D2950, March, 1971.

(96) "The AASHO Road Test Report No. 5: Flexible Pavement Research". Highway Research Special Report No. 61 E, 1962, p 60.

(97) "Theoretical Analysis of Structural Behavior of Road Test Flexible Pavements". Highway Research Board Special Report No. 10, p 31.

(98) "Thickness Design for Full Depth Asphalt Pavement Structures for Highways and Streets." Asphalt Institute Manual Series No. 1 (MS-1), December, 1969.

(99) Troxler Laboratories, "Instruction Manual for Series 2400 Compac Surface Moisture/Density Gages". Troxler Electronic Laboratories, Inc., Raleigh, North Carolina.

(100) Volterra, E., and J. H. Gaines, "Beams on Elastic Foundations". Advanced Strength of Materials, Englewood, N.J.: Prentice-Hall, 1971.

(101) Wallace, H. A., and J. R. Martin, "Reconstruction of Old Pavement". Asphalt Pavement Engineering, New York: McGraw-Hill, 1967.

(102) Walker, R. D., et al., "Significance of Layer Deflection Measurements". Highway Research Board, Bulletin 321, 1962, pp 63-81.

(103) "WAASHO Road Test Part 2: Test Data, Analysis, Findings." Highway Research Board, Special Report 22, 1955, p 212.

(104) Wiendick, K. W., "Theoretical Evaluation of the Shear-to-Normal Stress Ratio at the Soil-Wheel Interface". Journal of Terra Mechanics Volume 5, No. 4, 1968, pp 9-25.

(105) Winnitoy, W. E., "Rating Flexible Pavement Surface Condition". Highway Research Record 300, 1969.

(106) Witczak, M. W., and J. F. Shook, "Full-Depth Asphalt Airfield Pavements". Proceedings, ASCE Journal of Transportation Engineering, Vol. 101, No. TE 2, May, 1975, p 297.

(107) Wong, J. Y., and A. R. Reece, "Prediction of Rigid Wheel Performance Based on the Analysis of Soil-Wheel Stresses". Journal of Terra Mechanics Volume 4 No. 1, 1967, Part I, pp 81-95; Volume 4, No. 2, Part II, pp 7-25.

(108) Woods, K. B., "Influence of Heavy Loads on Pavement Design Trends". Proceeding, ASCE Volume 76, 1950, p 3.

(109) Worona, V., "Evaluation of Nuclear Bituminous Pavement Density Gages". Final Report of Phase I, Pennsylvania Department of Highways, Bureau of Public Roads, H RP-PR, March, 1969.

(110) Yoder, E. J., "Performance of Flexible Pavements". Principles of Pavement Design, New York: Wiley & Sons Book Co., 1959.

(111) Yoder, E. J., and R. T. Milhous, "Comparison of Different Methods of Measuring Pavement Condition". Interim Report, NCHRP Report 7, 1964, p 29.

(112) Zube, E., et al., "Service Performance of Cement-Treated Bases Used in Composite Pavements". Highway Research Record 291, 1969.

APPENDIX A

DESCRIPTION OF TEST SITES

TABLE III

DESCRIPTION OF TEST

TEST SITE #	LOCATION	SECTION TYPE	BASE TYPE	AGE (MONTHS)	LOCATION OF MARKER (ORANGE PLATE)
10	Interstate 40, Westbound Lanes, Muskogee,County, Oklahoma, approx. 12.50 miles East of McIntosh County line	Fill	Hot Mix Sand Asphalt	36	North right-of-way fence
20	Interstate 40, Westbound Lanes, Seminole County, Oklahoma, approx. 2.4 miles East of Pottawatomie County line	Fill	Black Base	82	North right-of-way fence
30	Interstate 40, Westbound Lanes, Sequoyah County, Oklahoma, approx. 13.0 miles East of Muskogee County line	Cut	Black Base	56	North right-of way fence
40	Interstate 40, Eastbound Lanes, Sequoyah County, Oklahoma, approx. 12.6 miles East of Muskogee County line	Fill	Black Base	56	South right-of-way fence
50	Interstate 40, Westbound Lanes, Seminole County, Oklahoma, approx. 4.5 miles East of Pottawatomie County line	Slight Cut	Black Base	86	North right-of-way fence
60	Interstate 40, Westbound Lanes, Beckham County, Oklahoma, approx. 19.0 miles East of Texas-Oklahoma State line	Slight Fill	Hot Mix Sand Asphalt	169	North right-of-way fence
70	Interstate 40, Westbound Lanes, Beckham County, Oklahoma, approx. 20.50 miles East of Texas-Oklahoma State line	Slight Fill	Hot Mix Sand Asphalt	169	North right-of-way fence
80	Interstate 35, Southbound Lanes, Kay County, Oklahoma, approx. 25.0 miles North of Noble County line	Slight Fill	Stabilized Aggregate Base Course	165	West right-of-way fence
90	Interstate 35, Southbound Lanes, Kay County, Oklahoma, approx. 26.0 miles North of Noble County line	Slight Fill	Stabilized Aggregate Base Course	165	West right-of-way fence
100	Interstate 35, Southbound Lanes, Cleveland County, Oklahoma, approx. 4.5 miles North of McClain County line	Slight Fill	Stabilized Aggregate Base Course	158	West right-of-way fence
110	Interstate 40, Westbound Lanes, Cleveland County, Oklahoma, approx. 12.0 miles East of Oklahoma County line	Slight Fill	Stabilized Aggregate Base Course	158	West right-of-way fence
120	Interstate 40, Eastbound Lanes, Pottawatomie County, Oklahoma, approx. 12.0 miles East of Oklahoma County line	Slight Fill	HMSA	105	North right-of-way fence
130	Interstate 40, Eastbound Lanes, Washita County, Oklahoma, approx. 9.0 miles East of Beckham County line	Slight Fill	Soil-Cement Base	148	South right-of-way fence
140	Interstate 40, Westbound Lanes, Washita County, Oklahoma, approx. 12.25 miles East of Beckham County line	Fill	Soil-Cement Base	148	North right-of-way fence
170	Interstate 40, Eastbound Lanes, Beckham County, Oklahoma, approx. 26.4 miles East of Texas-Oklahoma State line	Fill	Soil-Cement Base	169	South right-of-way fence
180	Interstate 40, Eastbound Lanes, Beckham County, Oklahoma, approx. 20.25 miles East of Texas-Oklahoma State line	Fill	Soil-Cement Base	196	South right-of-way fence

APPENDIX B

PRESENTATION OF TEST DATA

SITE NO.: 10 LOCATION: I-40 WEST MUSKOGEE CO. MILE 12.50 BASE COURSE TYPE: H.M.S.A. AGE (MONTHS): 36 CROSS-SLOPE (IN/FT): 0.195

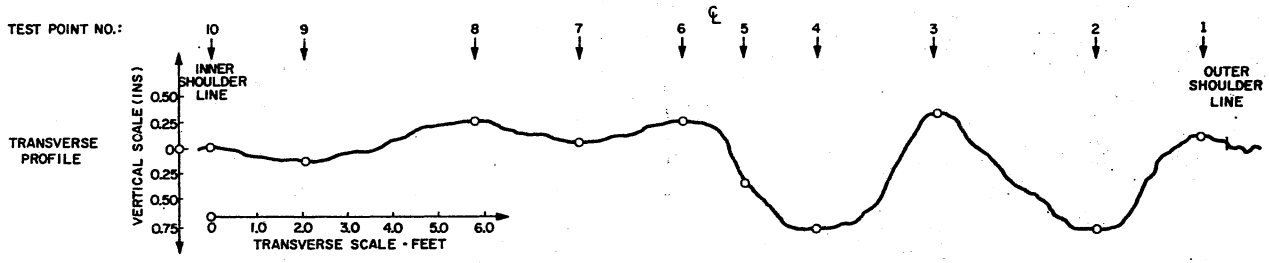

PROFILE MEAS. (INS): ["+" VALUE = RUT, "-" VALUE = HEAVE]	0.00	0.400	-0.400	0.350	0.00	0.350	0.990	-0.500	0.990	-0.200
BULK SP. GRAVITY										
LAYER A	2.27	2.30	2.28	2.31	2.31	2.30	2.31	2.30	2.31	2.31
LAYER B	2.30	2.31	2.30	2.32	2.32	2.30	2.34	2.30	2.34	2.30
LAYER C	2.17	2.34	2.18	2.19	2.18	2.18	2.20	2.18	2.18	2.18
LAYER D	2.21	2.25	2.22	2.26	2.21	2.20	2.21	2.20	2.41	2.20
LAYER E	2.20	2.22	2.20	2.17	1.86	2.16	2.19	2.16	2.19	2.16
RICE'S SP. GRAVITY										
LAYER A	2.33	2.33	2.30	2.33	2.33	2.33	2.33	2.33	2.32	2.33
LAYER B	2.35	2.36	2.35	2.37	2.37	2.33	2.37	2.33	2.36	2.35
LAYER C	2.42	2.43	2.42	2.42	2.41	2.41	2.42	2.41	2.45	2.41
LAYER D	2.41	2.41	2.41	2.40	2.41	2.41	2.41	2.41	2.43	2.41
LAYER E	2.41	2.41	2.41	2.41	2.41	2.41	2.41	2.41	2.41	2.41
PERCENT DENSITY										
LAYER A	97.42	98.70	97.85	99.14	99.14	98.71	99.14	98.71	99.57	99.14
LAYER B	97.90	97.88	97.87	97.89	97.89	98.71	98.73	97.87	99.15	97.87
LAYER C	89.67	96.30	90.08	90.50	90.46	90.46	90.91	90.46	89.00	90.46
LAYER D	91.70	93.36	92.12	94.17	91.70	91.29	91.70	91.28	99.18	91.29
LAYER E	91.28	92.12	91.28	90.04	77.18	89.63	90.87	89.63	90.87	89.63
NUCLEAR DENSITY										
LAYER A (PCF)	125.60	131.10	130.60	134.0	134.30	72.50*	____**	____**	____**	75.50*
ATTRITION [MAX. PROJECTIONS-INCHES]	0.016	0.008	0.016	0.004	0.016	0.008	0.004	0.024	0.016	0.063

* LOW VALUES CONSIDERED UNRELIABLE
** VALUES CONSIDERED ERORNEOUS

Figure 17. Data for Site #10

SITE NO.: 60 LOCATION: I-40 WEST BECKHAM CO MILE 19.0 BASE COURSE TYPE: H.M.S.A. AGE(MONTHS): 169 CROSS-SLOPE(IN/FT): 0.178

TEST POINT NO.:

TRANSVERSE PROFILE

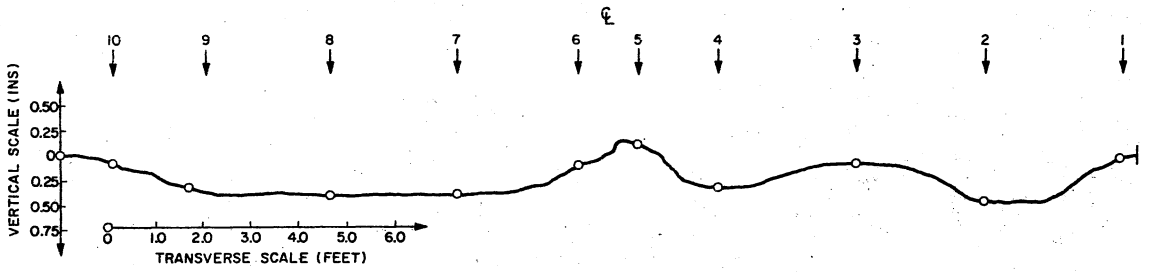

PROFILE MEAS. (INS)
["+" VALUE = RUT
"-" VALUE = HEAVE]

		0.094	0.130	0.214	0.214	0.094	-0.125	0.300	0.078	0.429	0.00
BULK SP. GRAVITY											
	LAYER A	2.34	2.37	2.33	2.38	2.35	2.34	2.46	2.37	2.45	2.40
	LAYER B	2.37	2.41	2.02	2.07	2.42	2.41	2.43	2.39	2.41	2.36
	LAYER C	1.90	1.90	1.60	1.61	1.91	1.92	1.92	1.91	1.92	1.91
	LAYER D	1.90	1.91	1.89	1.60	1.91	1.90	1.91	1.91	1.93	1.91
	LAYER E	1.89	1.92	1.88	1.93	1.90	1.91	1.88	1.90	1.90	1.91
RICE'S SP. GRAVITY											
	LAYER A	2.51	2.48	2.42	2.52	2.52	2.47	2.52	2.50	2.48	2.51
	LAYER B	2.47	2.48	2.46	2.46	2.49	2.48	2.48	2.49	2.50	2.48
	LAYER C	2.42	2.48	2.41	2.44	2.46	2.42	2.23	2.42	2.42	2.43
	LAYER D	2.41	2.35	2.43	2.42	2.47	2.42	2.21	2.43	2.41	2.43
	LAYER E	2.43	2.42	2.39	2.47	2.42	2.41	2.20	2.40	2.38	2.43
PERCENT DENSITY											
	LAYER A	93.23	95.56	96.28	94.44	93.25	94.74	97.62	94.80	98.79	95.62
	LAYER B	95.95	97.18	82.11	84.15	97.19	97.18	97.98	95.98	96.40	95.16
	LAYER C	78.51	76.61	66.40	65.98	77.84	79.34	86.10	78.93	79.34	78.60
	LAYER D	78.84	81.28	77.78	66.12	77.33	78.51	86.43	78.60	80.08	78.60
	LAYER E	77.78	79.34	78.61	78.14	78.51	79.25	85.45	79.17	79.83	78.60
NUCLEAR DENSITY											
	LAYER A	158.00*	155.00*	153.50*	154.30*	157.00*	108.40	154.50	103.50	162.00*	156.00*
ATTRITION (MAX. PROJECTIONS):		0.016	0.002	0.002	0.031	0.008	0.047	0.031	***	***	***

* VALUES CONSIDERED UNRELIABLE
*** BAD PHOTOS

Figure 18. Data for Site #60

SITE NO.: 70 LOCATION: I-40 WEST BECKHAM CO. MILE 20.5 BASE COURSE TYPE: HMSA AGE (MONTHS): 169 CROSS-SLOPE(IN/FT): 0.152

TEST POINT NO.:

TRANSVERSE PROFILE

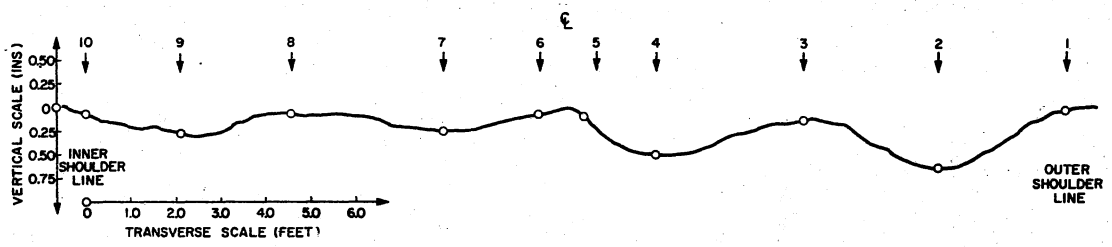

PROFILE MEAS. (INS) ("-" VALUE = RUT, "+" VALUE = HEAVE)										
	0.000	0.143	0.036	0.125	0.000	0.000	0.464	0.125	0.574	0.000
BULK SP. GRAVITY										
LAYER A	2.30	2.35	2.30	2.35	2.30	2.35	2.42	2.34	2.46	2.43
LAYER B	2.34	2.42	2.43	2.43	2.42	2.45	2.43	2.43	2.46	2.43
LAYER C	1.92	1.98	1.96	1.96	1.96	1.97	2.00	2.00	1.99	1.99
LAYER D	1.88	1.92	1.91	1.91	1.90	1.90	1.92	1.94	1.91	1.95
LAYER E	1.88	1.92	1.90	1.89	1.87	1.84	1.84	1.91	1.82	1.85
RICE'S SP. GRAVITY										
LAYER A	2.52	2.51	2.52	2.51	2.52	2.49	2.50	2.50	2.48	2.51
LAYER B	2.49	2.49	2.51	2.50	2.49	2.51	2.52	2.52	2.51	2.52
LAYER C	2.42	2.43	2.43	2.43	2.44	2.43	2.35	2.41	2.44	2.44
LAYER D	2.45	2.43	2.44	2.51	2.44	2.41	2.29	2.39	2.41	2.42
LAYER E	2.40	2.40	2.40	2.47	2.43	2.43	2.30	2.43	2.42	2.41
PERCENT DENSITY										
LAYER A	91.27	93.63	91.27	93.63	91.27	94.38	96.80	93.60	99.18	96.81
LAYER B	93.98	97.19	96.81	97.20	97.19	97.61	96.43	96.43	98.01	96.43
LAYER C	79.34	81.48	80.66	80.66	80.33	81.07	85.11	82.99	81.56	81.56
LAYER D	76.73	79.01	78.28	76.10	77.87	78.84	83.84	81.17	79.25	80.58
LAYER E	78.33	80.00	79.17	76.52	76.95	75.72	80.00	78.60	75.21	76.76
NUCLEAR DENSITY (PCF)										
LAYER A	104.50	104.00	150.50**	92.00**	105.00	154.00**	157.50**	157.00**	158.50**	158.50**
ATTRITION MEAS. (INS) (MAX. PROJECTIONS)	0.006	0.006	0.008	0.008	0.002	***	***	***	***	0.002

** HIGH VALUES CONSIDERED ERRORNEOUS
*** BAD PHOTOS

Figure 19. Data for Site #70

SITE NO.: 120 LOCATION: I-40 WEST POTTAWATOMIE CO. MILE 12.0 BASE COURSE TYPE: H.M.S.A. AGE (MONTHS): 105 CROSS-SLOPE (IN/FT): 0.364

TRANSVERSE PROFILE

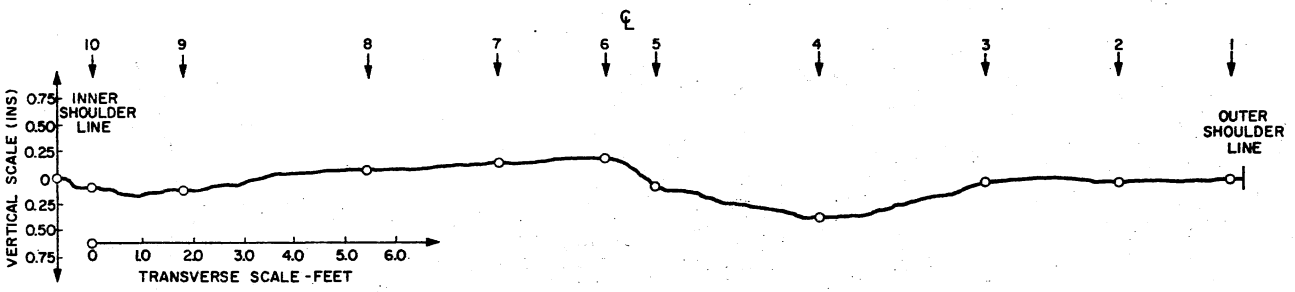

PROFILE MEAS. (INS) ["+" VALUE = RUT, "-" VALUE = HEAVE]	0.000	0.160	0.030	0.000	0.000	0.000	0.380	0.000	0.000	0.000
BULK SP. GRAVITY										
LAYER A	2.15	2.25	2.26	2.32	2.31	2.32	2.38	2.27	2.31	2.23
LAYER B	2.27	2.33	2.30	2.29	2.31	2.26	2.33	2.32	2.33	2.24
LAYER C	1.93	1.95	1.93	1.95	1.91	1.90	1.92	1.91	1.93	1.91
LAYER D	1.95	1.99	1.96	1.97	1.90	1.88	1.91	1.90	1.91	1.89
LAYER E	1.93	1.93	1.93	1.93	1.89	1.92	1.93	1.94	1.94	1.91
RICE'S SP. GRAVITY										
LAYER A	2.44	2.44	2.45	2.42	2.49	2.49	2.42	2.41	2.38	2.38
LAYER B	2.42	2.43	2.41	2.40	2.41	2.39	2.41	2.40	2.39	2.41
LAYER C	2.44	2.44	2.44	2.44	2.43	2.44	2.43	2.43	2.43	2.43
LAYER D	2.43	2.42	2.42	2.43	2.42	2.42	2.44	2.42	2.42	2.45
LAYER E	2.43	2.40	2.43	2.44	2.43	2.42	2.44	2.41	2.42	2.44
PERCENT DENSITY										
LAYER A	88.11	92.21	92.24	95.87	92.77	93.17	98.35	94.19	97.06	93.70
LAYER B	93.80	95.88	95.44	95.42	95.85	94.56	96.68	96.67	97.49	92.95
LAYER C	79.10	79.92	79.10	79.92	78.60	77.87	79.01	78.60	79.42	78.60
LAYER D	80.25	82.23	80.99	81.07	78.51	77.69	78.28	78.51	78.93	77.14
LAYER E	79.42	80.41	79.42	79.10	77.78	79.34	79.10	80.50	80.17	78.28
NUCLEAR DENSITY (PCF)										
LAYER A	149.68	150.95	148.00	151.30	152.05	154.17	155.92	152.92	153.80	147.18
ATTRITION MEAS. (INS) (MAX. PROJECTIONS)	0.094	0.047	0.024	0.008	0.016	0.031	0.002	0.016	0.002	0.031

Figure 20. Data for Site #120

SITE NO.: 50 LOCATION: I-40 WEST SEMINOLE CO. MILE 4.5 BASE COURSE TYPE: B.B. AGE (MONTHS): 86 CROSS-SLOPE (IN/FT): 0.275

TEST POINT NO.: 10 9 8 7 6 5 4 3 2 1

TRANSVERSE PROFILE

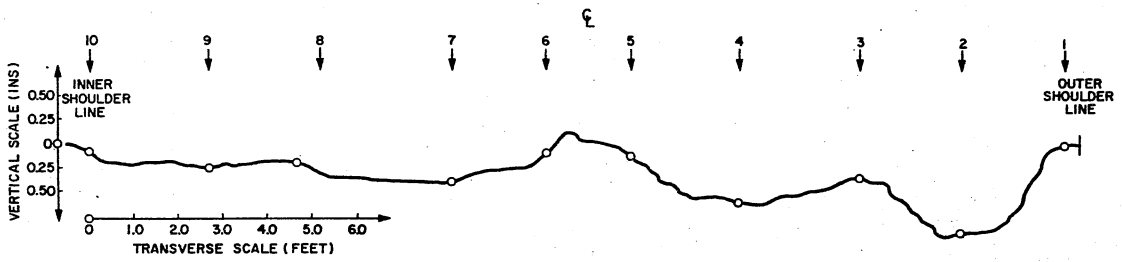

PROFILE MEAS. (INS) ["+" VALUE = RUT "-" VALUE = HEAVE]	0.00	0.090	0.054	0.232	0.00	0.094	0.464	0.411	0.786	0.00
BULK SP. GRAVITY										
LAYER A	2.24	2.27	2.27	2.24	2.25	2.26	2.28	2.26	2.27	2.26
LAYER B	2.22	2.25	2.23	2.23	2.23	2.23	2.26	2.22	2.23	2.23
LAYER C	2.18	2.16	2.19	2.12	2.11	2.20	2.17	2.13	2.19	2.15
LAYER D	2.21	2.23	2.23	2.22	2.20	2.22	2.24	2.21	2.22	2.21
LAYER E	2.20	2.23	2.20	2.22	2.20	2.20	2.22	2.22	2.19	2.20
RICE'S SP. GRAVITY										
LAYER A	2.43	2.45	2.43	2.44	2.43	2.40	2.41	2.45	2.42	2.41
LAYER B	2.47	2.44	2.49	2.43	2.46	2.48	2.45	2.45	2.44	2.44
LAYER C	2.47	2.43	2.48	2.42	2.42	2.46	2.44	2.41	2.44	2.43
LAYER D	2.48	2.48	2.48	2.48	2.44	2.47	2.46	2.42	2.47	2.42
LAYER E	2.48	2.48	2.48	2.48	2.44	2.45	2.44	2.45	2.42	2.45
PERCENT DENSITY										
LAYER A	92.18	92.65	93.42	91.80	92.59	94.17	94.61	92.24	93.80	93.78
LAYER B	89.88	92.21	89.56	91.77	90.65	91.13	92.24	90.61	91.39	91.39
LAYER C	88.26	88.89	88.31	87.60	87.19	89.43	88.93	88.38	89.75	88.48
LAYER D	89.11	89.92	89.92	89.52	90.16	89.88	91.06	91.32	89.88	91.32
LAYER E	88.71	89.92	88.71	89.52	90.16	89.80	90.98	89.80	90.50	89.80
NUCLEAR DENSITY										
LAYER A	143.00	145.50	144.50	147.50	140.50	120.20	143.50	126.00	148.50	145.00
ATTRITION (INS) [MAX. PROJECTIONS]	0.016	0.023	0.016	0.016	0.031	0.078	0.094	***	***	***

*** BAD PHOTOS

Figure 21. Data for Site #50

SITE NO.: 20 LOCATION: I-40 WEST SEMINOLE CO. MILE 240 BASE COURSE TYPE: B.B. AGE (MONTHS): 82 CROSS-SLOPE (IN/FT): 0.270

TEST POINT NO.:

TRANSVERSE PROFILE

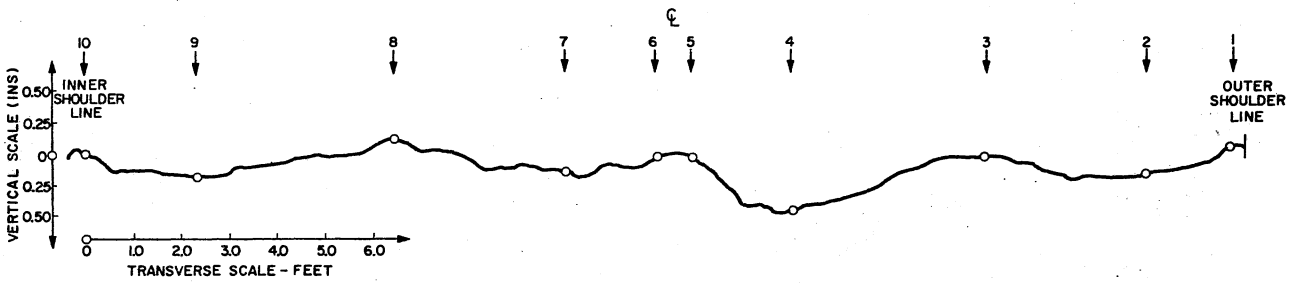

PROFILE MEAS. (INS) ["+" VALUE = RUT, "-" VALUE = HEAVE]	0.00	0.170	-0.054	0.161	0.00	0.00	0.571	0.078	0.250	0.00
BULK SP. GRAVITY										
LAYER A	2.40	2.44	2.41	2.34	2.40	2.41	2.43	2.42	2.44	2.40
LAYER B	2.18	2.25	2.22	2.20	2.18	2.22	2.24	2.23	2.22	2.20
LAYER C	2.20	2.25	2.26	2.25	2.24	2.23	2.19	2.19	2.28	2.19
LAYER D	2.21	2.37	2.22	2.25	2.28	2.34	2.21	2.19	2.22	2.22
LAYER E	2.30	2.27	2.21	2.27	2.37	2.30	2.20	2.18	2.22	2.22
RICE'S SP. GRAVITY										
LAYER A	2.45	2.45	2.44	2.44	2.46	2.45	2.45	2.46	2.45	2.45
LAYER B	2.47	2.48	2.44	2.44	2.45	2.44	2.46	2.47	2.44	2.45
LAYER C	2.43	2.46	2.44	2.44	2.46	2.44	2.44	2.45	2.45	2.40
LAYER D	2.41	2.47	2.42	2.44	2.46	2.47	2.44	2.47	2.42	2.44
LAYER E	2.47	2.46	2.42	2.45	2.47	2.45	2.44	2.44	2.42	2.45
PERCENT DENSITY										
LAYER A	97.96	99.59	98.77	95.90	97.56	98.37	99.18	98.37	99.59	97.96
LAYER B	88.26	90.73	90.98	90.16	88.98	90.98	91.06	90.28	90.98	89.80
LAYER C	90.54	91.46	92.62	92.21	91.06	91.39	89.75	89.39	93.06	91.25
LAYER D	91.70	95.18	91.74	92.21	92.68	94.74	90.57	88.66	91.74	90.98
LAYER E	93.12	92.28	91.32	92.65	95.95	93.88	90.16	89.34	91.74	90.61
NUCLEAR DENSITY (P.C.F.)										
LAYER A	80.00*	79.0 *	138.00	81.00*	130.50	___**	139.50	87.00*	79.50*	133.50
ATTRITION										
MAX. PROJ. (INS)	___***	0.016	0.008	___***	0.032	0.004	0.079	0.008	___***	___***

* LOW VALUES CONSIDERED UNRELIABLE
** VALUES CONSIDERED ERRORNEOUS
*** BAD PHOTOS

Figure 22. Data for Site #20

SITE NO.: 30 LOCATION: I-40 WEST SEQUOYAH CO. MILE 13.0 BASE COURSE TYPE: B.B. AGE (MONTHS): 56 CROSS-SLOPE (IN/FT): 0.208

TEST POINT NO.: 10 9 8 7 6 ℄ 5 4 3 2 1

TRANSVERSE PROFILE

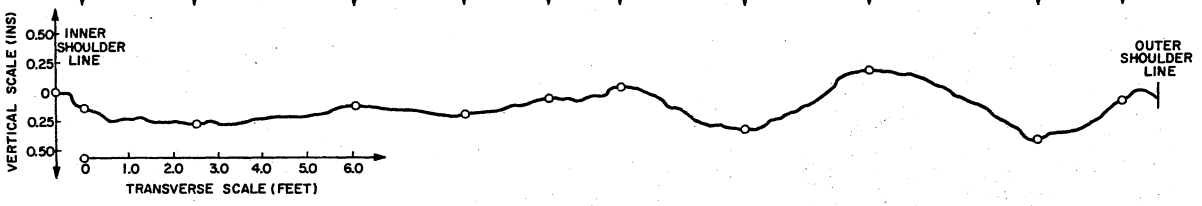

PROFILE MEAS. (INS) ["+" VALUE = RUT "-" VALUE = HEAVE]	0.00	0.250	0.125	0.146	0.070	-0.094	0.536	-0.233	0.607	-0.042
BULK SP. GRAVITY										
LAYER A	2.24	2.27	2.23	2.16	2.23	2.30	2.31	2.30	2.31	2.30
LAYER B	2.21	2.25	2.30	2.24	2.26	2.28	2.31	2.29	2.32	2.29
LAYER C	2.22	2.24	2.30	2.24	2.30	2.09	2.34	2.28	2.34	2.29
LAYER D	2.25	2.25	2.30	2.18	2.25	2.25	2.34	2.25	2.34	2.25
LAYER E	2.26	2.26	2.26	2.22	2.26	2.26	2.20	2.26	2.20	2.26
RICE'S SP. GRAVITY										
LAYER A	2.34	2.32	2.32	2.29	2.33	2.33	2.32	2.32	2.32	2.32
LAYER B	2.36	2.33	2.34	2.33	2.37	2.36	2.37	2.37	2.34	2.37
LAYER C	2.36	2.35	2.37	2.35	2.37	2.36	2.36	2.34	2.36	2.36
LAYER D	2.36	2.36	2.36	2.36	2.36	2.36	2.36	2.36	2.36	2.36
LAYER E	2.34	2.34	2.34	2.34	2.34	2.34	2.32	2.34	2.32	2.34
PERCENT DENSITY										
LAYER A	95.73	97.84	96.12	94.32	95.71	98.71	99.57	99.14	99.57	99.14
LAYER B	93.64	96.57	98.29	96.14	95.36	96.61	97.47	96.62	99.14	96.62
LAYER C	94.07	95.32	97.05	95.32	97.05	88.56	99.15	97.43	99.15	97.03
LAYER D	95.34	95.34	97.46	92.37	95.34	95.34	99.15	95.34	99.15	95.34
LAYER E	96.58	96.58	96.58	94.87	96.58	96.58	94.83	96.58	94.83	96.58
NUCLEAR DENSITY										
LAYER A	107.50	124.00	111.00	116.20	115.70	126.00	127.50	130.50	131.20	129.00
ATTRITION (INS) [MAX. PROJECTION]	***	***	***	***	***	***	***	***	***	***

*** BAD PHOTOS

Figure 23. Data for Site #30

SITE NO.: 40 LOCATION: I-40 EAST SEQUOYAH CO. MILE 12.6 BASE COURSE TYPE: B.B. AGE (MONTHS): 56 CROSS-SLOPE (IN/FT): 0.225

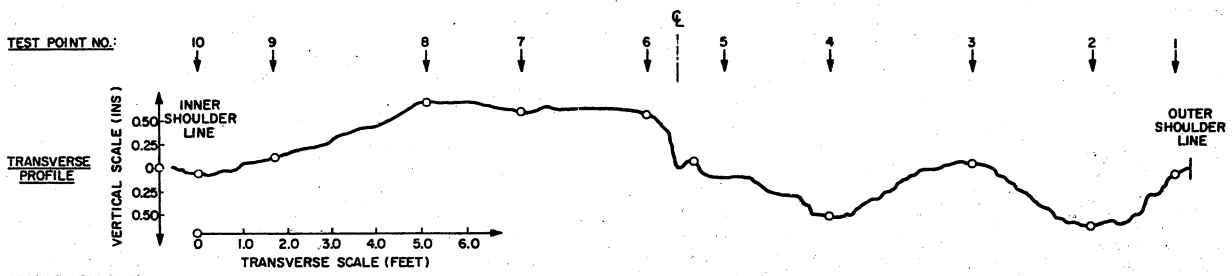

PROFILE MEAS. (INS) ["+" VALUE = RUT, "-" VALUE = HEAVE]	0.031	0.233	0.00	0.094	0.00	-0.078	0.607	-0.078	0.643	0.00
BULK SP. GRAVITY										
LAYER A	2.22	2.28	2.25	2.28	2.27	2.24	2.35	2.27	2.30	2.30
LAYER B	2.15	2.17	2.17	2.21	2.15	2.24	2.29	2.25	2.28	2.24
LAYER C	2.23	2.24	2.22	2.24	2.24	2.29	2.30	2.29	2.31	2.27
LAYER D	2.20	2.19	2.25	2.25	2.22	2.20	2.22	2.20	2.22	2.21
LAYER E	2.18	2.19	2.25	2.25	2.18	2.20	2.18	2.20	2.18	2.21
RICE'S SP. GRAVITY										
LAYER A	2.45	2.44	2.42	2.43	2.44	2.43	2.44	2.45	2.45	2.43
LAYER B	2.30	2.31	2.32	2.32	2.32	2.31	2.36	2.32	2.32	2.31
LAYER C	2.36	2.35	2.35	2.37	2.37	2.39	2.39	2.38	2.38	2.39
LAYER D	2.37	2.36	2.36	2.37	2.34	2.36	2.34	2.36	2.34	2.37
LAYER E	2.35	2.36	2.36	2.37	2.37	2.36	2.37	2.36	2.37	2.37
PERCENT DENSITY										
LAYER A	90.61	93.44	92.98	93.83	93.03	92.18	96.31	92.65	93.98	94.65
LAYER B	93.48	93.94	93.53	95.26	92.67	96.97	97.03	98.98	98.28	96.97
LAYER C	94.49	95.32	94.47	94.51	94.51	95.82	96.23	96.22	97.06	95.00
LAYER D	92.83	92.80	95.34	94.94	94.87	93.22	94.87	93.22	94.87	93.25
LAYER E	92.77	92.80	95.34	94.94	91.98	93.22	91.98	93.22	91.98	93.25
NUCLEAR DENSITY (PCF)										
LAYER A	131.60	136.00	135.50	136.50	134.00	132.00	140.50	139.00	140.50	135.10
ATTRITION (INS.) [MAX. PROJECTIONS]	0.002	***	***	0.008	***	0.032	0.016	0.008	***	0.002

*** BAD PHOTOS

Figure 24. Data for Site #40

SITE NO.: 80 LOCATION: I-35 SOUTH KAY CO. MILE: 25.0 BASE COURSE TYPE: S.A.B.C. AGE(MONTHS): 165 CROSS-SLOPE(IN/FT): 0.205

TRANSVERSE PROFILE

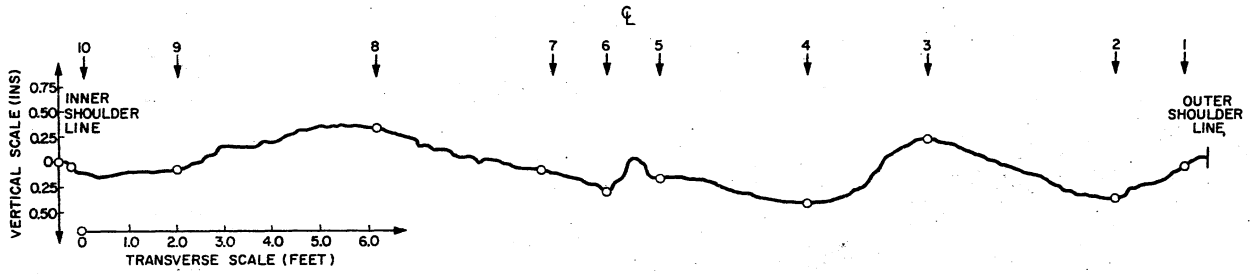

PROFILE MEAS. (INS) ["+" VALUE = RUT "-" VALUE = HEAVE]	0.000	0.125	0.000	0.196	0.000	0.000	0.571	-0.200	0.482	0.000
BULK SP. GRAVITY										
LAYER A	2.16	2.27	2.23	2.37	2.25	2.29	2.32	2.31	2.31	2.19
LAYER B	2.33	2.40	2.33	2.41	2.34	2.35	2.35	2.36	2.35	2.35
LAYER C										
LAYER D										
LAYER E										
RICE'S SP. GRAVITY										
LAYER A	2.39	2.39	2.38	2.40	2.38	2.45	2.39	2.39	2.39	2.39
LAYER B	2.45	2.46	2.40	2.45	2.41	2.41	2.39	2.41	2.39	2.38
LAYER C										
LAYER D										
LAYER E										
PERCENT DENSITY										
LAYER A	90.38	94.98	93.70	98.75	94.54	93.47	97.07	96.65	96.65	91.63
LAYER B	95.10	97.56	97.08	98.37	97.10	97.51	98.32	97.93	98.33	98.74
LAYER C										
LAYER D										
LAYER E										
NUCLEAR DENSITY (PCF)										
LAYER A	82.00*	141.00	144.00	93.80*	142.60	146.50	151.50	101.20	149.50	87.00*
ATTRITION MEAS. (INS) (MAX. PROJECTION)	0.047	0.062	0.062	0.078	0.078	0.047	0.031	0.016	0.047	0.031

* LOW VALUES CONSIDERED UNRELIABLE

NB: NON-BITUMINOUS MATERIALS EXCLUDED

Figure 25. Data for Site #80

SITE NO.: 90 LOCATION: I-35 SOUTH, KAY CO. MILE 26.0 BASE COURSE TYPE: S.A.B.C. AGE (MONTHS): 165 CROSS-SLOPE (IN/FT): 0.296

TEST POINT NO.: 10 9 8 7 6 ℄ 5 4 3 2 1

TRANSVERSE PROFILE

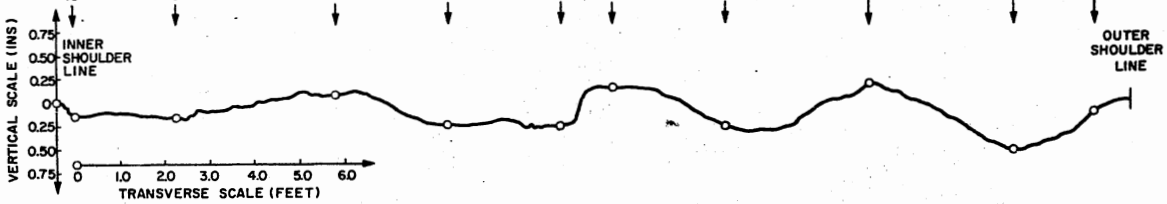

PROFILE MEAS. (INS.) ("+" VALUE = RUT, "-" VALUE = HEAVE)	0.000	0.116	-0.054	0.161	0.000	-0.167	0.500	-0.250	0.625	0.000
BULK SP. GRAVITY										
LAYER A	2.20	2.24	2.23	2.26	2.24	2.23	2.30	2.26	2.30	2.28
LAYER B	2.33	2.34	2.33	2.34	2.34	2.32	2.35	2.34	2.37	2.36
LAYER C										
LAYER D										
LAYER E										
RICE'S SP. GRAVITY										
LAYER A	2.40	2.40	2.40	2.40	2.41	2.39	2.40	2.40	2.40	2.40
LAYER B	2.44	2.44	2.44	2.45	2.45	2.44	2.44	2.45	2.44	2.44
LAYER C										
LAYER D										
LAYER E										
PERCENT DENSITY										
LAYER A	91.67	93.33	92.92	94.17	92.95	93.31	95.83	94.17	95.83	95.00
LAYER B	95.49	95.90	95.49	95.51	95.51	95.08	96.31	95.51	97.13	96.72
LAYER C										
LAYER D										
LAYER E										
NUCLEAR DENSITY										
LAYER A	139.50	87.00**	91.50*	87.00*	140.00	86.80*	95.00*	138.50	84.00*	98.50*
ATTRITION MEAS. (INS) (MAX. PROJECTIONS)	0.070	0.031	0.008	0.031	0.078	0.109	0.031	0.016	0.008	0.078

* VALUES CONSIDERED UNRELIABLE

Figure 26. Data for Site #90

SITE NO.: 100 LOCATION: I-35 SOUTH CLEVELAND CO. MILE 4.5 BASE COURSE TYPE: S.A.B.C. AGE (MONTHS): 158 CROSS-SLOPE (IN/FT): 0.27

TEST POINT NO.: 10 9 8 7 6 ℄ 5 4 3 2 1

TRANSVERSE PROFILE

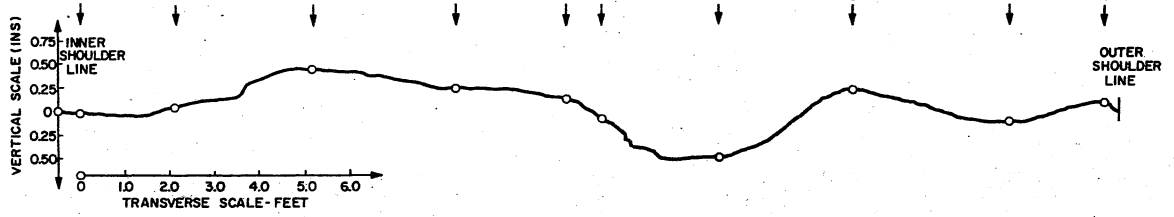

PROFILE MEAS. (INS) ["+" VALUE = RUT, "-" VALUE = HEAVE]	0.000	0.200	0.000	0.078	0.000	0.000	0.607	-0.232	0.250	-0.094
BULK SP. GRAVITY										
LAYER A	2.31	2.35	2.29	2.36	2.33	2.33	2.39	2.38	2.40	2.39
LAYER B	2.32	2.36	2.39	2.40	2.27	2.36	2.41	2.38	2.39	2.32
LAYER C										
LAYER D										
LAYER E										
RICE'S SP. GRAVITY										
LAYER A	2.44	2.43	2.43	2.42	2.47	2.44	2.42	2.43	2.43	2.44
LAYER B	2.44	2.44	2.44	2.43	2.38	2.48	2.46	2.47	2.44	2.45
LAYER C										
LAYER D										
LAYER E										
PERCENT DENSITY										
LAYER A	94.67	96.71	94.24	97.52	94.33	95.49	98.76	97.94	98.77	97.95
LAYER B	95.08	96.72	97.95	98.77	95.38	95.16	97.97	96.36	97.95	94.69
LAYER C										
LAYER D										
LAYER E										
NUCLEAR DENSITY (PCF)										
LAYER A	150.50	155.00	103.00	85.50*	106.50	150.70	152.70	152.00	157.00	115.50
ATTRITION MEAS. (INS) (MAX. PROJECTIONS)	***	***	***	***	***	***	***	***	***	***

* LOW VALUES CONSIDERED UNRELIABLE
*** BAD PHOTOS
NB: NON-BITUMINOUS MATERIALS EXCLUDED

Figure 27. Data for Site #100

SITE NO.: 110 LOCATION: I-35 SOUTH CLEVELAND CO. MILE 4.75 BASE COURSE TYPE: S.A.B.C. AGE(MONTHS): 158 CROSS-SLOPE(IN/FT): 0.202

TEST POINT NO.: 10 9 8 7 6 5 4 3 2 1

TRANSVERSE PROFILE

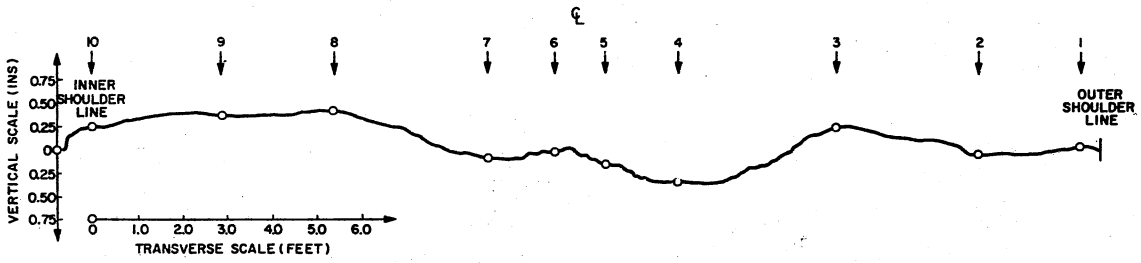

PROFILE MEAS. (INS) ["+" VALUE = RUT, "-" VALUE = HEAVE]										
	0.000	0.047	0.000	0.250	-0.031	0.000	0.482	-0.214	0.200	-0.031
BULK SP. GRAVITY										
LAYER A	2.40	2.41	2.35	2.41	2.30	2.32	2.37	2.36	2.38	2.36
LAYER B	2.26	2.33	2.27	2.32	2.30	2.31	2.43	2.40	2.38	2.36
LAYER C										
LAYER D										
LAYER E										
RICE'S SP. GRAVITY										
LAYER A	2.48	2.47	2.49	2.49	2.46	2.48	2.43	2.44	2.42	2.44
LAYER B	2.44	2.45	2.43	2.44	2.43	2.43	2.50	2.48	2.47	2.48
LAYER C										
LAYER D										
LAYER E										
PERCENT DENSITY										
LAYER A	96.77	97.57	94.38	96.79	93.50	93.55	97.53	96.72	98.35	96.72
LAYER B	92.62	95.10	93.42	95.08	94.65	95.06	97.20	96.77	96.36	95.16
LAYER C										
LAYER D										
LAYER E										
NUCLEAR DENSITY (PCF)										
LAYER A	156.30	154.48	155.40	157.50	150.00	79.90*	155.80	156.67	156.45	153.35
ATTRITION MEAS. (INS) (MAX. PROJECTIONS)	***	***	***	***	***	***	***	***	***	***

* LOW VALUES CONSIDERED UNRELIABLE
*** BAD PHOTOS

Figure 28. Data for Site #110

SITE NO.: 130 LOCATION: I-40 EAST WASHITA CO. MILE: 9.0 BASE COURSE TYPE: S.C.B. AGE (MONTHS): 148 CROSS-SLOPE (IN/FT): 0.165

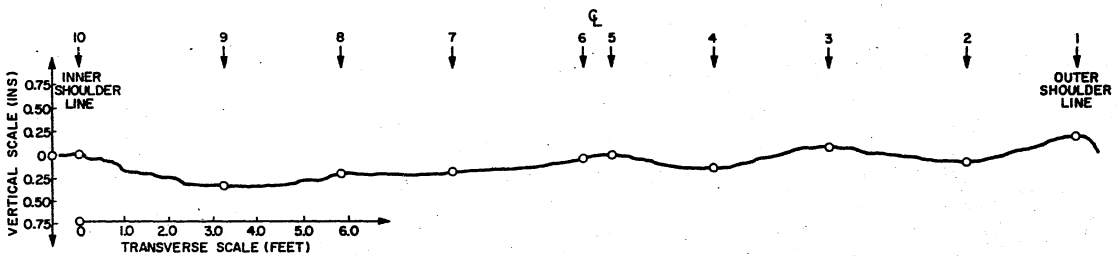

PROFILE MEAS. (INS) ["+" VALUE = RUT, "-" VALUE = HEAVE]	0.000	0.200	0.183	0.097	0.000	0.000	0.200	-0.062	0.219	-0.184
BULK SP. GRAVITY										
LAYER A	2.30	2.35	2.34	2.36	2.35	2.40	2.42	2.38	2.42	2.37
LAYER B	2.45	2.46	2.42	2.46	2.45	2.44	2.46	2.42	2.43	2.41
LAYER C										
LAYER D										
LAYER E										
RICE'S SP. GRAVITY										
LAYER A	2.48	2.47	2.48	2.47	2.48	2.48	2.48	2.48	2.48	2.47
LAYER B	2.50	2.51	2.50	2.50	2.50	2.53	2.51	2.50	2.49	2.51
LAYER C										
LAYER D										
LAYER E										
PERCENT DENSITY										
LAYER A	92.74	95.14	94.35	95.55	94.76	96.77	97.58	95.97	97.58	95.95
LAYER B	98.00	98.01	98.60	98.40	98.00	96.44	98.01	96.80	97.59	96.02
LAYER C										
LAYER D										
LAYER E										
NUCLEAR DENSITY (PCF)										
LAYER A	152.20	152.67	149.45	151.77	151.40	156.42	158.05	156.42	160.17	157.67
ATTRITION MEAS. (INS) (MAX. PROJECTIONS)	***	***	***	***	***	***	***	***	***	***

*** BAD PHOTOS
NB: NON-BITUMINOUS MATERIALS EXCLUDED

Figure 29. Data for Site #130

SITE NO.: 140 LOCATION: I-40 WEST WASHITA CO. MILE 12.25 BASE COURSE TYPE: S.C.B. AGE (MONTHS): 148 CROSS-SLOPE (IN/FT): 0.358

TEST POINT NO.:

TRANSVERSE PROFILE

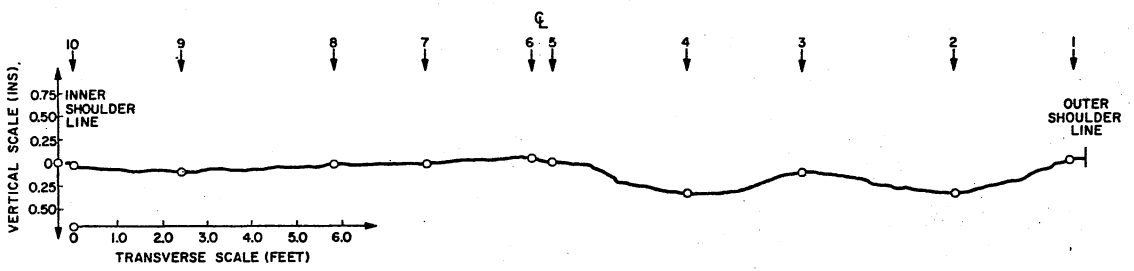

PROFILE MEAS. (INS) ["+" VALUE = RUT, "-" VALUE = HEAVE]	0.000	0.098	0.000	0.043	-0.030	0.000	0.257	0.183	0.289	0.000
BULK SP. GRAVITY										
LAYER A	2.28	2.31	2.28	2.31	2.31	2.36	2.44	2.41	2.44	2.41
LAYER B	2.37	2.39	2.36	2.42	2.42	2.38	2.45	2.40	2.44	2.43
LAYER C										
LAYER D										
LAYER E										
RICE'S SP. GRAVITY										
LAYER A	2.49	2.48	2.48	2.48	2.49	2.48	2.48	2.47	2.48	2.48
LAYER B	2.50	2.50	2.50	2.50	2.50	2.49	2.50	2.50	2.48	2.48
LAYER C										
LAYER D										
LAYER E										
PERCENT DENSITY										
LAYER A	91.57	93.15	91.94	93.15	92.77	95.16	98.39	97.57	98.39	97.17
LAYER B	94.80	95.60	94.40	96.80	96.80	95.58	98.00	96.00	98.39	97.98
LAYER C										
LAYER D										
LAYER E										
NUCLEAR DENSITY (PCF)										
LAYER A	148.43	152.05	150.92	150.42	152.05	152.83	160.07**	159.25**	161.32**	157.57**
ATTRITION MEAS. (INS) (MAX. PROJECTIONS)	0.002	0.008	0.003	0.006	0.0	0.03	0.016	0.008	0.016	0.003

** HIGH VALUES CONSIDERED ERRORNEOUS

Figure 30. Data for Site #140

SITE NO.: 170 LOCATION: I-40 EAST BECKHAM CO., MILE: 26.4 BASE COURSE TYPE: S.C.B. AGE(MONTHS): 169 CROSS-SLOPE(INS/FT): 0.214

TEST POINT NO.: 10 9 8 7 6 ℄ 5 4 3 2 1

TRANSVERSE PROFILE

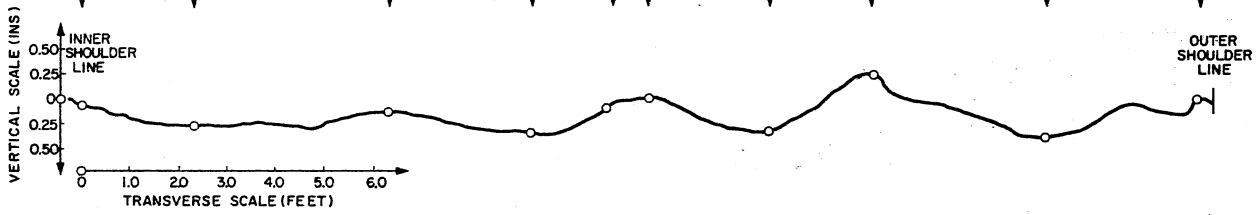

PROFILE MEAS. (INS.) ["+" VALUE = RUT, "-" VALUE = HEAVE]	0.000	0.200	0.125	0.300	0.000	-0.030	0.500	-0.250	0.500	-0.125
BULK SP. GRAVITY										
LAYER A	2.37	2.43	2.42	2.41	2.39	2.42	2.43	2.43	2.43	2.40
LAYER B	2.36	2.39	2.41	2.40	2.37	2.39	2.45	2.43	2.44	2.41
LAYER C										
LAYER D										
LAYER E										
RICE'S SP. GRAVITY										
LAYER A	2.48	2.48	2.49	2.49	2.48	2.48	2.47	2.49	2.47	2.49
LAYER B	2.46	2.45	2.49	2.48	2.49	2.49	2.49	2.48	2.48	2.48
LAYER C										
LAYER D										
LAYER E										
PERCENT DENSITY										
LAYER A	95.56	97.98	97.19	96.79	96.37	97.58	98.38	97.59	98.38	96.39
LAYER B	95.94	97.55	96.79	96.77	95.18	95.98	98.39	97.98	98.39	97.18
LAYER C										
LAYER D										
LAYER E										
NUCLEAR DENSITY (PCF)										
LAYER A	159.25*	162.60*	163.97*	157.57*	162.20*	163.45*	162.60*	165.65*	164.35*	162.20*
ATTRITION MEAS. (INS) (MAX. PROJECTIONS)	0.016	0.047	0.003	0.031	0.008	0.047	0.008	0.000	0.002	0.003

* HIGH VALUES CONSIDERED UNRELIABLE

Figure 31. Data for Site #170

SITE NO.: 180 LOCATION: I-40 EAST BECKHAM CO. MILE 20.25 BASE COURSE TYPE: SCB AGE (MONTHS): 169 CROSS-SLOPE (IN/FT): 0.183

TEST POINT NO.:

TRANSVERSE PROFILE

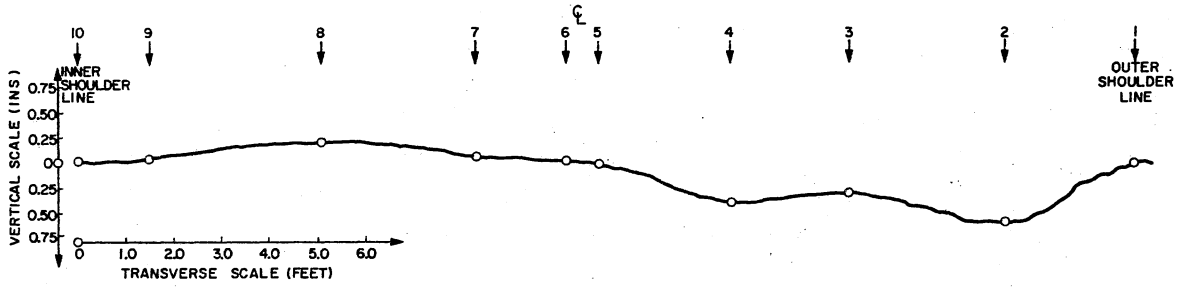

PROFILE MEAS. (INS) ["+" VALUE = RUT, "-" VALUE = HEAVE]	0.000	0.055	0.00	0.043	0.000	0.000	0.289	0.217	0.478	0.000
BULK SP. GRAVITY										
LAYER A	2.35	2.38	2.32	2.34	2.33	2.36	2.43	2.38	2.43	2.32
LAYER B	2.40	2.43	2.40	2.41	2.41	2.43	2.47	2.45	2.47	2.41
LAYER C										
LAYER D										
LAYER E										
RICE'S SP. GRAVITY										
LAYER A	2.51	2.50	2.49	2.47	2.51	2.49	2.50	2.50	2.48	2.51
LAYER B	2.50	2.51	2.50	2.51	2.53	2.52	2.49	2.50	2.50	2.50
LAYER C										
LAYER D										
LAYER E										
PERCENT DENSITY										
LAYER A	93.63	95.20	93.17	94.74	92.83	94.78	97.20	95.20	97.98	92.43
LAYER B	96.00	96.81	96.00	96.02	95.26	96.43	99.20	98.00	98.80	96.40
LAYER C										
LAYER D										
LAYER E										
NUCLEAR DENSITY (PCF)										
LAYER A	156.67	159.25*	155.92*	156.67*	153.42*	157.05	160.07*	158.42*	160.42*	155.42*
ATTRITION MEAS. (INS) (MAX. PROJECTIONS)	0.062	0.040	0.031	0.047	0.016	0.062	0.031	0.016	0.031	0.016

* HIGH VALUES CONSIDERED UNRELIABLE

Figure 32. Data for Site #180

APPENDIX C

COMPUTER ANALYSIS OF TEST DATA

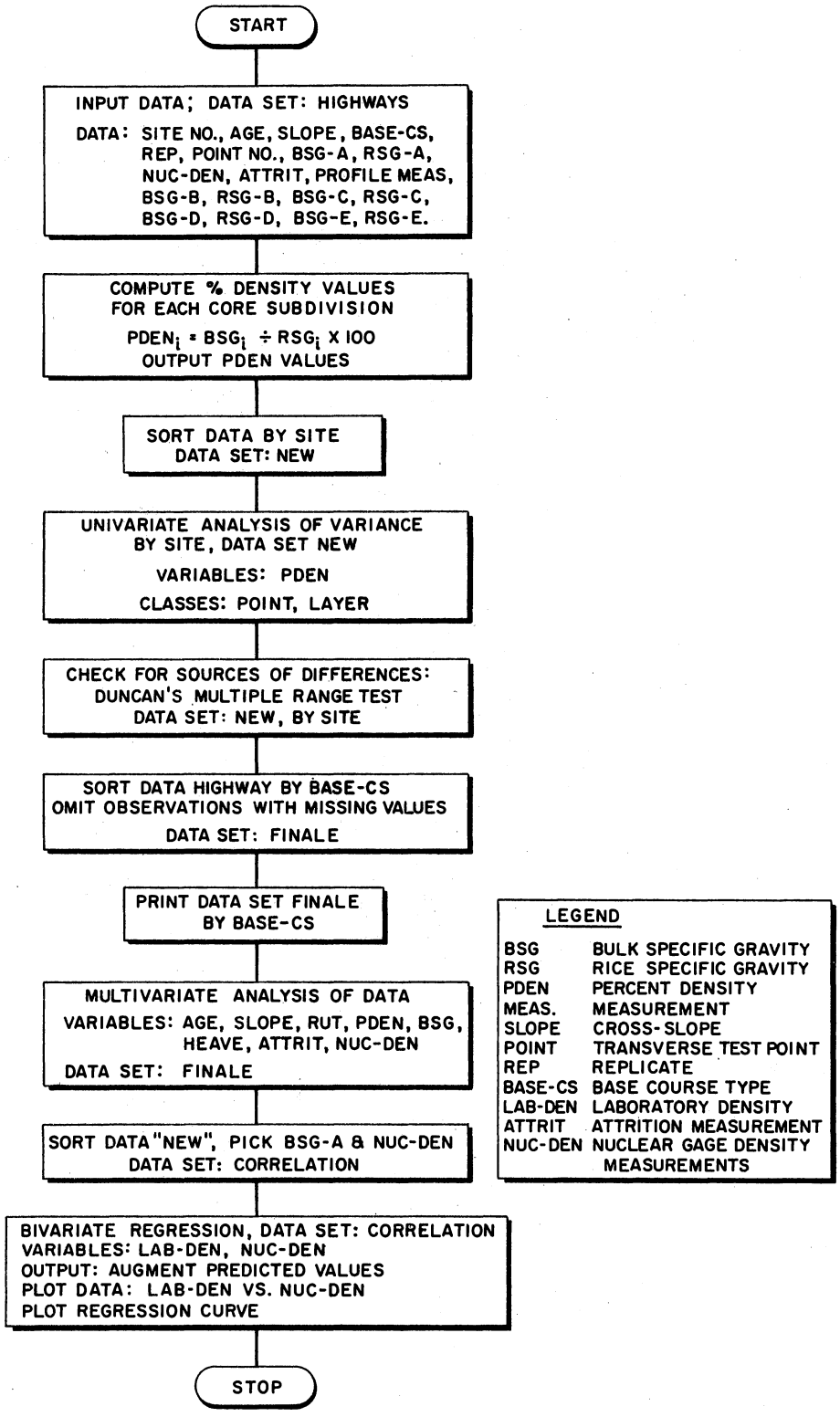

Figure 33. Flow Diagram: Computer Analysis of Test Data Using the SAS Computer Program

APPENDIX D

DENSITY CURVES

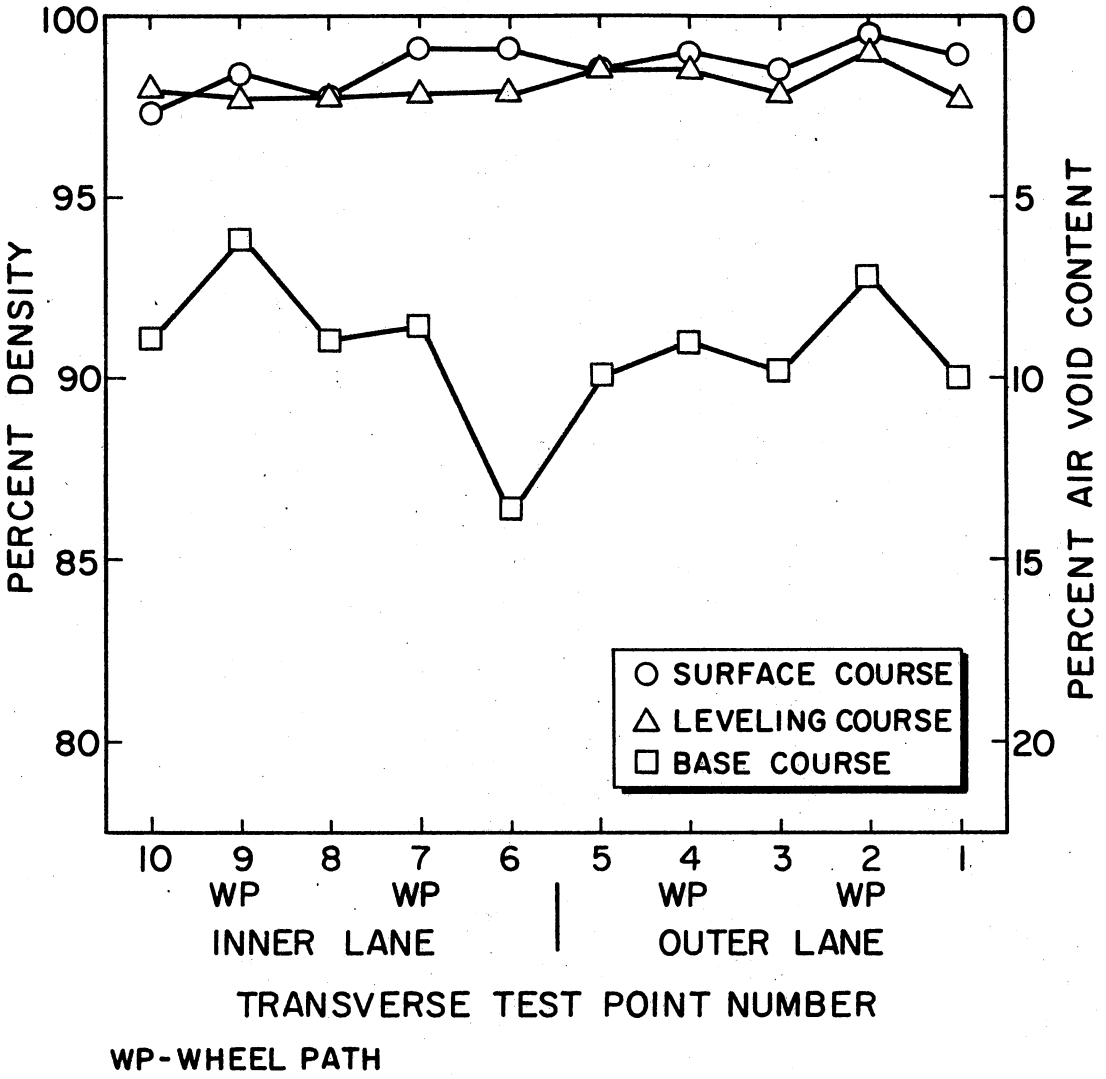

Figure 34. Percent Density Versus Transverse Test Point Site #10, Base Type--HMSA

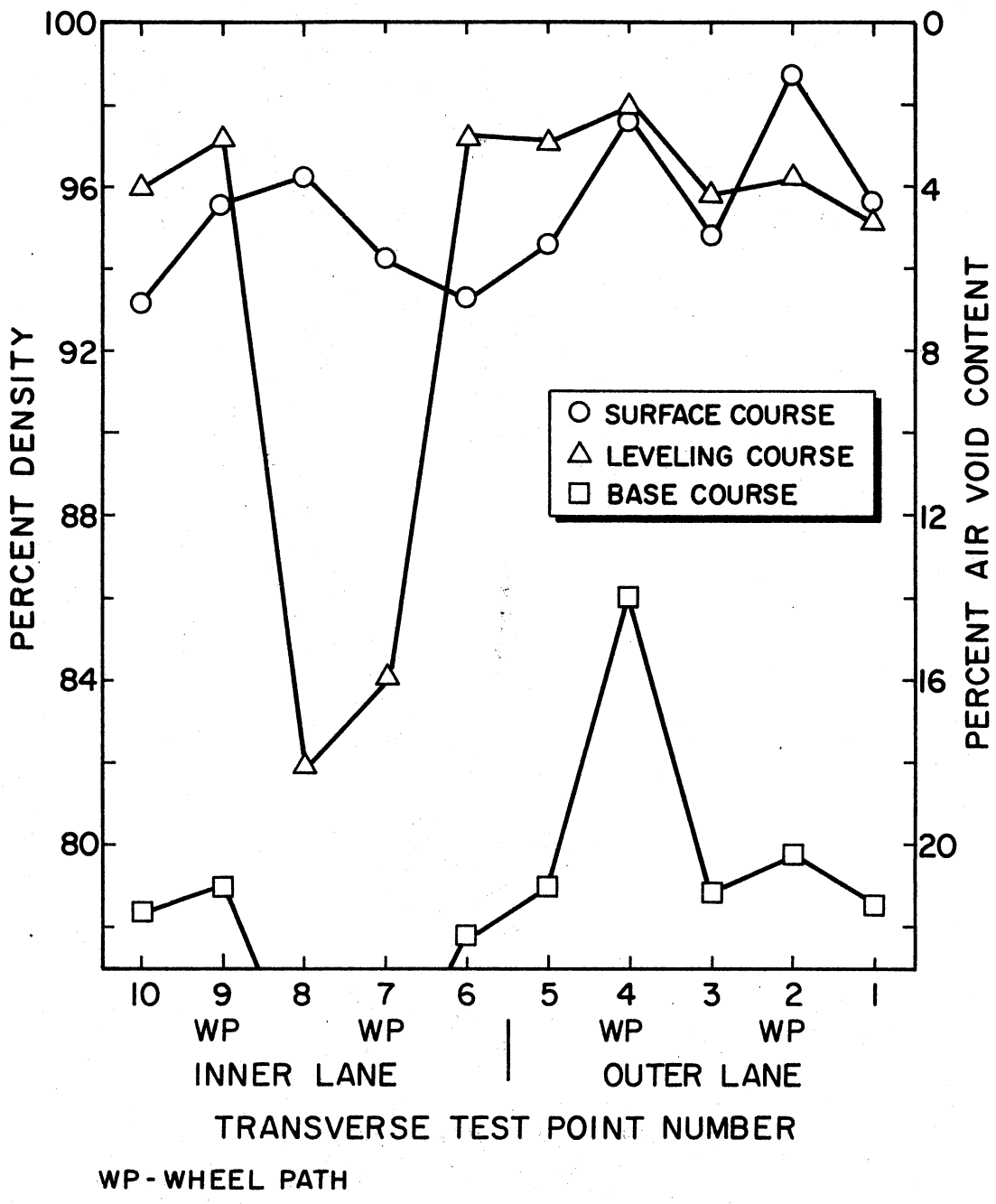

Figure 35. Percent Density Versus Transverse Test Point Site #60, Base Type--HMSA

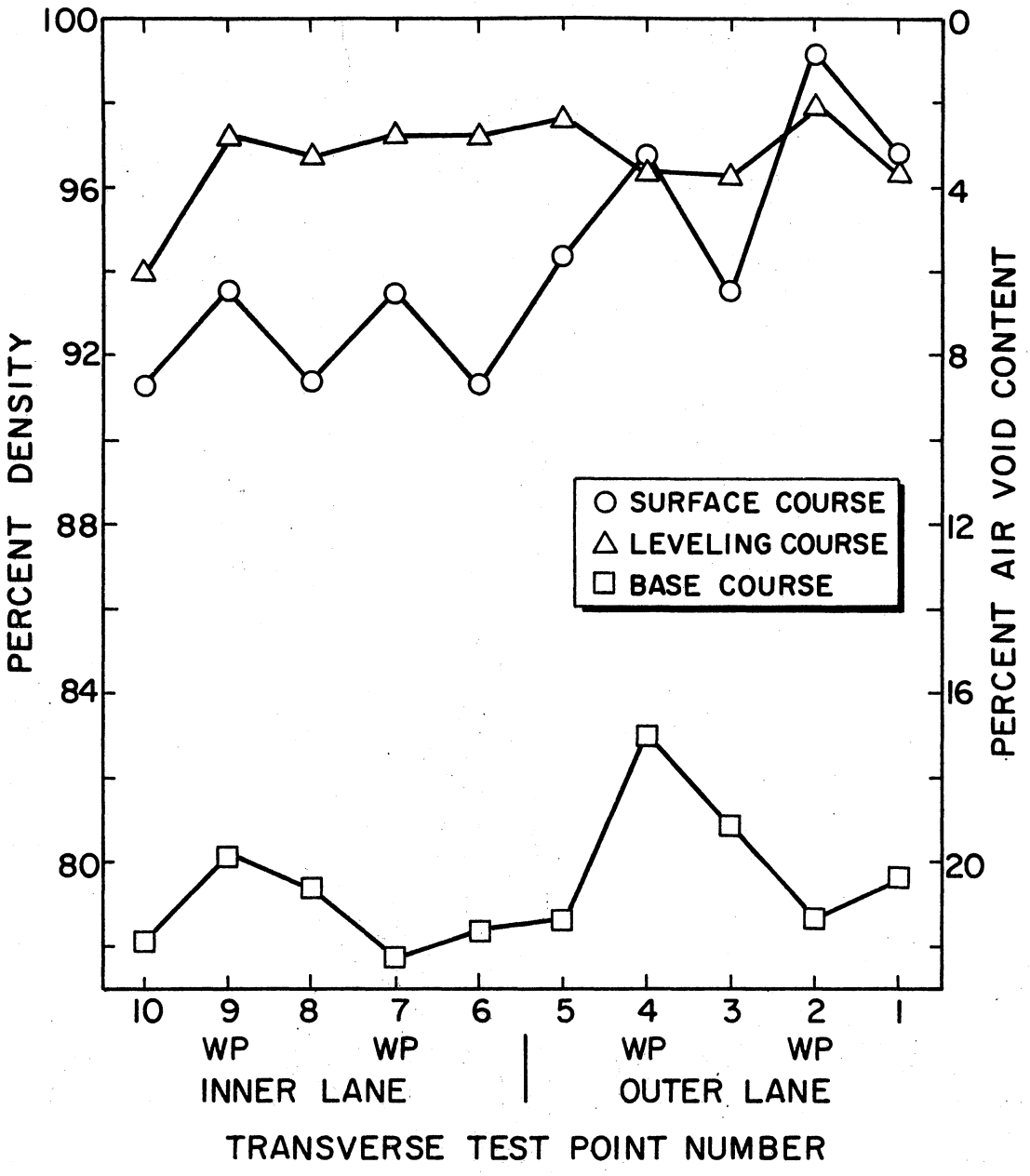

Figure 36. Percent Density Versus Transverse Test Point Site #70, Base Type--HMSA

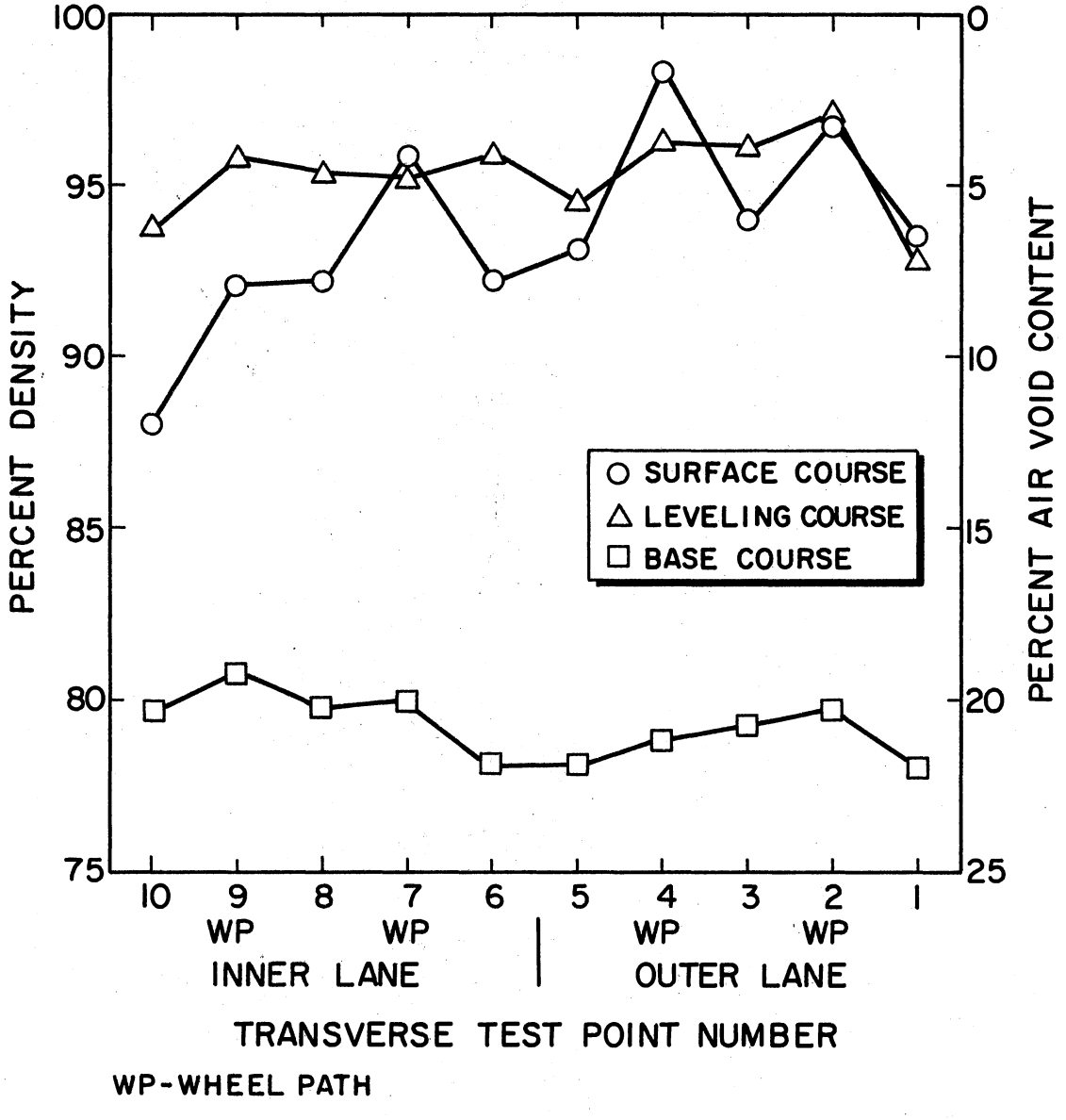

Figure 37. Percent Density Versus Transverse Test Point Site #120, Base Type--HMSA

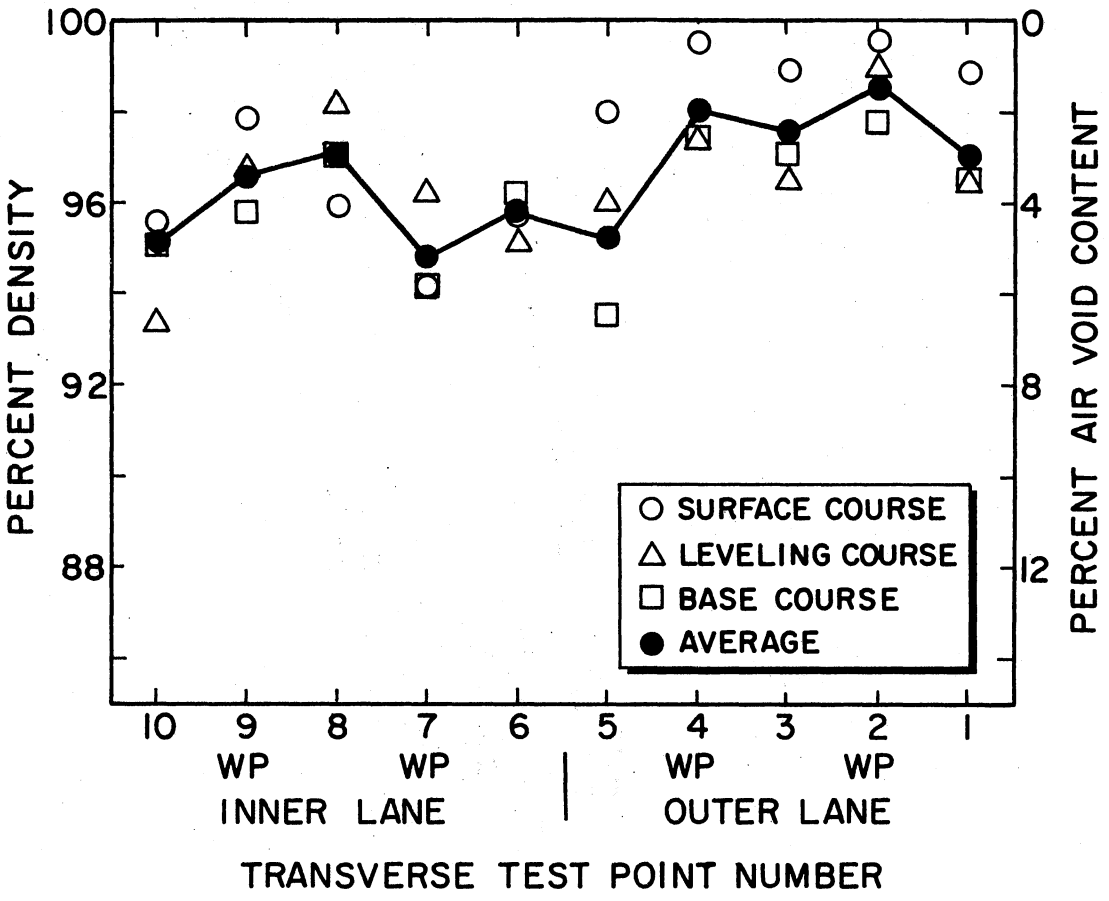

Figure 38. Percent Density Versus Transverse Test Point Site #30, Base Type--BB

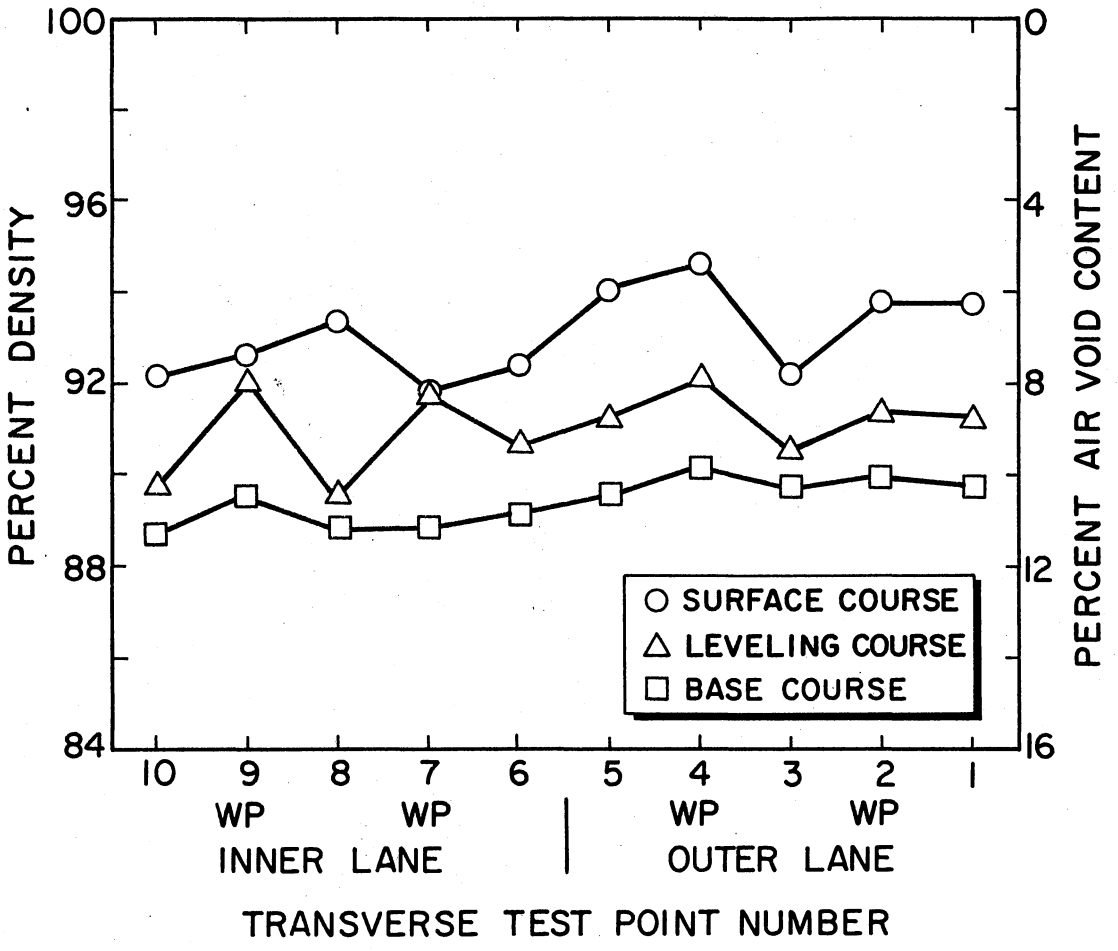

Figure 39. Percent Density Versus Transverse Test Point Site #50, Base Type--BB

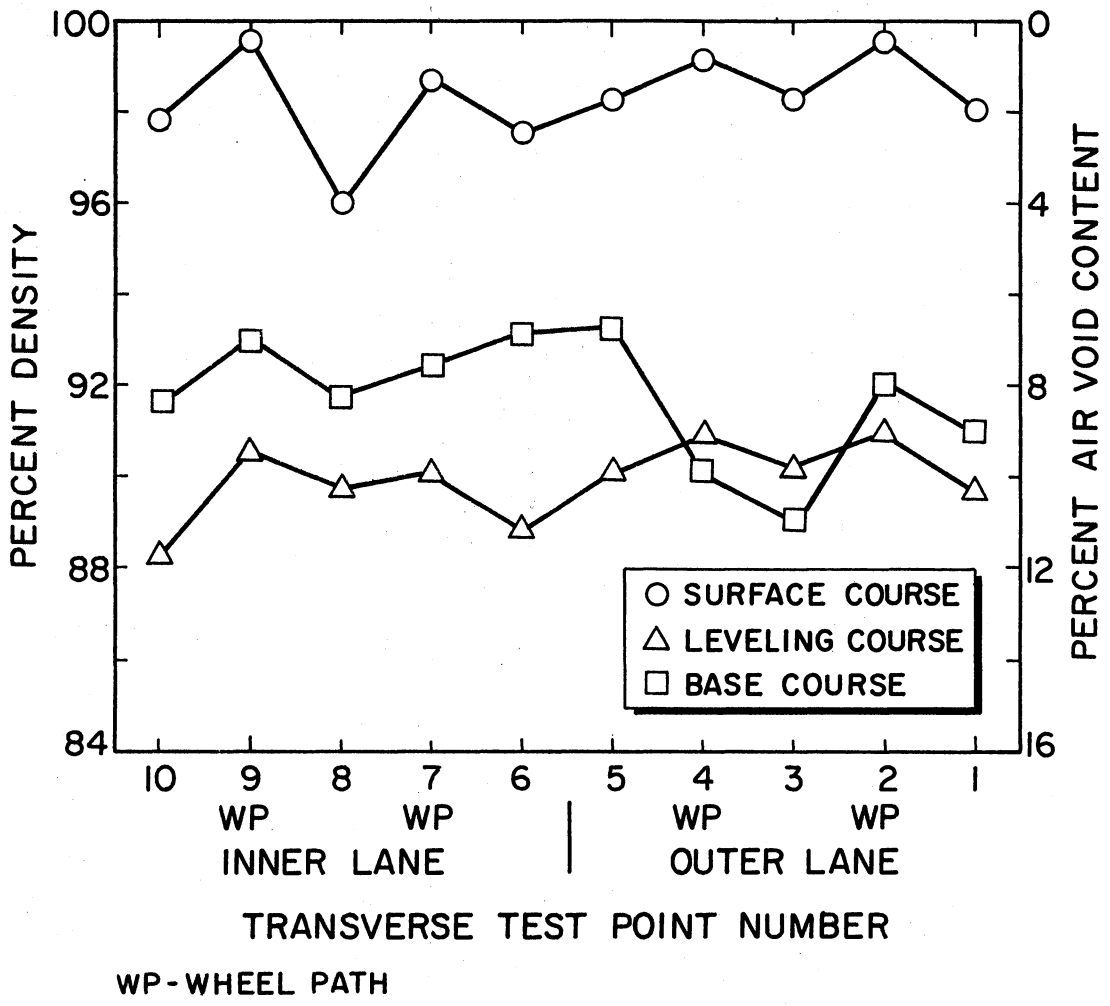

Figure 40. Percent Density Versus Transverse Test Point
Site #20, Base Type--BB

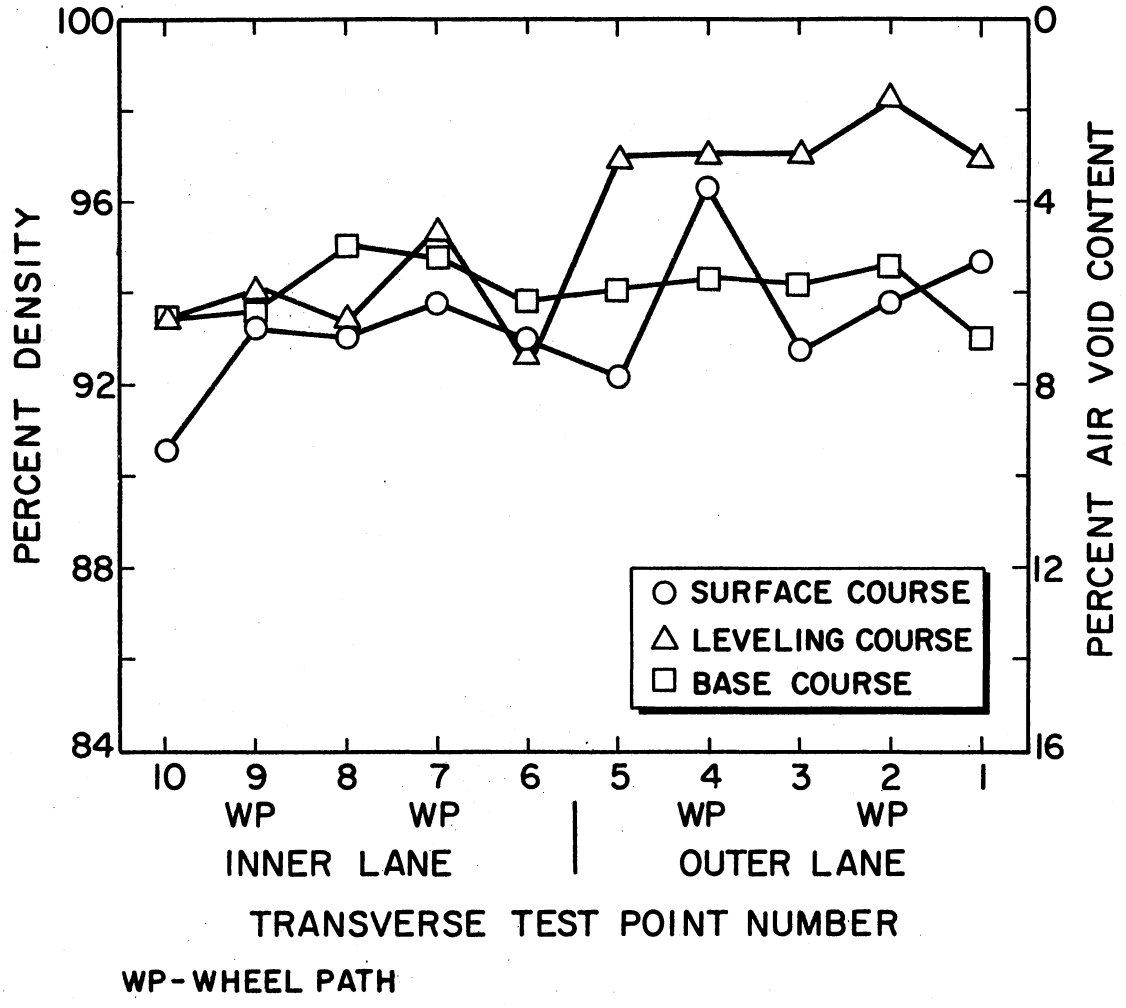

Figure 41. Percent Density Versus Transverse Test Point Site #40, Base Type--BB

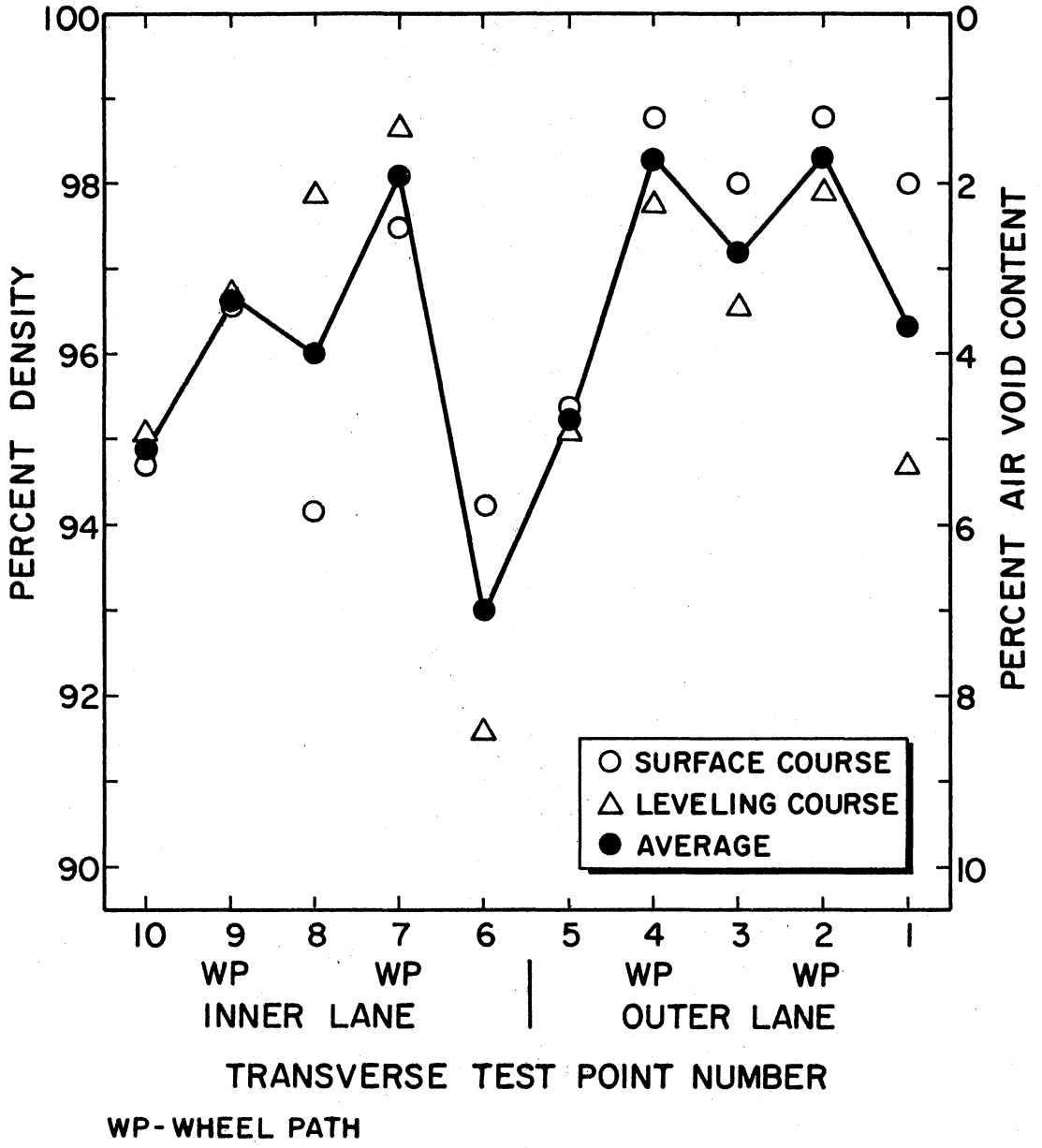

Figure 42. Percent Density Versus Transverse Test Point Site #100, Base Type--SABC

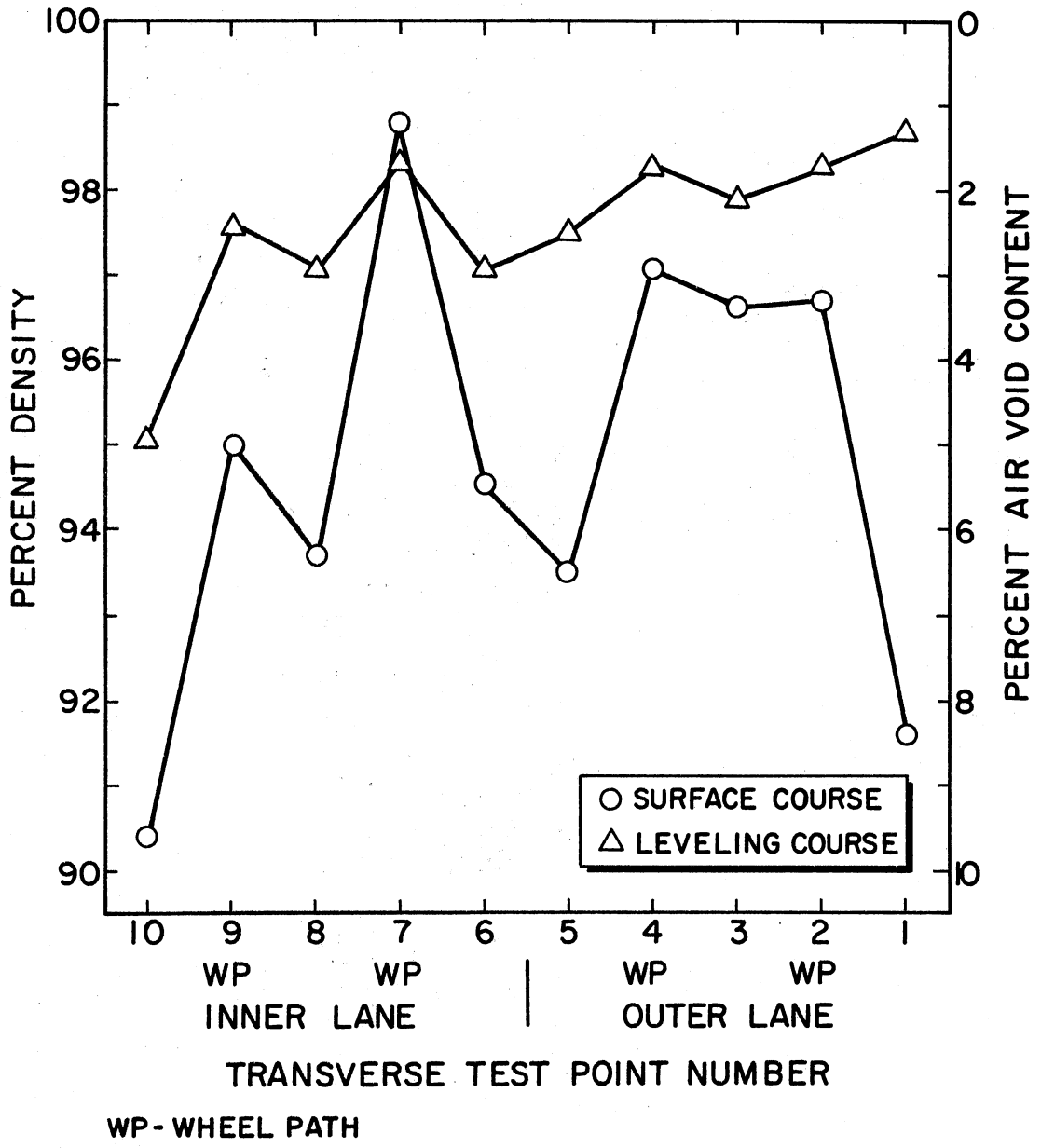

Figure 43. Percent Density Versus Transverse Test Point
Site #80, Base Type--SABC

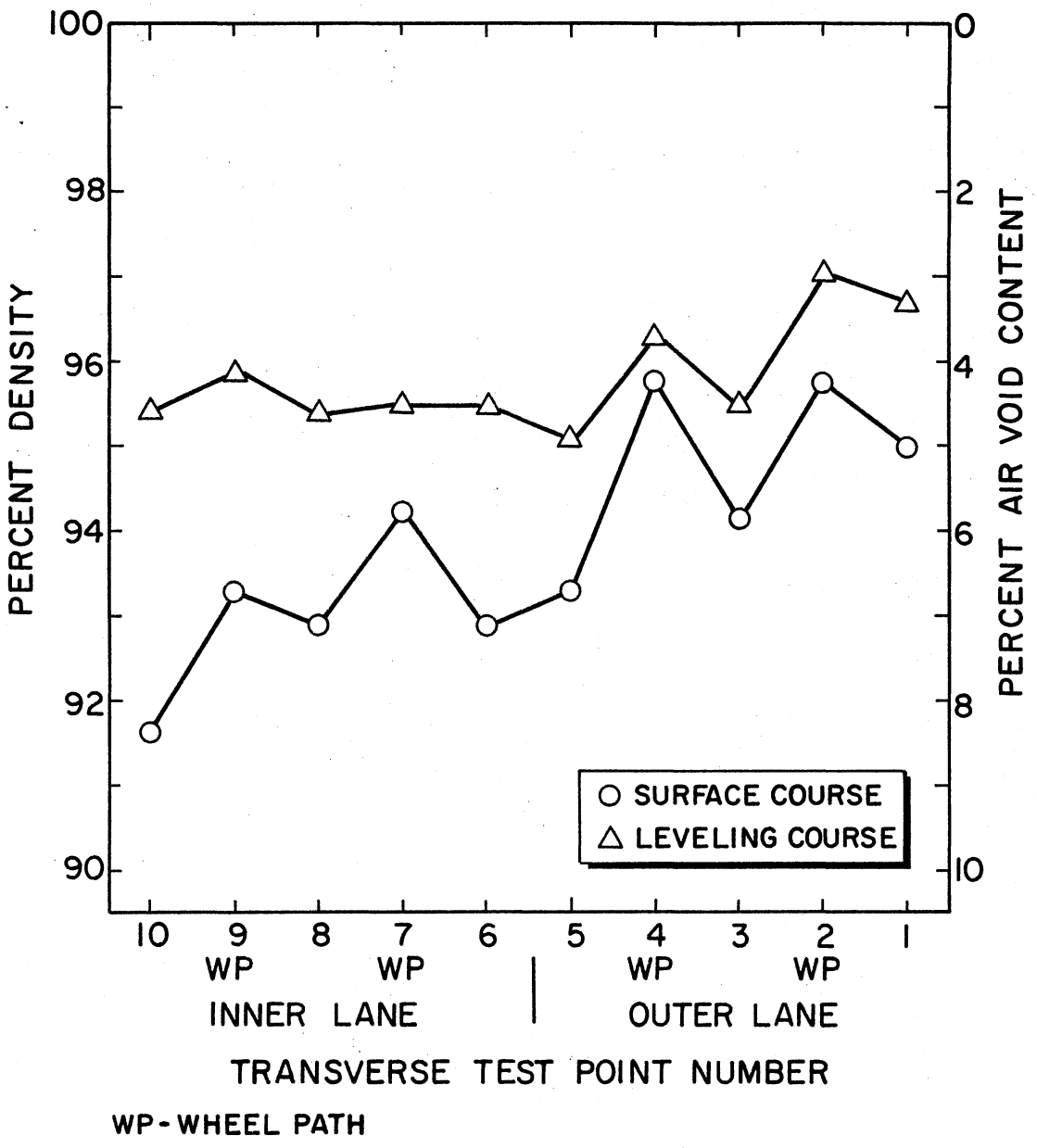

Figure 44. Percent Density Versus Transverse Test Point Site #90, Base Type--SABC

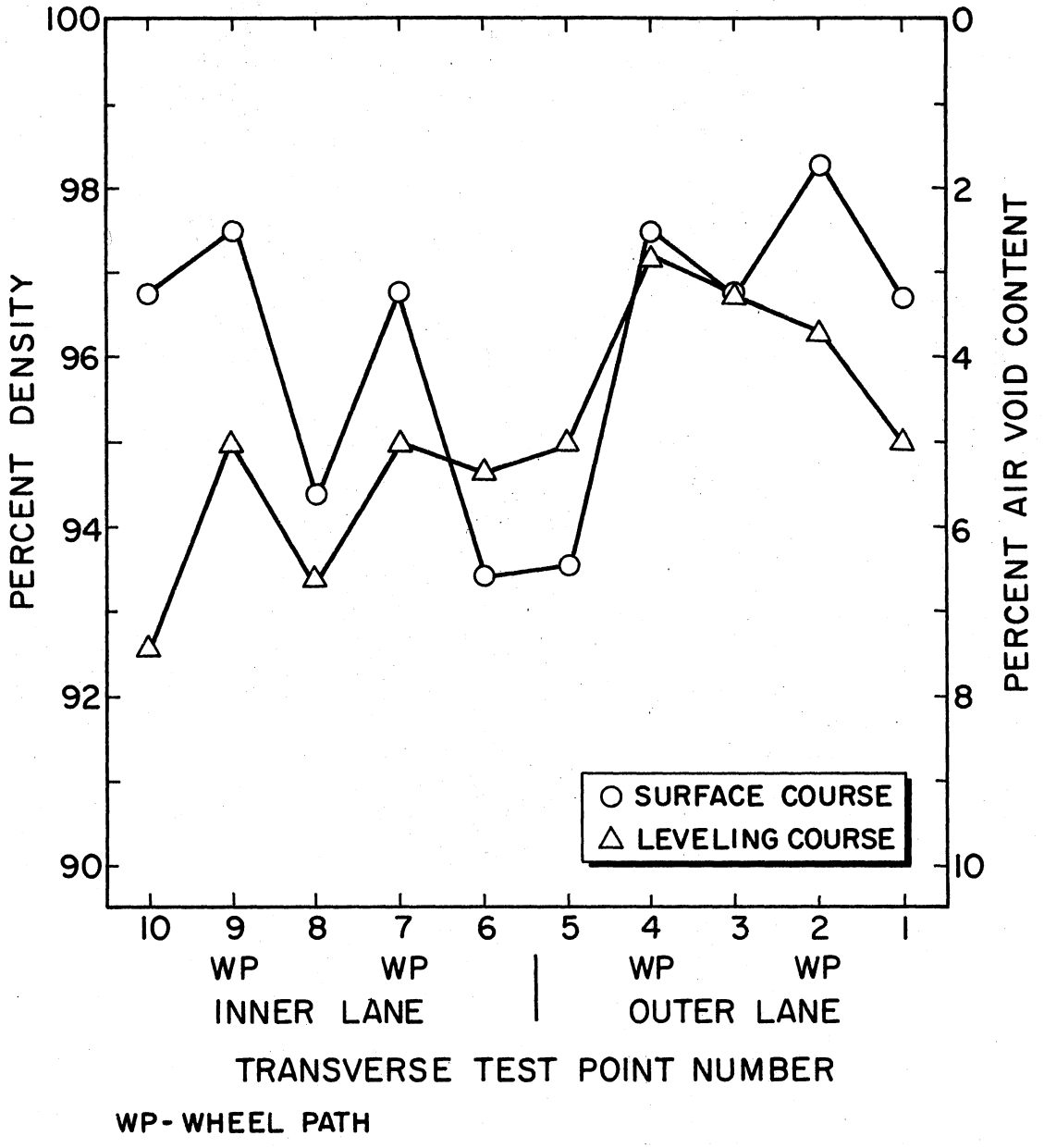

Figure 45. Percent Density Versus Transverse Test Point Site #110, Base Type--SABC

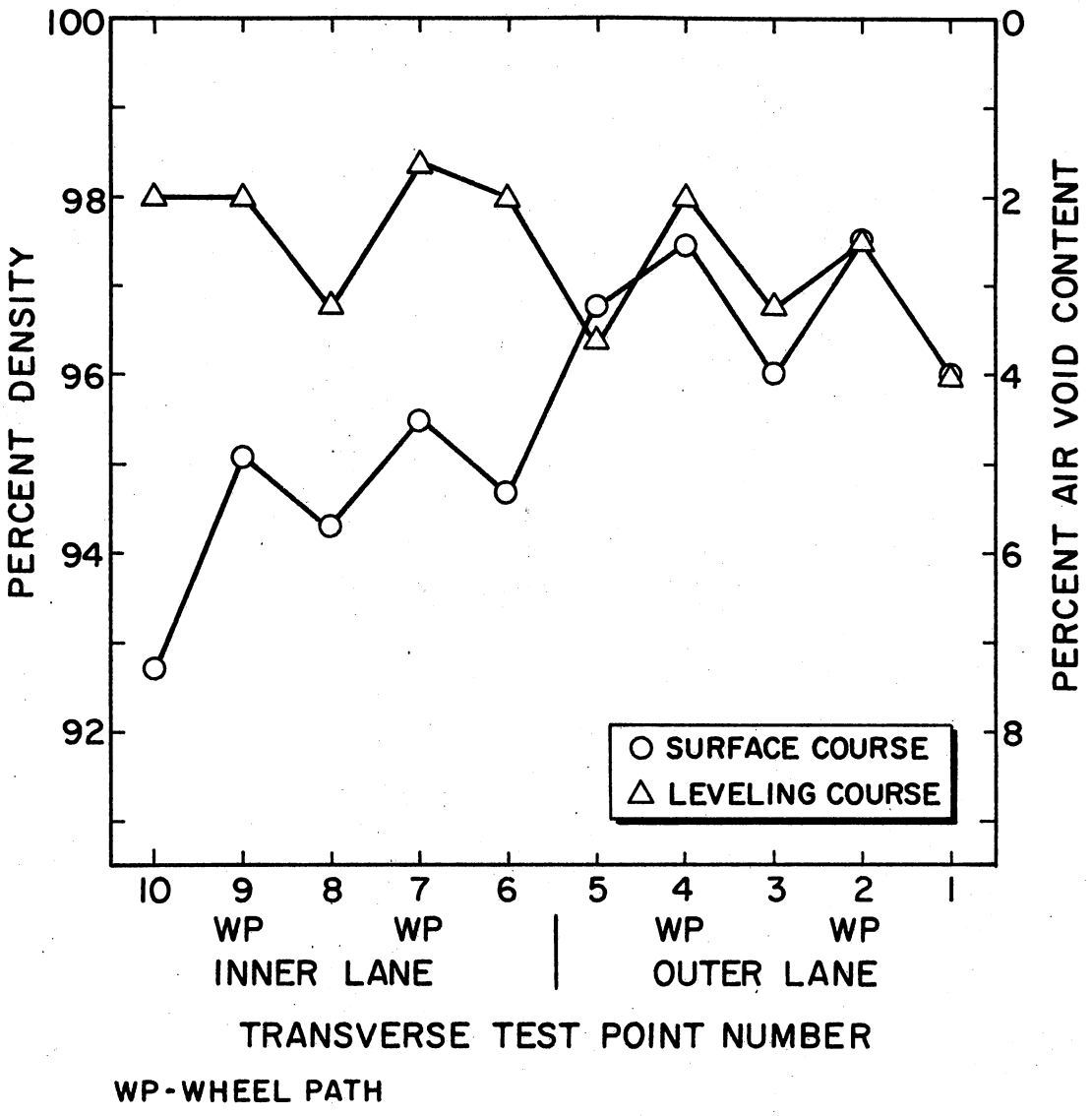

Figure 46. Percent Density Versus Transverse Test Point Site #130, Base Type--SCB

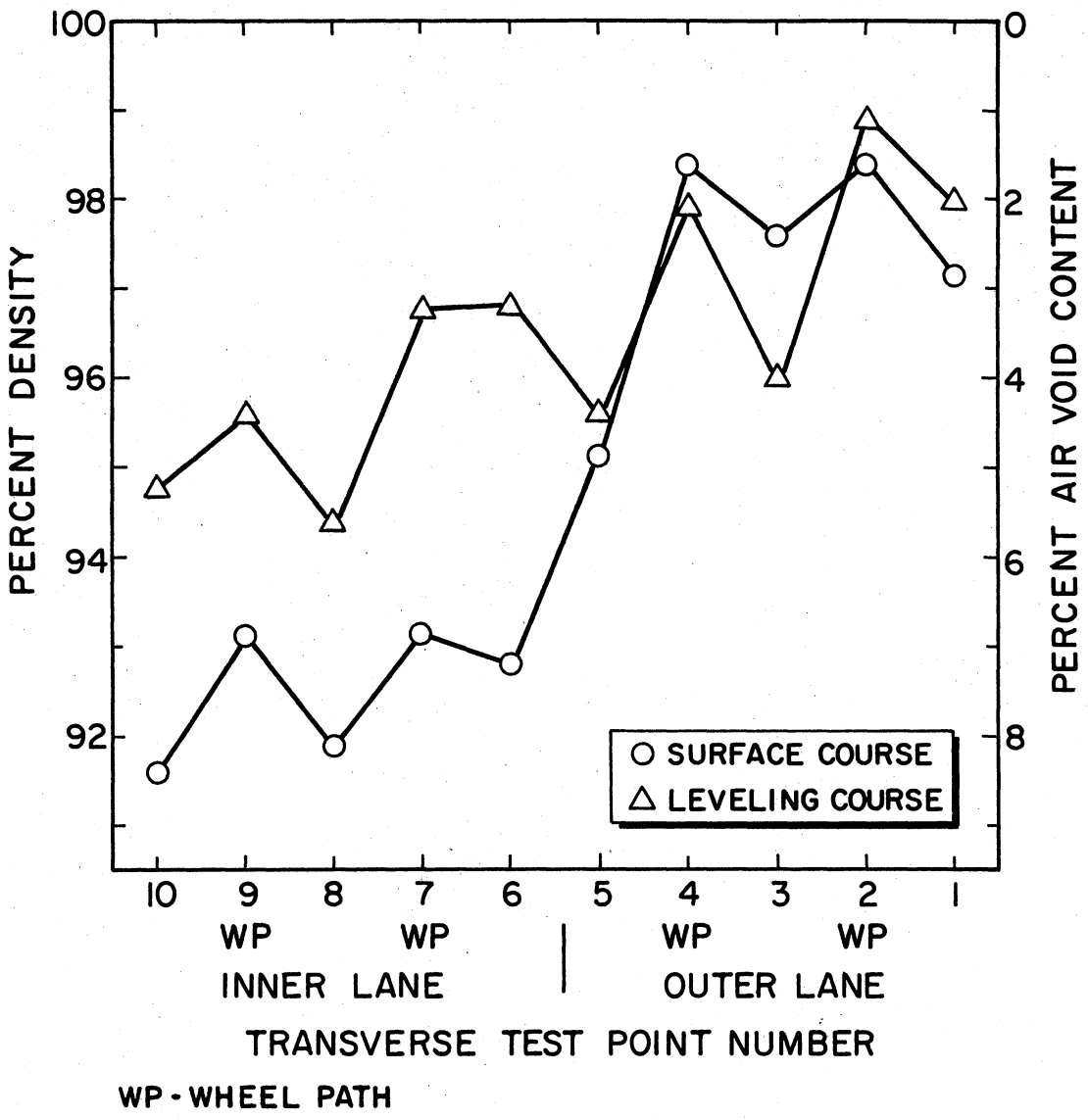

Figure 47. Percent Density Versus Transverse Test Point Site #140, Base Type--SCB

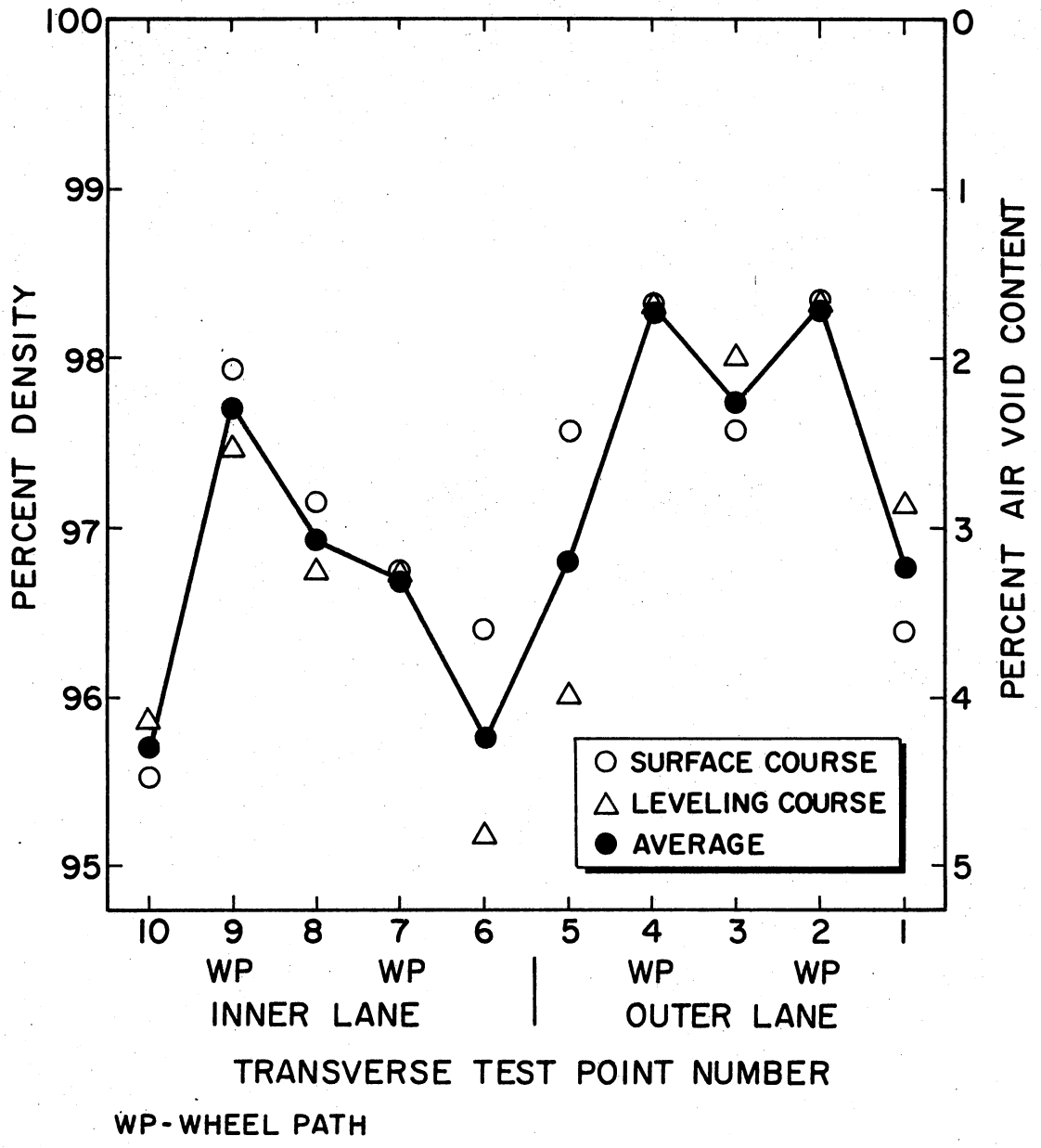

Figure 48. Percent Density Versus Transverse Test Point
Site #170, Base Type--SCB

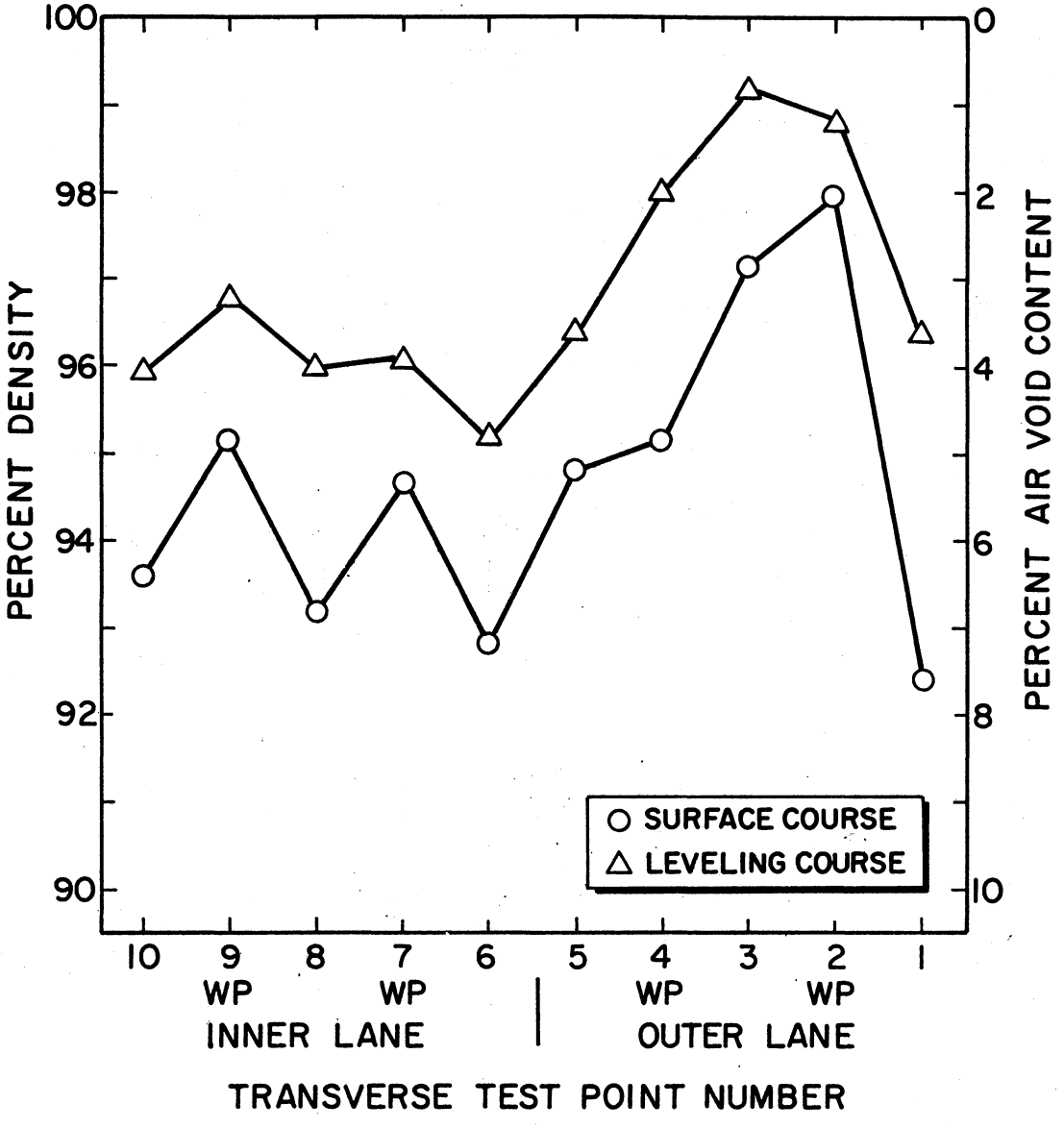

Figure 49. Percent Density Versus Transverse Test Point
Site #180, Base Type--SCB

APPENDIX E

CORRELATION BETWEEN NUCLEAR GAGE DENSITY AND LABORATORY DENSITY VALUES

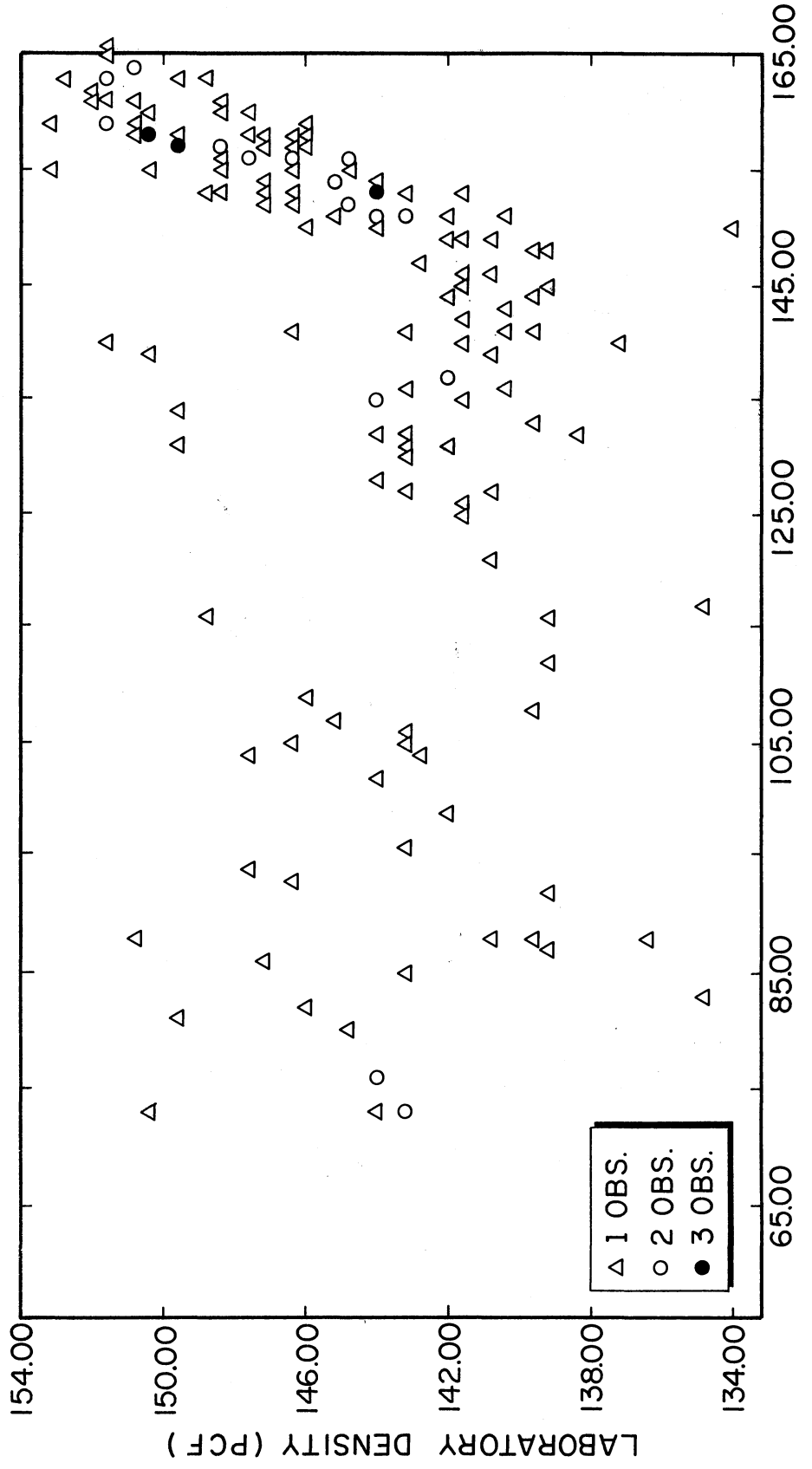

Figure 50. Plot of Nuclear Density Versus Laboratory Density

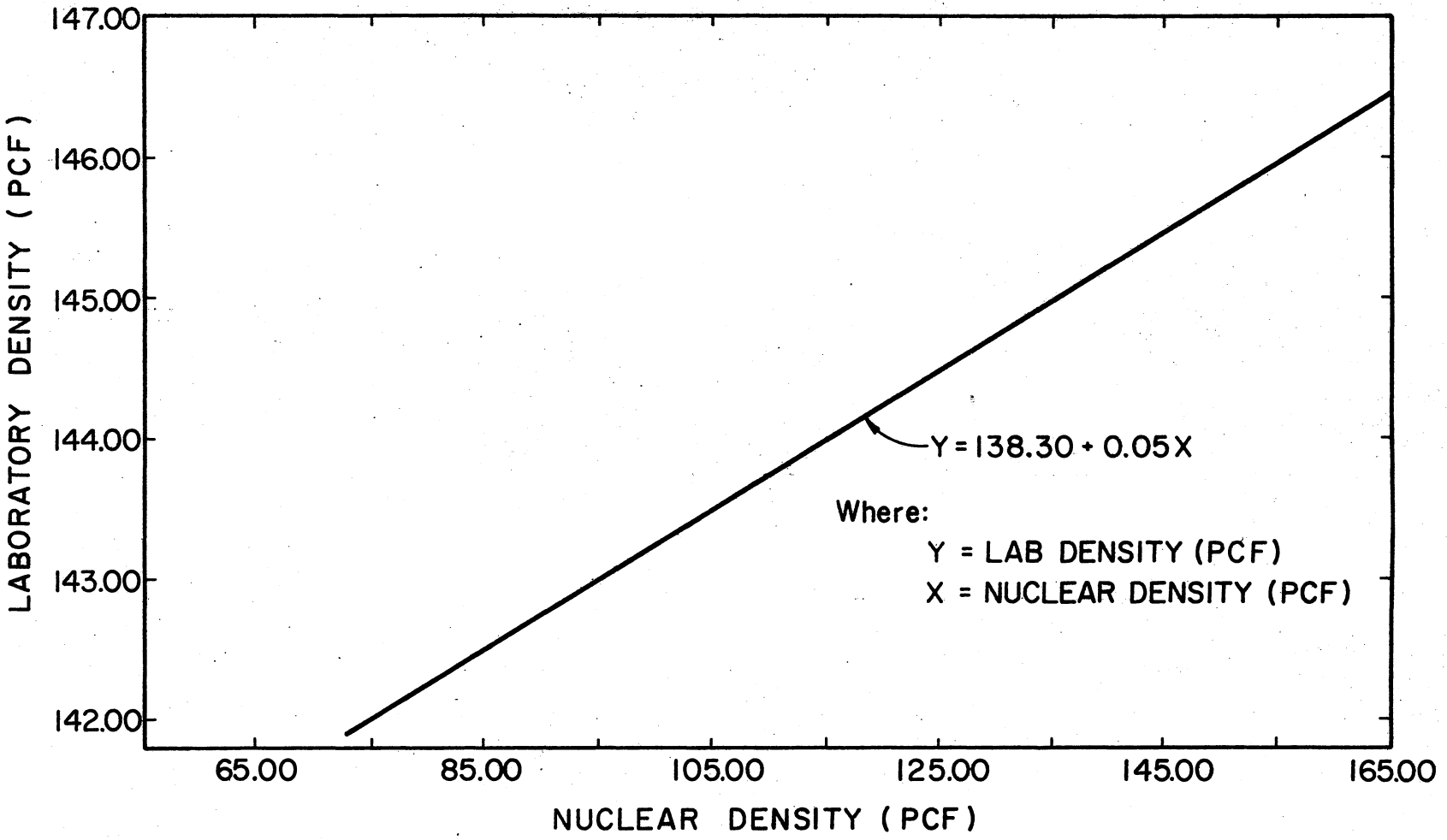

Figure 51. Correlation Curve

VITA[2]

Samuel Oteng-Seifah

Candidate for the Degree of

Doctor of Philosophy

Thesis: CHARACTERISTICS OF RUTTING ON HIGH QUALITY BITUMINOUS HIGHWAY PAVEMENTS

Major Field: Civil Engineering

Biographical:

Personal Data: Born in Apromasi near Kumasi, Republic of Ghana, July 3, 1943, the son of Kwame Adjei and Akosua Afrakoma. Married Mary Doris Agyemang, August, 1970.

Education: Attended the Takoradi Govt. Polytechnic Institute, 1962-1965, received the Ordinary National Cert. (City & Guilds, London) and the Advanced Level G.C.E. of the British Associated Examining Board in June, 1965; attended the University of Science & Technology, Kumasi, Ghana, 1965-1969 and received the Bachelor of Science degree in Building Technology in June, 1969; received the Master of Science degree in Civil Engineering from the Montana State University, Bozeman, in January, 1972; completed requirements for the Doctor of Philosophy degree at Oklahoma State University in December, 1975.

Professional Experience: Research Assistant, Kumasi University, summer 1966; Assistant Engineer (Quantities Surveying), Kumasi University, summer 1967; Assistant Engineer, Kumasi City Council, Ghana, summer 1968; Assistant Engineer, State Construction Corporation, Accra, Ghana, summer 1969; Engineer, Civil Engineering, Ashanti Goldfields Corporation, Ghana, 1969-1970; Research Assistant, Civil Engineering, Oklahoma State University, 1973-1975.

Professional Organizations: Associate Member, American Society of Civil Engineers; Transportation Research Board; Association of Asphalt Paving Technologists; Member, Chi Epsilon.